TRITA - FKT 2000:48
ISSN 1103 - 470X
ISRN KTH/FKT/D--00/48--SE

Carbody and Passengers in Rail Vehicle Dynamics

Doctoral thesis

by

Pelle Carlbom

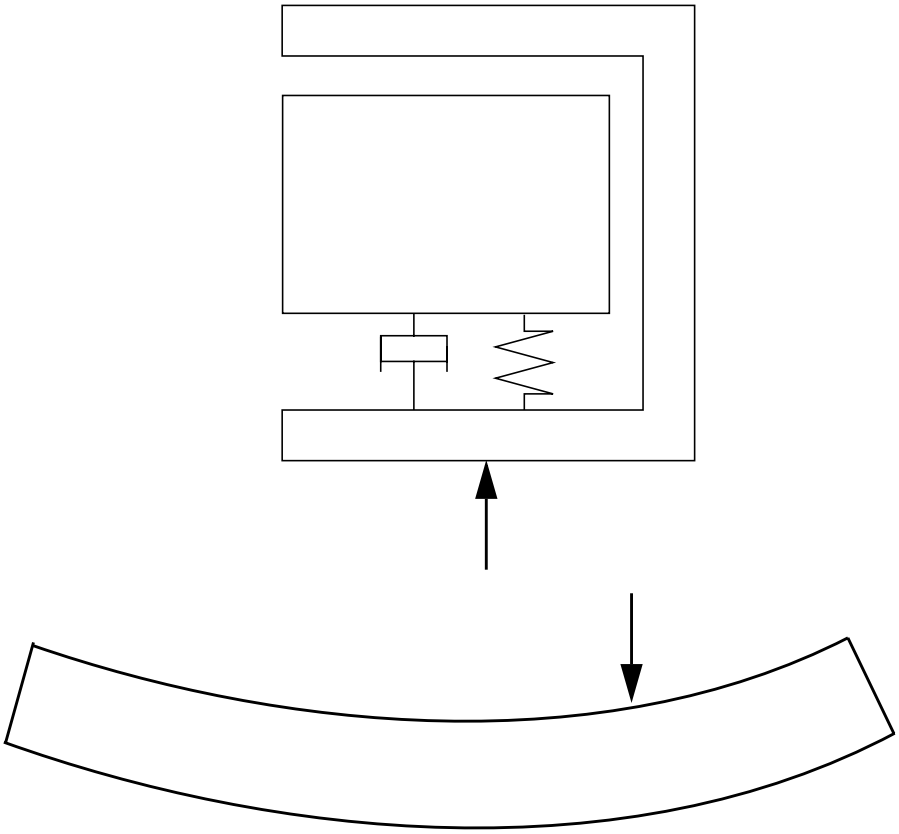

Stockholm
2000

Railway Technology
Department of Vehicle Engineering
Royal Institute of Technology

TRITA - FKT 2000:48
ISSN 1103 - 470X
ISRN KTH/FKT/D--00/48--SE

Carbody and Passengers in Rail Vehicle Dynamics

Doctoral thesis

by

Pelle Carlbom

Postal address
Kungl Tekniska Högskolan
Järnvägsteknik
100 44 Stockholm

Visiting address
Teknikringen 8, 2 tr
Stockholm

Phone
08-790 60 00
Fax:
08-790 76 29

Preface

Rail vehicle dynamics is a subject that is necessary to master for many rail vehicle engineers, with many practical problems to overcome. It is also a source of interesting problems for the theoretically interested. Working on this thesis I have made an effort to understand both the engineer's and the theorist's points of view, and I hope that both find something interesting to read here.

The work is a part of the project SAMBA, an abbreviation for "SAMverkan fordon-BAna" (Vehicle-track interaction) which was initiated jointly by the Swedish railway industry (Adtranz, SJ and Banverket) and KTH. The overall aim of the project is to deepen the knowledge of rail-vehicle dynamics to the benefit of railway industry. The present work addresses the issue of development of modelling and simulation techniques for the prediction of carbody vibrations and ride comfort.

The financial support from Adtranz Sweden, SJ, Banverket and NUTEK (The Swedish National Board for Industrial and Technical Development) is gratefully acknowledged.

I owe a great Thank You to my supervisor Dr. Mats Berg for his continuous and reliable support. I thank Professor Evert Andersson for his enthusiastic and efficient advice. The interest shown by the representatives of Adtranz, in particular Lars Ohlsson, Nils Nilstam, Magnus Hermodsson, Jens Borg, Mikael Norman and Håkan Andersson, is greatly appreciated. Ingemar Persson at DEsolver AB brought many ideas. I thank Dr. Ulf Carlsson at KTH and linguistic reviewer Everett Ellestad for valuable comments on the manuscript. I am also grateful to all of you who helped me with the measurements, especially Kent Lindgren and Fredrik Sundberg at KTH. I appreciate the swift and service-minded actions of Bertil Degerholm and Mikael Wrang at SJ and the help from Åke Lindén at Banverket. I will remember the friendly daily-life among my colleagues at the department. And Sister, Mum and Dad, thank you for being there.

Stockholm, anno MM

Pelle Carlbom

Abstract

The carbody plays an important role in rail vehicle dynamics. This thesis aims at developing validated modelling methods to study its dynamics, how it is excited on track and how it interacts with the passengers. The primary interest is ride comfort, considering vibrations up to 20 Hz. In this frequency range, the structural flexibility of the carbody is of major concern. The models are intended for use in time-domain simulation, calling for small-sized models to reduce computational time and costs. Key parameters are proposed to select carbody eigenmodes for inclusion in a flexible multibody model, and to quantify the interaction between passengers and carbody.

Extensive comparisons between measurements and corresponding simulations are carried out in a case study. On-track measurements are performed to obtain operating deflection shapes and power spectral densities of the accelerations in the carbody. The complete vehicle is modelled using the pieces of software GENSYS (flexible multibody model) and ANSYS (finite element model of the carbody). Actual, measured track irregularities are used as input. In order to investigate the influence of passenger load, experimental modal analysis of the carbody is performed with and without passengers. Also, amplitude dependence is examined. Simple models, based on human-body models from literature, of the passenger-carbody system are proposed and validated. Vertical seating dynamics is considered. The models are implemented and tested in the case study. Finally, ideas on model reduction and approximation are presented and applied.

The main conclusions drawn from the study are that
- the structural flexibility of the carbody must be taken into account when predicting vertical vibration comfort. It is possible to predict which carbody modes that will contribute most to the vibrations.
- the carbody dynamical properties depend on the excitation amplitude.
- passengers and carbody interact significantly.
- the proposed models describe the interaction quite well. The proposed passenger-carbody model gives an upper boundary on the interaction.
- the proposed passenger-seat-carbody model can be used to study the influence of the seat parameters on the interaction. This merits to be investigated further, however.

Keywords: Carbody, Experimental modal analysis, Human-body dynamics, Model reduction, Multibody dynamics, Operating deflection shapes, Rail-vehicle dynamics, Ride comfort, Seating dynamics, Structural dynamics.

Contents

1 Introduction

1.1 Carbody, passengers and ride comfort

If you as a passenger riding in a rail vehicle do not think about vibration, that is because rail-vehicle-dynamics engineers have succeeded in achieving good ride comfort. A low vibration level is one of the important factors of a good ride comfort [58][1]. The vibrations are mainly caused by track irregularities, from which they are transmitted via the bogies and the carbody to the passengers. The carbody is not rigid, but bends and twists from the excitation coming from the bogies. In some cases, this carbody structural flexibility accounts for half of the perceived vibrations, the rest being due to rigid body motions [13]. The current trend towards lighter vehicles and higher speeds makes the issue of carbody structural flexibility crucial in the design and development of competitive vehicles. Also, the demand for a high comfort standard calls for a better understanding of the passenger-carbody interaction.

Engineers have two tools to assess vibrations: measurements and simulations. Measurements are, however, not possible during the design phase of a new vehicle. Here, simulations based on rail vehicle dynamics models offer a possibility to predict ride comfort, but, in order to be reliable, the simulation models must be validated. There is, therefore, a need for validated methods in analysing and modelling the structural dynamics of the carbody.

The present work addresses the issue of carbody structural dynamics. It examines the role played by the structural flexibility of the carbody, and, in particular, it aims at developing validated modelling methods to analyse the dynamics of the carbody, how it is excited on track and how it interacts with the passengers.

Figure 1-1 below shows a common Swedish rail vehicle, the SJ-B7M, which serves as a case study in the present work. Measurements were also carried out on a variant of it furnished for office-working, the SJ-S4M. The carbody and the bogies are indicated in the figure.

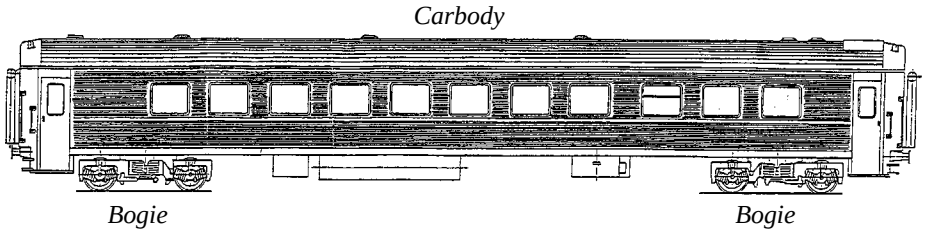

Figure 1-1 The SJ-B7M (SJ-S4M) rail vehicle. *Length 26.4 metres.*

1. References are found in Appendix A.

1.2 Related fields and work

The subject of “carbody and passengers in rail vehicle dynamics” deals with the areas of rail-vehicle dynamics, structural dynamics, ride comfort, human-body dynamics and seating dynamics. Each area is a vast field of its own. For instance, quoting [44], “human vibration involves physics, psychology, mathematics, physiology, engineering, medicine and statistics”.

Rail-vehicle dynamics is a subject of its own [8][26], and the study of rail-vehicle dynamics dates back to the 19th century. Then, vehicle stability [30] was one of the main interests. Of more recent date is the study of rail-vehicle dynamics based on simulation and applied to ride comfort, which began in the late 1960s with the advent of sufficiently powerful computers. Many of the computer codes for rail-vehicle dynamics that are commercially available today [27] have roots in that time. The simulation codes have been developed in industry, as well as at universities. Rail-vehicle dynamics and carbody structural flexibility is well supported by the framework of flexible multibody-dynamics [23][35].

The study [12] reviews structural dynamics models for rail vehicle dynamics. There are several studies on carbody structural flexibility, e.g. [19][20][21][22][25][31][32][33] and [34], often with application to ride comfort. Floating floors have been investigated [37]. The models range from simple beam models to detailed finite-element models. In most cases, modal models obtained from experimental modal analysis and finite-element calculation are used in the analysis. The number of investigations made by rail-vehicle manufacturers on the issue ought to be significant, but are seldom published.

The first international standard on ride comfort and whole body vibrations was published in 1975 [56], but already in 1941 [55] “equivalent comfort contour” curves for seated persons vibrated in the frequency range of 1 to 12 Hz were produced. These curves were developed to become the “Wertungsziffer” (Wz), which, for a long time, was widely used by European railways. The current standard is a modified ISO-2631 from 1997 [57]. There are, however, differing opinions, in particular on the “weighting filters” prescribed by this standard and a new standard is proposed [53]. Traditionally, only frequencies up to 20 Hz have been considered, but current standards also take higher frequencies into account, up to 80 Hz [37]. A thorough discussion on ride comfort is found in [44] and [54].

The sensitivity to vibration must not be confused with the actual vibration of the human body and its interaction with the carbody. There are early contributions to the field of human-body modelling and measurements [38], but the most quoted early experiments are the investigations of Dieckmann 1957 [42] and Coermann 1964 [40]. They worked independently on single-degree-of-freedom and two-degree-of-freedom models of the human body subjected to vertical vibrations. Coermann based his modelling on measurements of eight men. Miwa [48] extended the work and studied factors that might influence the measurements, such as body posture. The ISO-5982 standard 1981 [47] reports 39 people having been measured in the sitting position up to that date. This standard prescribes two-degree-of-freedom models for the human body in sitting, standing and supine (outstretched) position. Extensive studies including measurements of 60 people were recently performed by Wei and Griffin [51].

A whole chapter is devoted to seating dynamics in [44]. The interest in seating dynamics has, so far, been low in the rail vehicle industry, but “increased focus on customer seat comfort can be foreseen in the future” according to [49]. Seat models consisting either of filters or of mass-spring-damper systems are sometimes used in industry to better match predicted floor acceleration to the reaction of the seated passengers.

Only a couple of studies on passenger-vehicle interaction are found in the literature. In an experimental study [7], the natural frequency of the vertical bending mode was measured at various stages during manufacture of a passenger rail vehicle. The influence of 53 sitting, and then standing, passengers was examined. For standing passengers, there is no change in natural frequency, but for sitting passengers there is a slight increase in the vertical-bending natural frequency. Based on these few observations, the investigators drew the conclusion that the passenger mass should not be modelled as unsprung. Moreover, they claim that it is hardly worthwhile to model passengers and seats as sprung masses. This claim is not motivated, however, and the investigators did not consider the influence on damping, for instance. In [11], an example is given of how to modify a carbody modal model to simulate passenger loading, where the passengers are modelled as unsprung masses, but the prediction is not compared to measurements.

1.3 This thesis

1.3.1 Aim and approach

The present work aims at developing modelling methods to study the dynamics of the carbody in the frequency range of 0 to 20 Hz, how it is excited on track and how it interacts with the passengers. The models are to be used in time-domain simulation of rail-vehicle dynamics and, since such a simulation tends to require extensive computing time, an important aspect is the possibility of obtaining small, reduced models. Therefore, an important goal has been to find key parameters that describe the important properties of the dynamical system, in order to achieve small-sized models. A theme of this work is “the combination of two dynamical systems”; in the first part of the work, the combination of carbody and bogies when studying track-induced vibrations, and, in the second part, the combination of carbody and passengers.

The approach towards the subject is, on the one hand, based on the traditional methods used in rail vehicle dynamics, such as on-track measurements, experimental modal analysis (EMA), multibody modelling and finite-element modelling (FEM). On the other hand, mathematical analysis and numerical experiments (using MATLAB [61]) are used to find the essential features of rail vehicle carbody dynamics.

The work focuses on three of the topics identified in the pilot study [12], namely on the importance of structural vibration, on model reduction and on the modelling of passengers.

1.3.2 Thesis contributions

The thesis draws attention to parameters that play an important, but often forgotten, role in the interaction between two dynamical systems. Here, they are called “modal contribution factor” and “passenger load parameter”. The parameters serve as guides performing model reduction. Criteria to accomplish model reduction from a practical point of view are also proposed. More specifically, the proposed criteria are intended to help identify important carbody eigenmodes.

The thesis work also extends traditional rail-vehicle measurements to include new features, namely operating-deflection-shape (ODS) analysis of carbody structural vibrations and experimental modal analysis including the passengers. The comparison made between simulation models and full-scale measurements strengthens the conclusions drawn from the thesis.

In particular, this thesis is believed to contribute to the fields of rail-vehicle dynamics and modelling as regards the following aspects:

- On-track measurements of carbody operating-deflection shapes, identifying excited carbody mode-shapes and their contribution to the vibration level on different track sections.
- Modelling of the same rail vehicle combining finite-element and multibody models and including the actual track irregularities. A thorough comparison between measured and simulated results with emphasis on the structural flexibility of the carbody, comprising acceleration time-histories and spectra, as well as comfort-weighted r.m.s. values.
- Proposal and test of criteria for model reduction of the carbody model, in particular what carbody modes to be retained for ride-comfort simulation.
- Experimental modal analysis of a similar carbody with and without passengers to investigate the passenger-carbody interaction. Investigation of the dependence on excitation amplitude.
- Proposal and validation of small-sized models of the passenger-carbody interaction and of key parameters to estimate the interaction.
- Modelling of vertical seat-dynamics. Proposal and validation of a simple seat model and studies on the influence of the seat properties on passenger-carbody interaction.
- Ideas on how to reduce and approximate passenger-carbody and similar systems, e.g. a generalized passenger model.

1.3.3 Present reports and papers

The full research work is documented in five reports, cf. Figure 1-2:

In the pilot study [12], common modelling and measurement methods in structural dynamics are presented. A review of structural flexibility models for rail vehicles found in literature is made. Finally, research topics are identified.

The report [13] presents an investigation of the Swedish passenger vehicle SJ-S4M. The aim is twofold: to get a picture of the structural dynamics of a common vehicle and to test various methods for evaluation of data, for modelling and for simulation. The report contains the following parts: on-track measurements, selection and processing of data, analysis of measurement results (repeatability, power spectral densities, operating

deflection shapes and comfort filtering), vehicle modelling (finite-element modelling and multibody modelling) and, finally, a comparison between simulation and measurements including sensitivity analysis. Attention is paid to differences between simulation and measurement results.

In [14] general equations of motion for a flexible body in an accelerating reference system are derived. Suitable approximations for rail vehicle dynamics applications are then made. Model reduction by global-deformation-shape representation is discussed in a finite-element context. Both free-body eigenmodes and arbitrary deformation-shapes are considered. Algorithms that orthogonalize arbitrary deformation-shapes for use in time-domain simulation are presented and tested.

The author's licentiate thesis [15] summarizes the reports [12], [13] and [14].

The present report constitutes the author's doctoral thesis and extends the work to passenger-carbody interaction, cf. Section 1.3.4.

Parts of the work have also been published as papers [16][17][18].

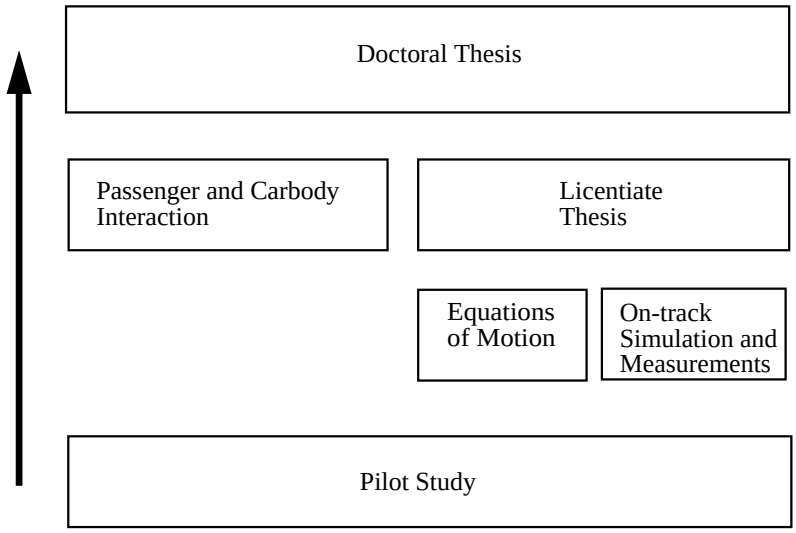

Figure 1-2 Present work.

1.3.4 Outline of doctoral thesis

Chapter 2 summarizes previous work of [13] and [15].

Chapter 3 presents measurements carried out to investigate the passenger-carbody interaction on a vehicle similar to the one in [13].

Chapter 4 reviews models of the human body, of seats and of the rail vehicle carbody that are judged to be suitable to use in studying passenger-carbody interaction.

Chapter 5 combines the models of Chapter 4 and proposes models of the passenger-carbody interaction, including models that consider seating dynamics. Methods to reduce and to approximate models are proposed.

Chapter 6 compares measurement results and model predictions to be able to validate the proposed models.

Chapter 7 applies models from Chapter 5 in the case study of [13].

Chapter 8 concludes and outlines further research.

References are given in Appendix A. Important definitions are given, and the notations are explained in Appendix B, which also comprises a short railway glossary.

2 Track-induced carbody dynamics

This chapter summarizes parts of the licentiate thesis that are relevant here, namely the case study and the proposed mode selection criteria. See also [13] and [15].

2.1 Case study

The Swedish passenger vehicle SJ-S4M was chosen as a basis for a case study consisting of on-track measurements and multibody and finite-element modelling as well as numerical simulation. Using general methods from the rail-vehicle industry for studying rail vehicle dynamics, e.g. on-track ride-comfort measurements and simulation with rail-vehicle dynamics software, an analysis of the role played by structural flexibility was undertaken [13][16]. The main aim may be summarized as answering a couple of questions raised in [12], namely “how important are the structural vibrations”? and “what set of carbody deformation shapes is the most efficient when studying rail vehicle dynamics” (and ride comfort)?

The main conclusion drawn from the case study is that structural flexibility dynamics must imperatively be considered when evaluating vertical comfort in such vehicles. The simulation results were also shown to be particularly sensitive to the modelling of the carbody-bogie interface and of non-structural masses in the carbody.

2.1.1 On-track measurements

On-track measurements provide information on how the vehicle behaves on the track and on the excitation induced by the track irregularities. On-track measurements are often carried out to verify ride-comfort and safety requirements, but sometimes more elaborated measurements are conducted to identify operating-deflection shapes (ODS). Results are however seldom published due to confidentiality. No published reference on rail-vehicle-carbody ODS has been found in the literature, but on other vehicles, e.g. buses [24].

An ODS [60] of a rail-vehicle carbody describes how the carbody vibrates at a particular frequency when the rail-vehicle is running on the track. Compared to eigenmodes of a carbody, which are determined by the dynamical properties alone, an ODS also depends on the magnitude and frequency content of the excitation forces. The acceleration must be measured at sufficiently many points of the carbody, so that the deformation shapes can be identified. It is important to obtain both a correct phase difference and relative magnitude between the acceleration signals in order to obtain an ODS.

A power spectral density (PSD) on the other hand shows how much a point of the carbody vibrates at various frequencies when the vehicle is running on the track, but it does not contain any information on the phase. The area under the PSD-curve corresponds to a mean square value. The peaks in the spectra are due to structural eigenmodes of the carbody structure, rigid-body eigenmodes of the complete vehicle or harmonics of the excitation induced by the track irregularities [31].

Together, ODS and PSD can provide information on which modes are excited on a particular track, and, in a sense, answer the question of what carbody mode shapes are important to include in a model.

The present on-track measurements were carried out on the SJ-S4M rail vehicle, see Figure 1-1, during its regular service. Twenty accelerometer positions were chosen to represent rigid-body modes as well as fundamental eigenmodes of the carbody such as bending and torsion, see Figure 2-1.

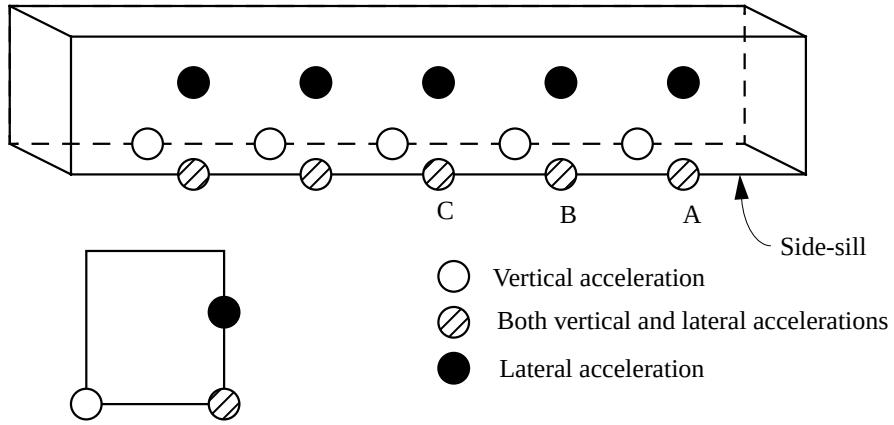

Figure 2-1 ***Accelerometer positions on carbody.*** *Results from positions A, B and C are presented below.*

In total, six test runs were made on a track section of about 65 kilometres between Västerås and Stockholm. At each run, fourteen acceleration signals were measured and recorded at a sampling rate of 6 kHz. Vehicle speed and position were recorded vocally for later reference. Suitable excerpts were chosen considering constant vehicle speed, constant curve radius and similarity of wheel-rail friction conditions between the runs. Chosen acceleration excerpts were then band-pass filtered in the interval of 0.3 Hz to 30 Hz, re-sampled at 200 Hz and scaled.

Track irregularity data of the actual track had been measured by Banverket, the Swedish National Rail Administration, and was analysed and customized for the simulation needs. Three track sections were used: a tangent track in good condition (10 seconds at 160 km/h), a tangent track in normal condition (20 seconds at 130 km/h) and a circular curve in normal condition (10 seconds at 130 km/h).

Figure 2-2 shows measurement results from the two tangent tracks presented as power spectral densities. Spectra of vertical acceleration are shown for three positions in one of the side-sills: over the bogie (A), in the carbody middle (C) and in between (B); see Figure 2-1.

The spectra are weighted to take ride comfort into account by applying (multiplying) the vertical comfort filter of Figure 2-12.

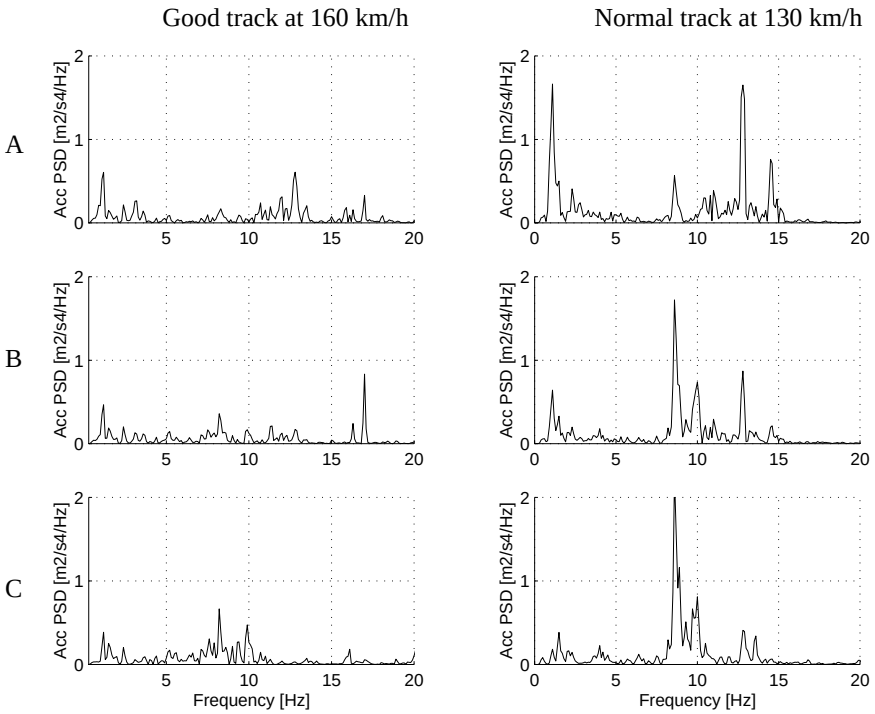

Figure 2-2 ***Comfort-weighted spectra of measured vertical carbody accelerations.***
Three locations in the side-sill, cf. Figure 2-1.
Left: good track, right: normal track.

The vibration spectral densities on the good and normal tracks differ not only in level, but also in shape; the peaks are different, though the repeatability of acceleration measurements performed on the same track is high. The peaks below 7 Hz belong essentially to rigid-body motion, whereas those above 7 Hz are due to carbody structural flexibility. In particular, the peak at 8.6 Hz corresponds to the first vertical bending mode and the peak at 12.8 Hz belongs to torsion while the peak at 17.2 Hz, excited only on the good track, corresponds to the second vertical bending mode. The ODS at these three frequencies are shown in Figure 2-3 to Figure 2-5. The shapes are based on measurements of vertical acceleration in 10 points of the side-sills, and essentially correspond to the floor of the carbody between the bogies. The four phases 0, 90, 180 and 270 degrees show that the shapes are not completely symmetric. The asymmetry may be due to asymmetrical mounting of exterior and interior equipment.

From the spectra in Figure 2-2, it may be seen that the first vertical bending mode and the torsion mode contribute considerably to the vertical acceleration level. They are, in this case, the two most important carbody modes from a ride comfort point of view.

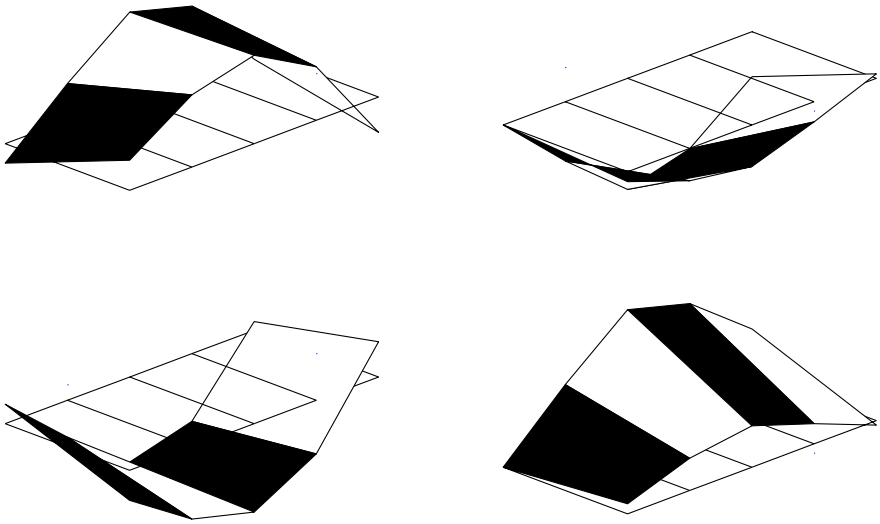

Figure 2-3 Measured operating-deflection-shape at 8.6 Hz (first vertical bending). *Four phases.*

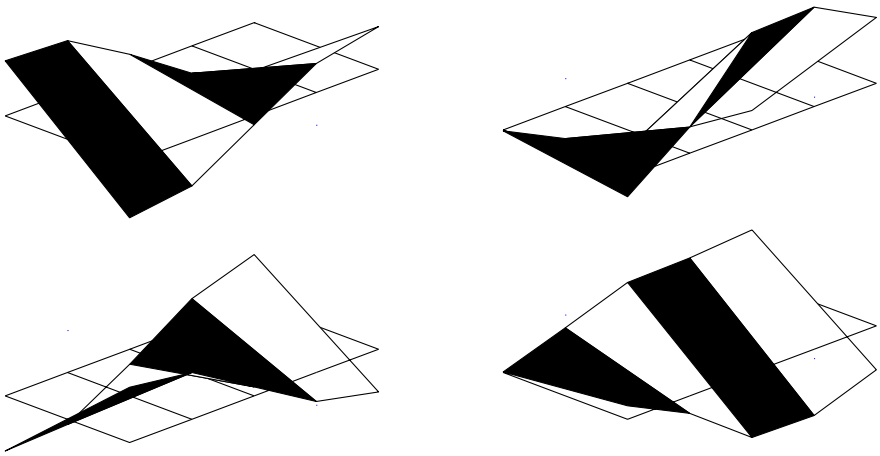

Figure 2-4 Measured operating deflection shape at 12.8 Hz (torsion). *Four phases.*

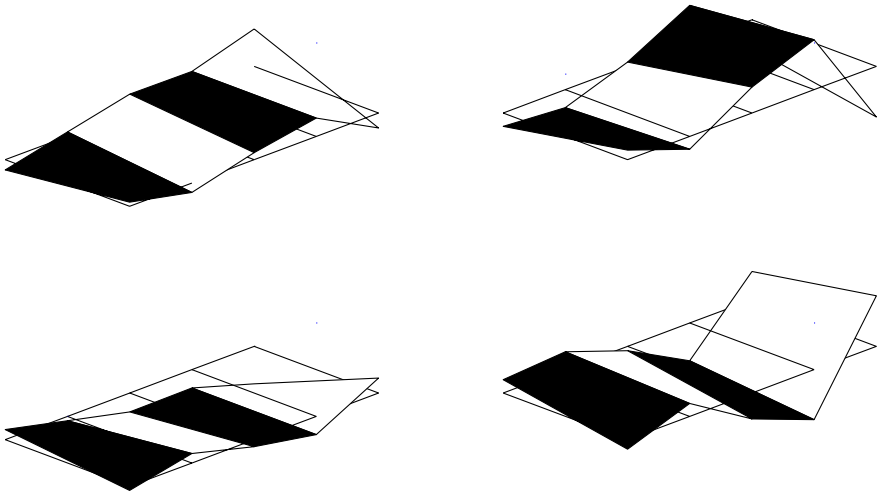

Figure 2-5 Measured operating-deflection-shape at 17.2 Hz (second vertical bending). *Four phases.*

2.1.2 Modelling and simulation

The bogie with its suspension and connections to the carbody influences, to a large extent, the vibrations transmitted from the track to the carbody, and, therefore, the models of bogies and track constitute important parts of the vehicle-track simulation model.

Figure 2-6 shows the design of the present bogies. The carbody rests, via two supports (yokes) and four coil-spring packages (two on each side), on a bolster beam. Between each bolster beam and the carbody, there are two traction rods, one on each side, that transmit longitudinal forces. Two vertical and two lateral dampers are also mounted between each bolster beam and the carbody.

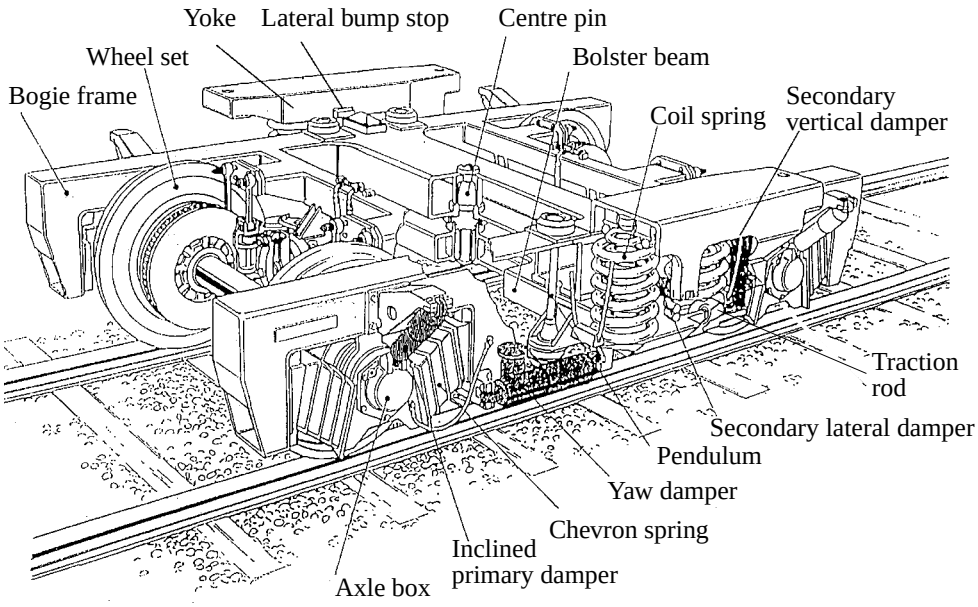

Figure 2-6 Bogie design [9].

Each bolster beam is attached to the bogie frame by one centre pin and four pendulums. This design allows yaw motions between carbody and bogie frame. Owing to flexibility in the centre pin and bolster beam a certain longitudinal motion between bogie frame and bolster beam is possible. The pendulums work, owing to the weight of the carbody, as a moderate yaw stiffness between bolster beam and bogie frame. Two yaw dampers are also mounted longitudinally to impede yaw motion between bogie frame and carbody. In the model, the yokes are considered to belong to the carbody.

The primary suspension of the bogies consists of rubber chevron springs, permitting radial self-steering, and inclined lateral/vertical hydraulic dampers.

A multibody model of the vehicle including carbody, suspension, bogies and track was set up using the commercial software GENSYS [27][59]. The vehicle is described as a system of rigid bodies interconnected via various suspension elements. The number of degrees of freedom is 54 excluding the flexible degrees-of-freedom. Non-linear characteristics of the suspension elements are taken into account. For instance, a model proposed by [10] is used for the rubber chevron springs. Another example is the yaw dampers, which are modelled as dampers with “force blow-off” and a series stiffness as illustrated in Figure 2-7. The series spring accounts for the reduced damping capability at higher frequencies.

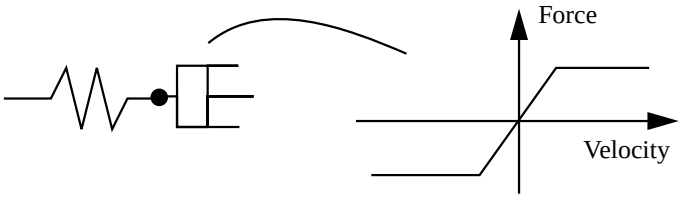

Figure 2-7 Model and characteristics of yaw dampers.

The contact mechanics between wheel and rail, see Figure 2-8, includes both creep forces, i.e. friction forces, and a non-linear wheel-rail contact geometry. The software GENSYS interpolates creep forces from a table that is previously calculated using Kalker's FASTSIM program [29]. The non-linear surface contact is modelled by so-called contact-geometry functions that describe, for instance, wheel rolling radius as a function of relative lateral displacement. Lateral track flexibility is modelled by means of a single-degree-of-freedom spring-damper-mass system, whereas vertical track flexibility is included in the wheel-rail contact modelling.

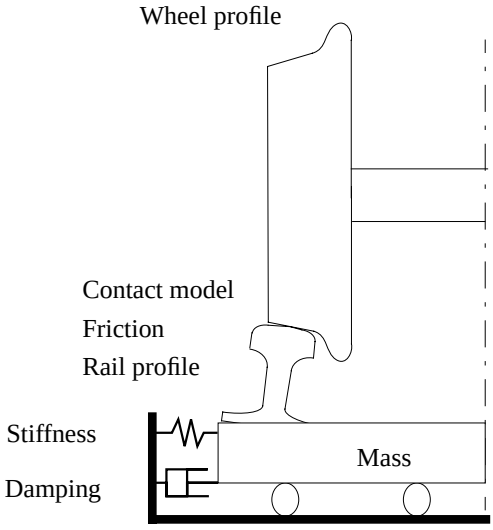

Figure 2-8 Wheel and track modelling.

The carbody is modelled by means of the commercial finite-element software ANSYS [62], giving a model with approximately 23,000 degrees of freedom. Orthotropic shell elements represent the corrugated plate. Non-structural masses, such as equipment and furniture, constitute about two thirds of the total mass.

The eight lowest free-body eigenmodes, disregarding the rigid-body modes, have undamped eigenfrequencies ranging from 9.1 Hz to 16.2 Hz according to the FE-calculations, see Figure 2-9 and Table 2-1. The mode shapes are typical for an oblong box (26.4 m x 3.4 m x 3.0 m), i.e. vertical and lateral bending shapes and torsion, as well as breathing modes.

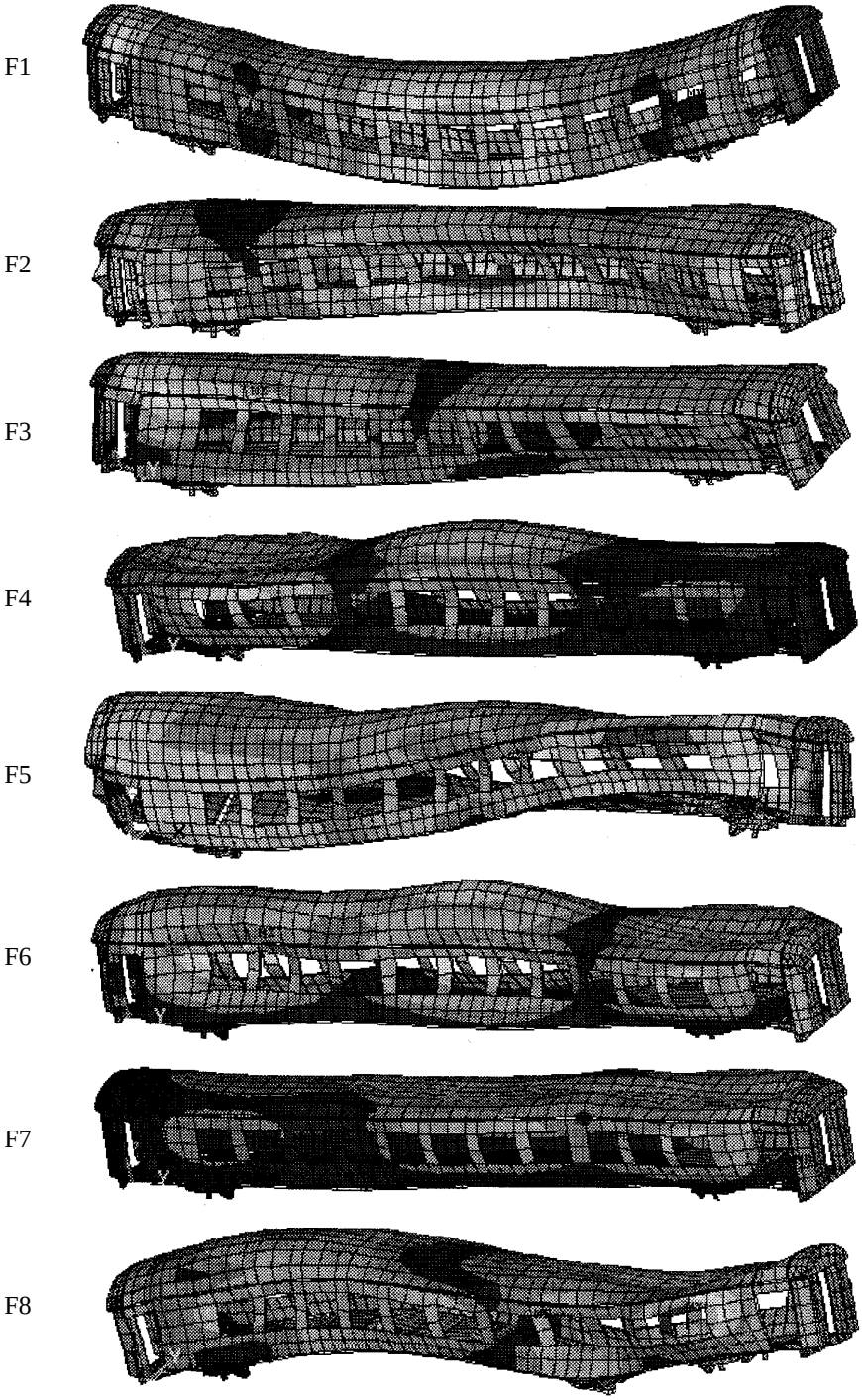

Figure 2-9 Eight carbody mode-shapes of the S4M vehicle calculated by FEM.

Table 2-1 Calculated mode shapes and undamped eigenfrequencies.

No.	Mode shape	Frequency [Hz]
F1	First vertical bending	9.1
F2	First lateral bending	12.2
F3	Torsion 1	12.8
F4	Breathing 1	13.4
F5	Torsion 2	13.9
F6	Breathing 2	14.3
F7	Breathing 3	15.0
F8	Second vertical bending	16.2

One may note that the first and second vertical bending modes are also excited at other frequencies on track, cf. Figure 2-2. This is quite normal, and is mainly due to the coupling to the bogies.

2.1.3 Comparison of results from measurement and simulation

The results from measurement and simulation can be compared in a number of ways. In the end, the simulation should reproduce the measured comfort values. Figure 2-10 shows measured and simulated comfort-weighted r.m.s.-values for the “tangent track in normal condition at 130 km/h”. The results are based on values from points in the side-sills. For the values “in carbody middle”, the average of two points is used: point C (cf. Figure 2-1) and the corresponding point in the other side-sill. For the values “over bogies”, the average of four points has been calculated, corresponding to A and the three other corresponding points.

White corresponds to the frequency interval from 0.3 to 7 Hz (essentially rigid-body vibration) and black corresponds to the frequency interval from 7 to 20 Hz (essentially structural flexibility vibration). As seen, structural flexibility is more important than rigid body motion in the vertical direction. This is to a large extent due to comfort-weighting in the vertical direction, see Figure 2-12. Structural flexibility is almost negligible in the lateral direction, also to a large extent depending on comfort-weighting.

In general, the agreement between simulated and measured values is quite good.

The cause for differences between simulated and measured results may be found by analysing the PSD. Such an analysis reveals that the measured distinct peak corresponding to torsion at 12.8 Hz is difficult to reproduce in the simulation. This is partly due to problems in modelling the carbody-bogie interface, e.g. dynamical properties of the vertical dampers at these frequencies. The carbody mode-shapes are also quite sensitive to the modelling of non-structural masses.

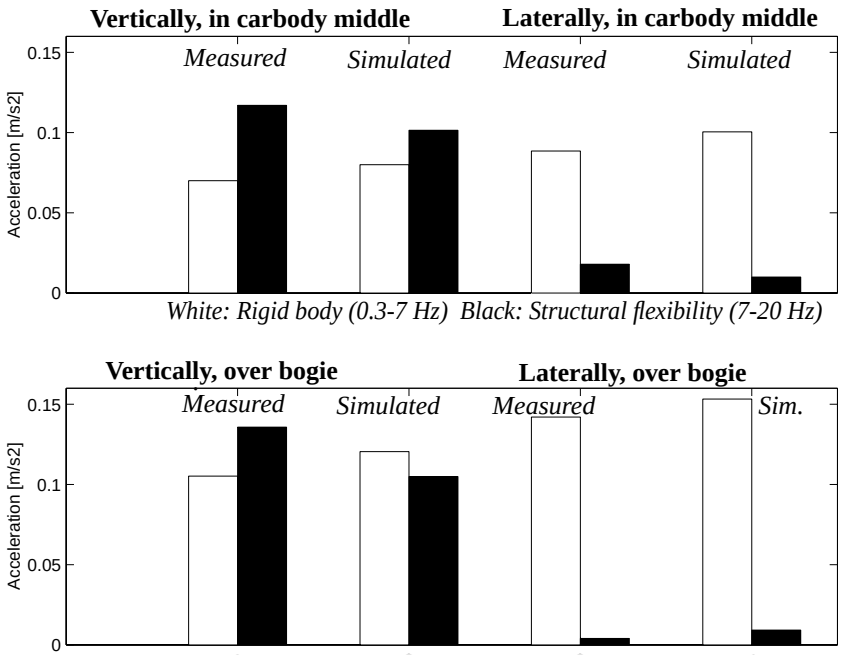

Figure 2-10 Measured and simulated comfort-weighted root mean square values. *White corresponds to rigid-body vibrations and black corresponds to structural-flexibility vibrations. Comfort filters according to Figure 2-12.*

2.2 Mode selection criteria

It is preferable to have models with a limited number of degrees-of-freedom in order to reduce computational time in a numerical simulation. Small models are also preferable, since they permit a better understanding of the essential system behaviour. It is important, however, not to miss the essential features when reducing a model. With the constant increase in computer capacity, finite element models tend to grow in size. Since the suitable model size for simulation is largely inferior to that of a finite-element model, there is a need for guidelines to accomplish the necessary model reduction [14][17].

Four consecutive criteria in selecting important carbody eigenmodes with respect to ride comfort are proposed to be used: modal participation factors (*MPF*), excitation spectra, modal contribution factors (*MCF*) and comfort filters. The concept of *MPF* is classical and found in many textbooks, e.g. [3]. *MCF*, which was introduced by the author in [15], is a natural parameter to describe the carbody dynamics from a ride comfort point of view. The present work puts this parameter in focus. The excitation spectra and the comfort filters may be seen as temporal counterparts of *MPF* and *MCF*, which are spatial quantities.

The *MPF* and *MCF* have been tested in the case study and implemented in GENSYS. In particular, the *MCF* seems to be a useful key parameter. It is easy to compute and is also closely related to the models of the passenger-carbody interaction proposed in this thesis.

2.2.1 Modal participation factors

In the case of a single excitation force, i.e. a force of the form $\boldsymbol{F}(t) = \alpha(t)\boldsymbol{R}$, it is customary, cf. for instance [3], to define a *MPF* as

$$MPF = \frac{\boldsymbol{n}_c^T \boldsymbol{R}}{\boldsymbol{n}_c^T \boldsymbol{M}_c \boldsymbol{n}_c} \tag{2-1}$$

where $\boldsymbol{R}$ is the force column-matrix excluding the time dependence, $\boldsymbol{n}_c$ is the mode-shape column-matrix and $\boldsymbol{M}_c$ is the finite-element-model mass-matrix. The subscript c refers to the carbody. A high value of *MPF* means that excitation of the mode shape $\boldsymbol{n}_c$ is sensitive to the force $\boldsymbol{F}$.

The carbody is excited by a number of independent sources, e.g. vertical and lateral track misalignment. It may therefore be justified to express the total force on the carbody as a sum of independent forces, each force having a specific spatial distribution

$$\boldsymbol{F}(t) = \alpha_1(t)\boldsymbol{R}_1 + \alpha_2(t)\boldsymbol{R}_2 + \alpha_3(t)\boldsymbol{R}_3 + \alpha_4(t)\boldsymbol{R}_4 + \ldots \tag{2-2}$$

For each such force, and mode, it is possible to define a modal participation factor

$$MPF_{ij} = \frac{\boldsymbol{n}_{cj}^T \boldsymbol{R}_i}{\boldsymbol{n}_{cj}^T \boldsymbol{M}_c \boldsymbol{n}_{cj}} \tag{2-3}$$

For instance, $\boldsymbol{R}_1$ may represent the simultaneous pushing of the traction rods towards the centre of the carbody. The quantity MPF_{1j} then tells how sensitive a mode shape $\boldsymbol{n}_{cj}$ is to this spatial force distribution. In a rail vehicle, the number of excitation sources and vibration paths are numerous, so the number of terms in (2-2) is high. Therefore, it is essential for both understanding and analysis to find the most important spatial distributions $\boldsymbol{R}_1$, $\boldsymbol{R}_2$ etc. An example of this application is found in [17].

Note that the *MPF* does not depend on the excitation-frequency content, only on the mode shape and positions and directions of applied forces. It is, therefore, a key parameter that describes spatial characteristics.

2.2.2 Excitation spectra

The actual track geometry results from a nominal, designed track to which track irregularities add. Vibrations in the carbody are mainly induced by these irregularities. It

is common to define these as shown in Figure 2-11: gauge irregularity, cant irregularity and lateral and vertical misalignment.

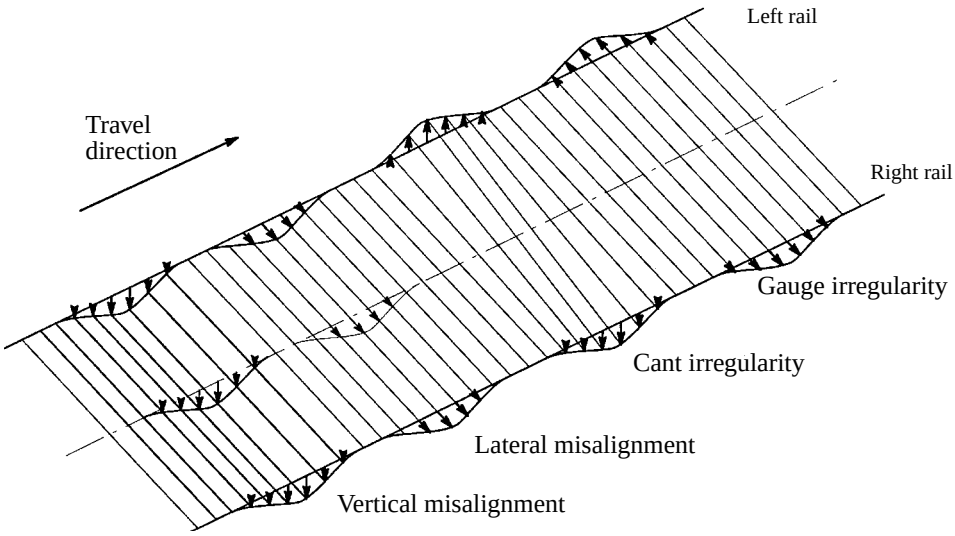

Figure 2-11 Definition of track irregularities.

In general, the amplitude of the track irregularities increases with increasing wavelength [8]. The high-frequency content of the excitation spectra therefore becomes more important as vehicle speed increases.

It is the track irregularities and the bogie characteristics that together determine the time-varying coefficients $\alpha_1(t)$, $\alpha_2(t)$ etc. in (2-2), and they may be determined by numerical simulation. However, it is possible to foresee some of the relations between the track irregularities and the excitation of the carbody mode-shapes. For instance, the excitation of torsion modes should be correlated with the cant irregularities of the track. And excitation of the vertical bending is often correlated with the bounce and pitch motion of the bogies induced by the vertical misalignment of the track.

The eigenfrequencies of the mode shapes certainly play an important role. Excitation at resonance frequencies should be avoided.

2.2.3 Modal contribution factors

It may be advocated that vibrations are important only if they are perceived by passengers. Under this assumption, deformations and vibrations are important only where passengers are seated. Having this in mind, it is possible to calculate a *spatial average* of the mode-shape values over the part of the carbody in which passengers are seated. Since comfort-weighted r.m.s.-values often are used as ride-comfort indices, it is convenient to use r.m.s.-values here also:

$$MCF_j = \sqrt{\sum_{i=1}^{N} d_{ij}^2 / N} \tag{2-4}$$

where MCF_j stands for Modal Contribution Factor of carbody mode number j. Here N "important locations" in the carbody are used. The vertical displacement of mode number j at a point numbered i is denoted by d_{ij}. *MCF* for lateral and longitudinal directions can also be defined. The parameter *MCF* was introduced by the author in [15]. Values from the case study corresponding to the shapes in Figure 2-9 are given in Table 2-2. The modes are supposed to be scaled to have a modal mass of 1 kgm^2.

Table 2-2 ***Calculated values of vertical MCF****. From [13]. Calculated by FEM using ten points in the side-sills.* $[mm]$ *(N=10).*

F1	F2	F3	F4	F5	F6	F7	F8
4.8	0.7	1.6	2.0	6.6	2.5	2.4	4.5

Thus, carbody mode F1 (first vertical bending), F5 (torsion) and F8 (second vertical bending) are the most important from a ride comfort point of view. This is in agreement with the PSD presented in Figure 2-2.

Note that the *MCF* does not depend on the frequency content, only on the mode shape and "important locations"; it is thus a key parameter that describes relevant spatial characteristics.

2.2.4 Comfort filters

In order to evaluate ride comfort, a number of methods have been worked out. Many are based on weighting functions describing human sensitivity vibrations. The weighting functions, see Figure 2-12, are multiplied with the Fourier-transformed acceleration signals to obtain comfort-weighted PSD.

According to present standards, humans are mainly sensitive to vertical vibrations in the interval of 5 to 15 Hz. The sensitivity reaches a maximum at 8 Hz, approximately. Human beings are sensitive to lateral vibrations in the interval of 1 to 2 Hz.

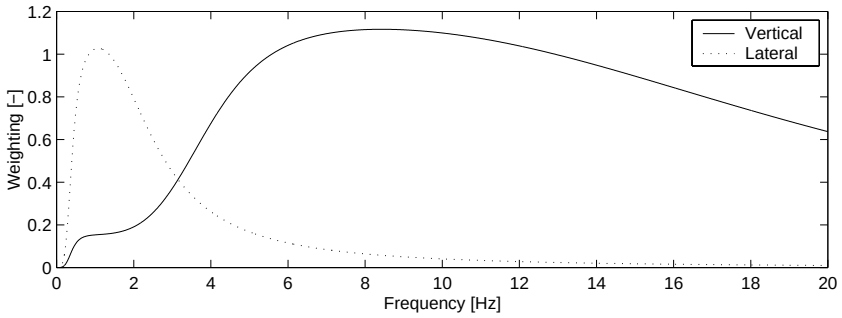

Figure 2-12 ISO-2631 comfort-weighting functions [57].

3 Measurements of passenger-carbody interaction

Measurements of passenger-carbody interaction were performed at the SJ depot in Hagalund during two weeks in the spring of 1999. The measurements consisted of experimental modal analysis of the SJ-B7M vehicle, shown in Figure 3-1. This vehicle is similar to the SJ-S4M vehicle, which had previously been studied [13], cf. Chapter 2. In order to investigate the passenger-carbody interaction, the vehicle was loaded with passengers during one afternoon.

Although the main aim was to study this interaction, other things were investigated as well during the two weeks, in particular the dependence on excitation amplitude. The results of the experimental modal analysis (EMA) were also to be compared to the previous operating-deflection-shape measurements and the finite-element modelling of the SJ-S4M vehicle. It was also of interest to measure the damping of the different mode-shapes. The effort was concentrated on the modes that had proved to be important in [13], namely the first vertical bending mode and the torsion modes. Additionally, seat-transmissibility measurements were taken in order to provide data for setting up a passenger-seat model.

The measurement conditions are described in Section 3.1. The results are presented and discussed in Section 3.2 and conclusions are stated in Section 3.3.

3.1 Measurement conditions

3.1.1 Setup, excitation and response

Valuable advice on how to set up the carbody for measurements was found in [2] and [28]. Ideally, the structure to be excited should be free. Therefore, all secondary suspension components except the vertical springs were dismounted: yaw dampers, vertical and lateral dampers and traction rods, cf. Figure 2-6. Distance blocks were inserted in the primary suspension to impede motion in the rubber chevron springs. Brakes were loosened. Next, the exciter was put into place, see Figure 3-1, where its location is indicated..

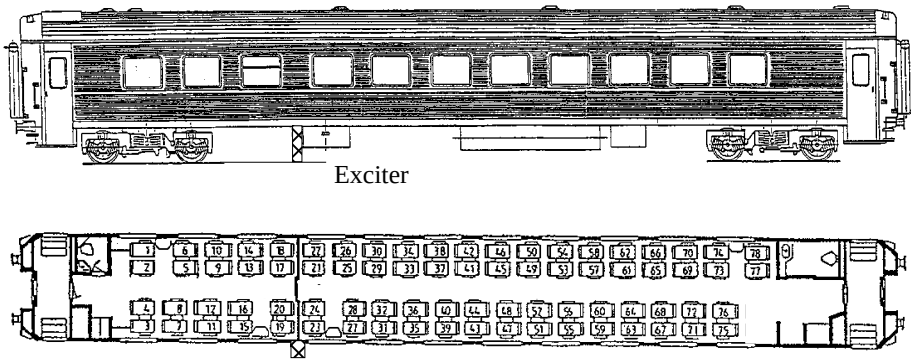

Figure 3-1 SJ-B7M vehicle and location of the vertical exciter.

The location of the exciter was selected so as to excite both the first vertical bending mode and the torsion modes, as well as other vertical modes. The exciter was fastened with bolts both to the ground and to one of the carbody side-sills, i.e. the two beams along the junction of floor and side walls, via a swivel connection to avoid moment excitation. A hydraulic shaker was used, see Table 3-1, where the measurement equipment is listed, and Figure 3-2, where the measurement setup is shown.

Table 3-1 Measurement equipment.

Item	Make
Exciter	MTS 242.03 Hydraulic Actuator
Controller	MTS 458.20 Microconsole
Pump	G.W. Hydraulic
Load sensor	Load Indicator AB, Type AB-50 - 4pole
15 accelerometers	BK 4398
Seat accelerometer	BK 4322
Amplifier	BK 2635 Charge Amplifier
FFT-analyser	HP VXI E1421B, E1432A, E1434A
Software	IDEAS-Test

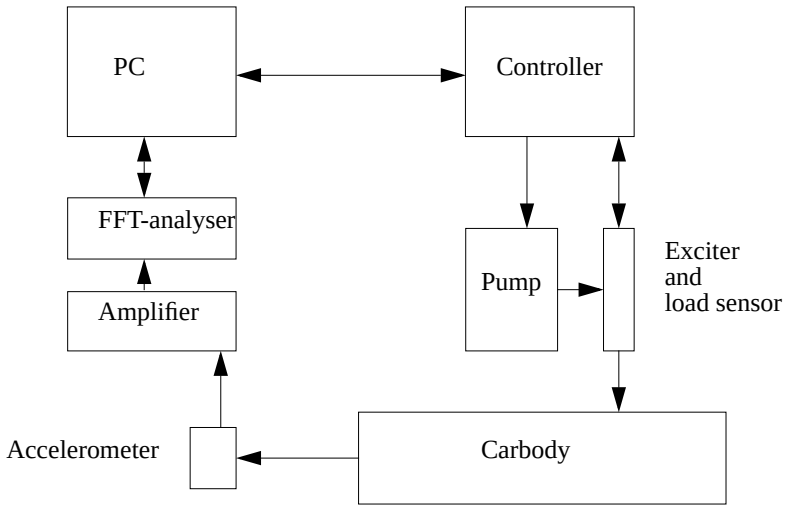

Figure 3-2 Measurement setup. *Principle.*

The hydraulic exciter needed a pump, and the system was controlled by the MTS 458.20 Microconsole. The signal from the load sensor mounted between the exciter and the swivel was used for feed-back control. The IDEAS-Test system together with an HP VXI FFT-analyser was used for monitoring the experiments.

The best excitation and sample combination was chosen among the possible ones allowed by the monitoring system. Random excitation was preferred not only because it gave shorter measuring times, but also because all frequencies are then measured simultaneously, avoiding the risk that passengers' moving around might disturb the measurements. Frequencies between 0.5 Hz and at least 20 Hz were to be measured, and, considering the anticipated half-width value of the frequency-response-function peaks, a frequency resolution of 0.05 Hz was judged sufficient. The form of force spectrum would not have to be "realistic", rather a dominance of higher frequencies is preferable in order to minimize the excitation of rigid-body modes, for safety reasons. Almost white-noise force-spectrum from 0.5 Hz to 39 Hz and a frequency resolution of 0.0488 Hz was used. The total time for one measurement is then approximately 10 minutes, using 25 to 30 time-frames for averaging purposes.

In order to investigate amplitude-dependency, four different excitation -amplitude levels were used, as summarized in Table 3-2. The levels were chosen to range from "better than good track" to "worse than bad track". The force level labelled "50%" corresponds to a vehicle running on main-line track, although the high frequency content is higher than normal.

Table 3-2 Excitation amplitudes*. Approximate force r.m.s.-levels.*

Level	Force [kN]
"100%"	1.6
"50%"	0.8
"25%"	0.4
"12.5%"	0.2

Fifteen channels were available for measuring the response. The BK 4398 accelerometers from the on-track measurements [13] were used. No amplifiers were used for these accelerometers, however. A seat accelerometer, BK 4322, was used together with a BK 2635 charge amplifier.

In order to be able to compare the measurement results with the previous on-track measurements, the same 10 vertical accelerometer positions in the side-sills were chosen, cf. Figure 3-3. These 10 positions allow to identify first and second vertical bending modes, as well as torsional modes.

The interest being focused closer to the passengers this time, 14 accelerometer positions were also chosen inside, on the inner floor, close to the feet of the seats, cf. Figure 3-3 and also Figure 3-5.

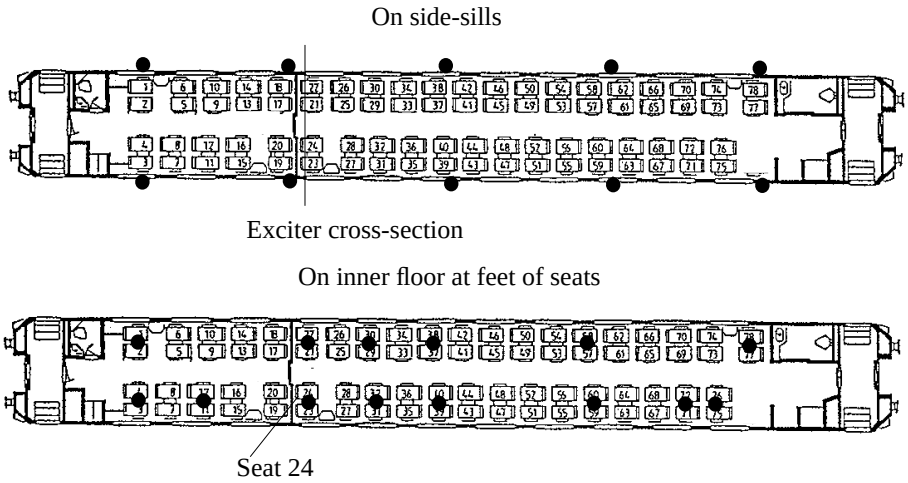

Figure 3-3 Accelerometer positions*. Ten in the side-sills and 14 on the inner floor.*

The behaviour of a carbody cross-section was investigated by putting 12 accelerometers in the cross-section of the exciter. Accelerometers were put both inside and outside, as shown in Figure 3-4. Some of the points correspond to those shown in Figure 3-5. Special measurements were also performed on one of the seats (number 24, indicated in Figure 3-3) with a passenger seated. The seat accelerometer BK 4322 was used to measure the acceleration at the seat pan, indicated in the figures by the letter *S*. One accelerometer was glued to the wooden plate, letter *W*. Accelerometers were also put on the consoles on which the wooden plate is mounted, i.e. position *C*.

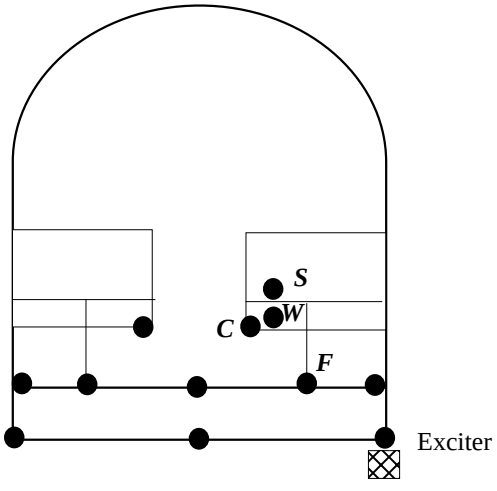

Figure 3-4 Accelerometer positions in the exciter cross-section. *Four points are indicated by letters*: *(F) floor, (C) console, (W) wooden plate of seat pan and (S) seat pan. See also Figure 3-5.*

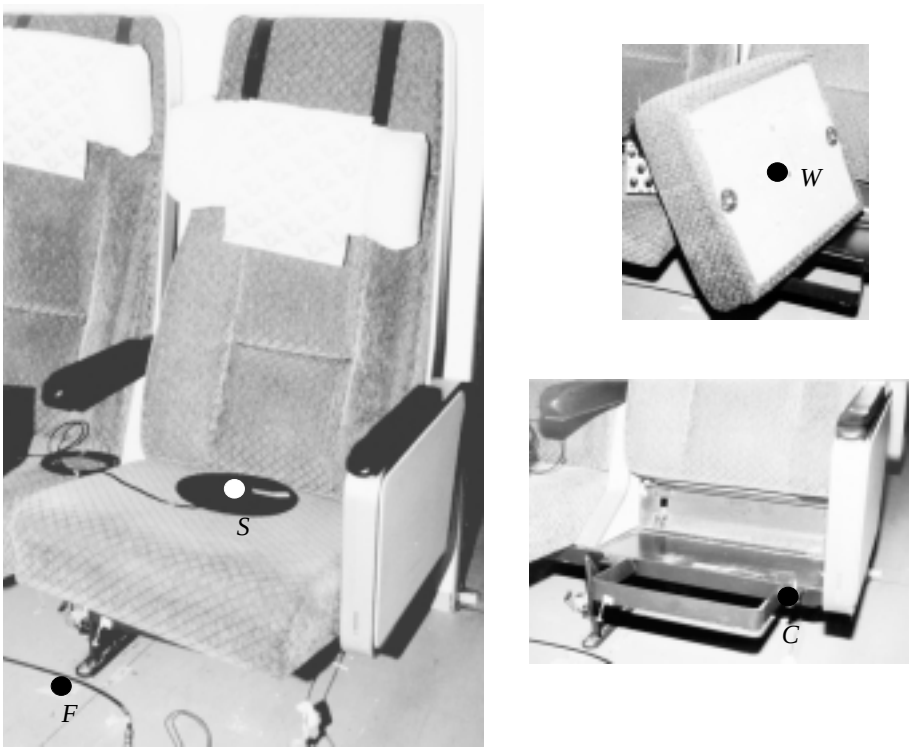

Figure 3-5 ***Four accelerometer positions on seat 24****. (F) floor, (C) console, (W) wooden plate of seat pan and (S) seat pan, which is dismounted in the figures to the right.*

3.1.2 Passengers

For three hours one afternoon, 35 persons, mainly students, came to act as passengers. The participants were asked about their weight, and the average was 66 kg with values ranging from 52 kg to 80 kg. The number of persons was chosen to make it possible to try different “passenger distributions”, with the aim of investigating the role of the “passenger load parameter”, cf. Section 5.1 and Appendix B, where important definitions are collected.

In order to calculate the sum in equation (B-8), each occupied seat must be assigned a passenger mass and a carbody deformation-shape-value, one for each mode. The inner floor positions in Figure 3-3 are used for this purpose. For each seat, the closest measurement point is used, and therefore the “passenger mass” is lumped and a mass is associated with each of the 14 accelerometer positions in Figure 3-3. The sum is then made of all accelerometer positions.

Two different passenger distributions were chosen: “Middle” with all passengers sitting as close to the middle as possible and “Ends” with the passengers sitting as close to the

carbody ends as possible. The “Middle” distribution was assumed to affect the first vertical bending mode the most, while the “Ends” distribution would affect the torsion modes. In Figure 3-6, the result of the passenger-mass lumping is shown for the two distributions. Unfortunately, there were only 33 passengers in the “Middle” distribution.

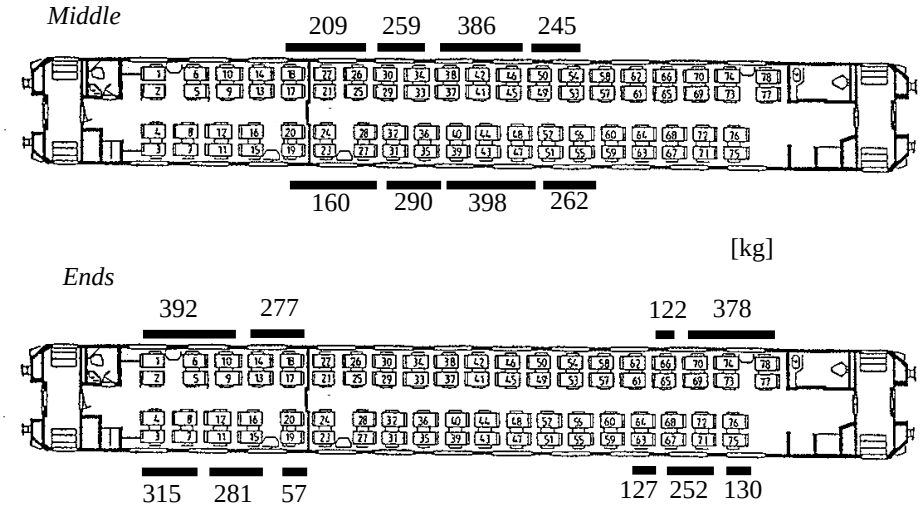

Figure 3-6 Passenger distributions “Middle” and “Ends”*. Lumped passenger masses.*

3.1.3 Measurement plan

The measurement plan set up before the measurements was followed roughly. Setting up the carbody, the exciter and the monitoring system took four days. Actual measurements were performed during five days, and bringing down the setup took half a day. Table 3-3 summarizes the measurements made during the five measurement days. In the column to the far left, the accelerometer configuration is described. Measurements were repeated to ensure repeatability.

Table 3-3 Measurements performed. *Number of repeated measurements.*

Accelerometer configuration	Excitation amplitude			
	“100%”	“50%”	“25%”	“12.5%”
Side sills and one seat (seat 24)	3	5	5	2
with passengers in the middle		2	1	
with passengers at the ends		2	2	
Inner floor	1	1	1	1
Exciter cross-section	3	2		1
with one passenger in seat 24	2	2		2

3.2 Results

3.2.1 Modal parameters and modal shapes, amplitude dependence

Autospectra of the exciting force and response accelerations, accelerance[1] functions and coherence functions were stored by the IDEAS-Test system.

A number of carbody modes can be identified: rigid-body modes and global-deformation modes as well as more local-deformation modes. A number of modes, in particular lateral bending modes and breathing modes cannot be identified by the present excitation and response-point setup. However, the modes on which the study focuses are identified. These are the global-deformation modes, labelled “G1” to “G5”. The identified modes shapes are listed in Table 3-4. Two rigid-body modes are identified, labelled “R1” and “R2”. Five local-deformation modes numbered “L1” to “L5” are identified in the exciter cross-section.

Eigenfrequency and relative damping vary with excitation amplitude, here, in Table 3-4, amplitude “50%” is shown as an example. The modal parameters are obtained using either the circle-fit method or the complex exponential method, see for instance [2]. The point-accelerance measurements are used. In some cases, the estimation of relative damping proved to be sensitive to the estimation method.

Table 3-4 Modal parameters of identified modes. *Amplitude,“50%”.*

No	Shape	Undamped eigenfrequency [Hz]	Relative damping [%]
R1	Bounce	1.2	2.4
R2	Roll	1.5	2.6
G1	Shear of cross-section	8.1	3.7
G2	First vertical bending	9.2	1.6
G3	Torsion 1	12.5	1.5
G4	Torsion 2	13.5	4.4
G5	Second vertical bending	18.2	3.4
L1	Bending of cross-section	20.8	5.0
L2	Bending of cross-section	24.2	2.4
L3	Bending of cross-section	30.5	3.7
L4	Bending of inner floor	33.7	3.7
L5	Local mode of seat 24	36.9	4.8

1. Definitions are found in Appendix B.

The five global modes shapes are shown in Figure 3-7.

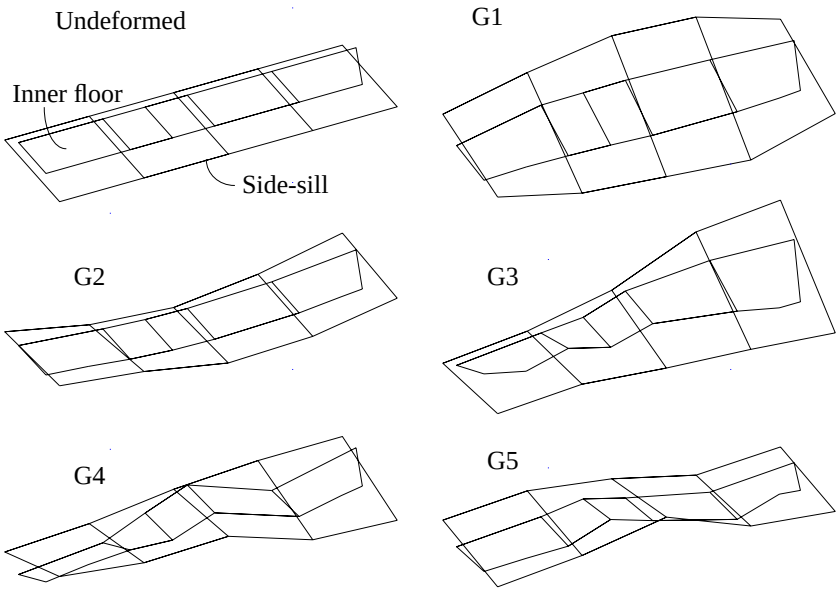

Figure 3-7 Modal shapes of five identified global modes. *Amplitude, "50%".*

The global mode shapes were obtained using the circle-fit method.

Examining the mode shapes in Figure 3-7, one finds that the two torsion modes G3 and G4 are not pure. The side-sills deform as in torsion, but the inner floor presents a more complex deformation. One explanation might be the inner wall in the exciter cross-section, cf. Figure 3-3, that would block parts of the inner floor. The mode shapes presented in Figure 3-7 are real, i.e. all parts of the carbody move in phase. But, if complex modes (that is when parts of the carbody move out-of-phase) are allowed in the modal model, then the torsion modes G3 and G4 are "more complex" than the other modes.

The shapes of Figure 3-7 may be compared with the operating deflection shapes and calculated finite-element mode-shapes in [13], cf. Chapter 2. Such a comparison in terms of eigenfrequency and peaks in spectra is presented in Table 3-5.

The results for the first vertical bending mode show good agreement. The coupling between carbody and bogies explains the fact that there are several peaks in the PSD. The first lateral bending mode and the breathing modes are not identified in the EMA owing to the choice of excitation and response points. The results for the torsion modes still show relatively good agreement, while the agreement for the second vertical bending is reasonable.

Table 3-5 ***Comparison between EMA and FEM (undamped) eigenfrequencies and ODS/PSD peaks [Hz].*** *FEM and ODS/PSD data from [13], cf. Chapter 2.*

Shape	EMA Eigenfrequency	FEM Eigenfrequency	ODS/PSD Peaks in spectra
Shear of cross-section	8.1		
First vertical bending	9.2	9.1	8.6, 9.3, 10.0
First lateral bending		12.2	10.0, 11.5, 12.0
Torsion 1	12.5	12.8	11.5, 12.8, 14.5
Torsion 2	13.5	13.9	
Breathing 1		13.4	
Breathing 2		14.3	
Breathing 3		15.0	
Second vertical bending	18.2	16.2	16.4, 17.2

It must be kept in mind that, firstly, the ODS and EMA correspond to somewhat different vehicles, and, secondly, that FEM results correspond to a free carbody while EMA results correspond to a carbody resting on vertical springs and that ODS/PSD results correspond to the carbody vibration of a running vehicle. No shear mode was discovered in [13]. Perhaps it was not excited on-track, but there ought to be one in the FEM results. Although it is not obvious from Figure 3-7 that G1 really is a shear mode, it nonetheless seems to be the case: firstly, a shear deformation of the inner-wall at the exciter cross-section was observed during the EMA measurements, and, secondly, it can be seen in Figure 3-7 that the deformation is larger in the middle of the carbody showing that the mode is not a rigid body mode.

Figure 3-8 illustrates the amplitude dependence of the undamped eigenfrequency and relative damping of the five modes G1 to G5. The accelerance of point F has been used for estimation.

The relative damping depends clearly on the excitation amplitude. As an example the increase in excitation amplitude from “25%” (corresponding to a good track) to “50%” (a normal track) results in an increase of relative damping of 1.0% for the mode G4 (from 2.2% to 3.2%). The vertical bending mode G2 is not significantly sensitive to excitation amplitude. The changes are comparable with those that are due to passenger loading, which are discussed in the Section 3.2.2.

Looking at Figure 3-8, one can see that the relative damping tends to increase with increased excitation-amplitude, in particular for modes G1 and G4. The eigenfrequency, on the other hand, decreases for increasing excitation amplitudes.

This may be explained by Coulomb friction, meaning that carbody surfaces stick to each other at low excitation amplitudes, whereas they release at higher excitation-amplitudes, thereby allowing frictional work and thus increased damping. This mechanism also gives lower stiffness at higher excitation-amplitudes, and, consequently, lower eigenfrequency at higher excitation-amplitudes.

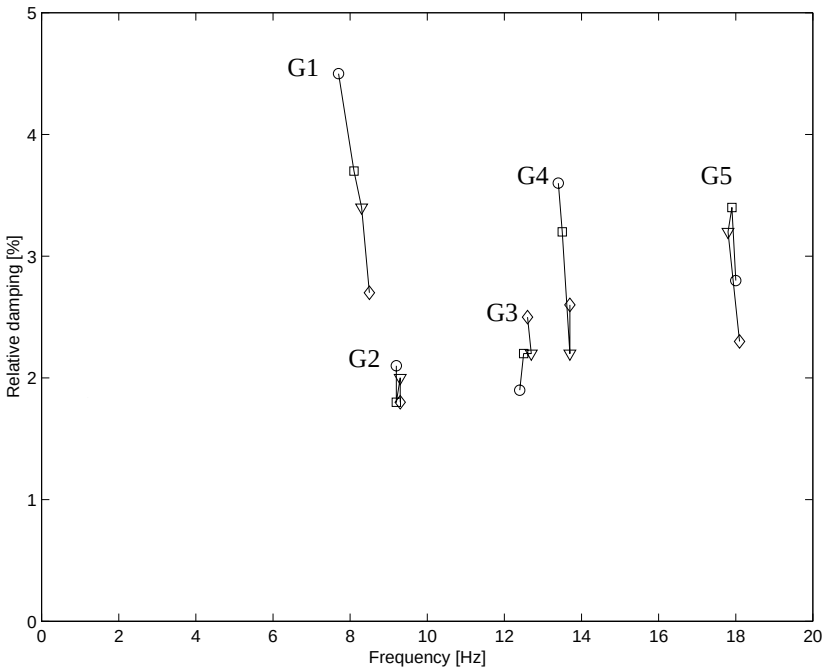

Figure 3-8 ***Undamped eigenfrequency and relative damping of global deformation modes as a function of the excitation-amplitude.*** *Based on response of point F. Circle: "100%" excitation, square: "50%", triangle: "25%" and diamond: "12.5%".*

3.2.2 Passenger-carbody interaction

From the measured response functions it is already obvious that passengers interact with the carbody dynamics, see Figure 3-9, where the point accelerance is shown. The point accelerance is defined as the frequency-response function "acceleration to force" at the excitation point. See the definition in Appendix B.1. Curves corresponding to no passengers as well as passenger distributions "Middle" and "Ends", here at the excitation amplitude of "50%", are shown.

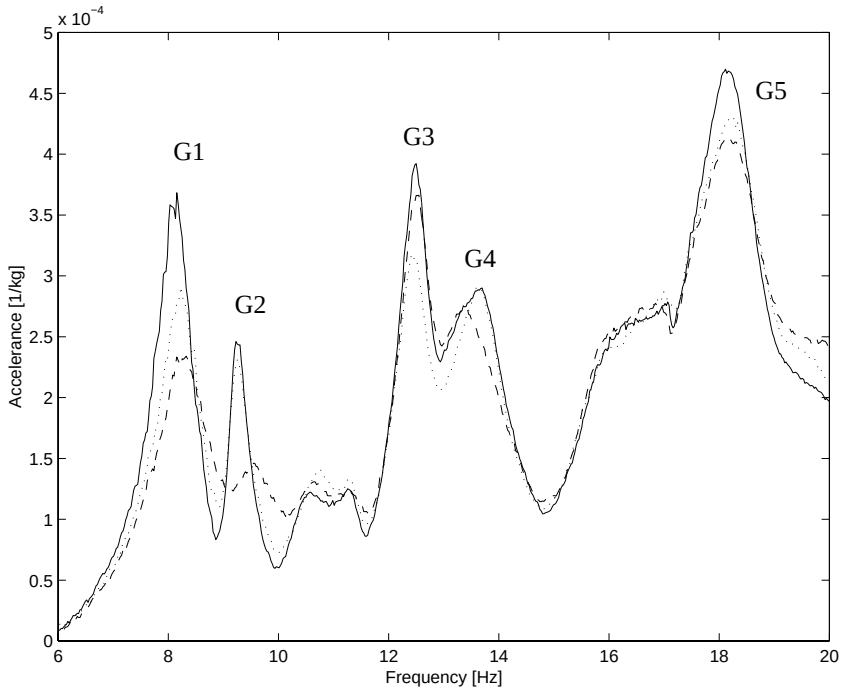

Figure 3-9 ***Measured point-accelerance (magnitude).*** *Amplitude "50%". Solid line: no passengers, dotted line: passenger distribution "Ends" and dashed line: passenger distribution "Middle".*

All five global deformation modes interact, more or less, with the passengers. Mode G2, the first vertical bending, with distribution "Middle", shows the strongest interaction.

A note on the use and interpretation of the measured point-accelerance in Figure 3-9 may be appropriate here. The modal parameters and mode shapes are estimated from the measured frequency-response functions by various curve-fitting methods.

In general, there is a rather large amount of freedom in how to perform the curve-fitting, e.g. which modes to include. Here, the complex exponential method, applied over the same frequency interval in all three cases, is used to estimate the undamped eigenfrequencies and relative damping. It was judged important to use the same frequency interval, the same method and the same response point for all passenger distributions, in order to obtain comparable results.

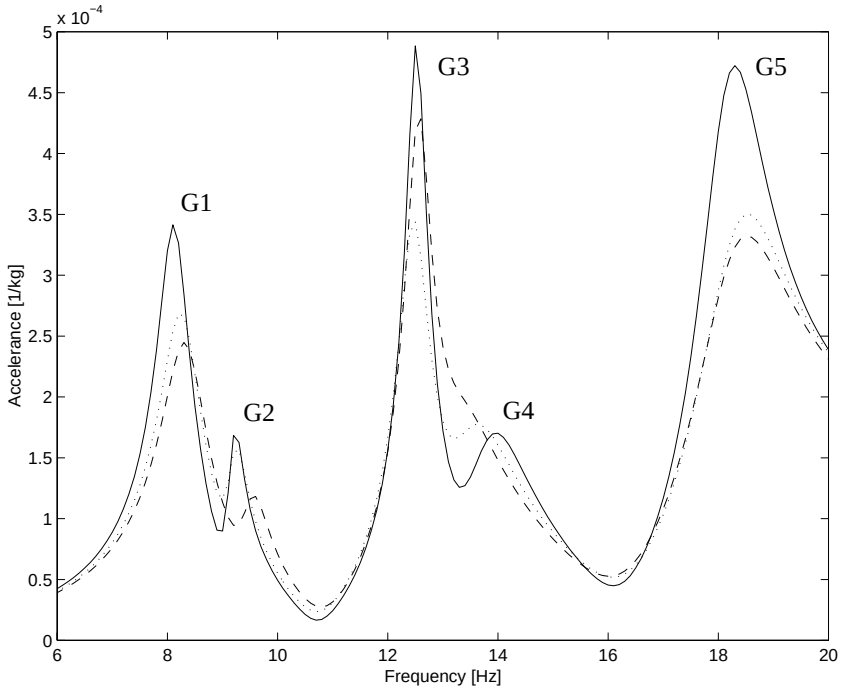

***Figure 3-10 Synthesized point accelerance (magnitude)**. Amplitude "50%". To be compared with Figure 3-9. Solid line: no passengers, dotted line: passenger distribution "Ends" and dashed line: passenger distribution "Middle"*

Figure 3-10 shows the present synthesized point-accelerance. The synthesized point-accelerance is calculated from the experimentally determined modal parameters and mode-shapes; it is synthesized.

All the features in the curves are not reproduced by the synthesized modal carbody model; only five global modes are retained here.

A comparison between the measured and synthesized point-accelerance reveals how faithful the estimated modal model is. For the sake of comparison, the measured and synthesized point-accelerance are shown in Figure 3-11, for the case of the empty carbody.

There are clear differences between the curves. The plateau at 16-17 Hz is not reproduced in the synthesized point-accelerance, for instance. Moreover, the two peaks between 10 Hz and 12 Hz correspond to modes that are not taken into account in this study. They might correspond to lateral modes, or breathing modes, but the present choice of accelerometer positions does not allow their being identified.

.

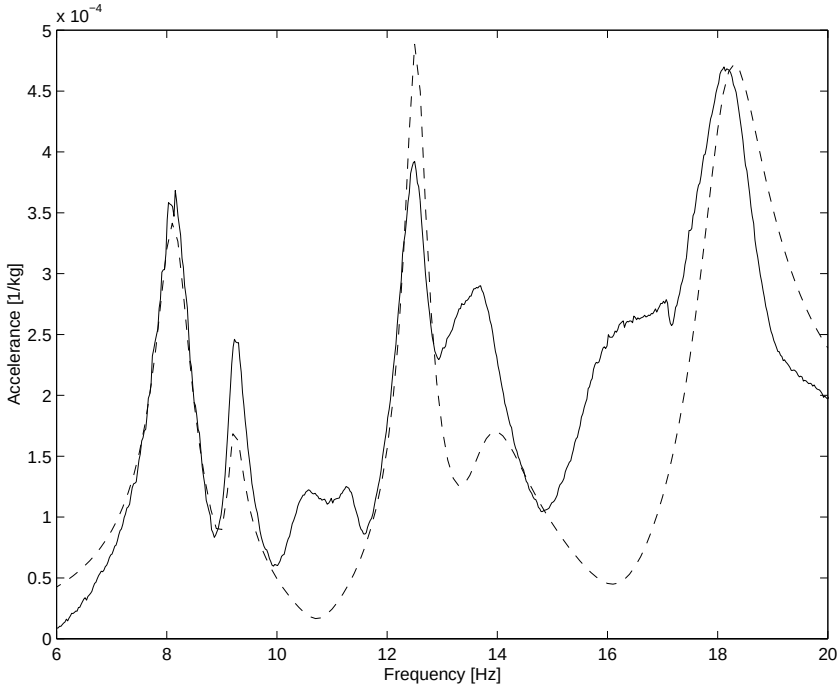

Figure 3-11 Comparison of measured (solid line) and synthesized (dashed line) point-accelerance for the empty carbody.

Looking closer at the peak G4 of the measured accelerance, one may notice that it seems to be composed of two peaks, indicating the difficulties in obtaining reliable relative damping estimates. A comparison to the corresponding synthesized peak suggests that this has led to the relative damping of mode G4 being overestimated.

The comparison between the measured and synthesized point accelerance thus shows that the relative damping seems to be overestimated for some modes, but also underestimated for other modes. It must be stressed that the estimates depend, to a relatively large extent, on the method of estimation, on how frequency intervals are chosen and on which response point is used etc.

The results of Figure 3-8 are based on another response point, namely *F*, which explains why results differ somewhat. In Figure 3-12, the accelerance of point *F* is shown. Damping and eigenfrequency estimates based on this function are somewhat different from those based on the point accelerance. In particular, there is no problem with the G4 peak.

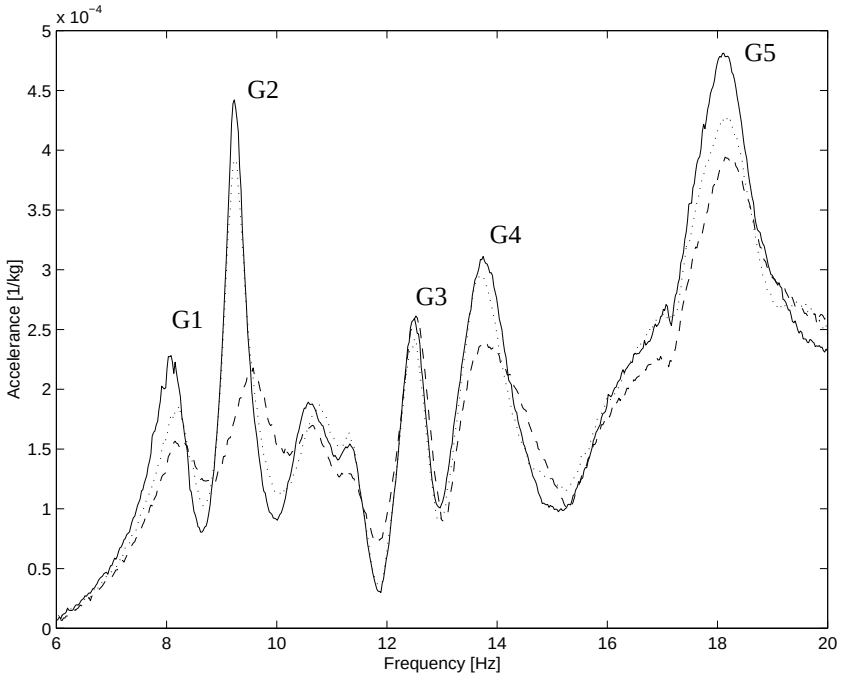

Figure 3-12 ***Measured accelerance of point F (magnitude).*** *Amplitude "50%". Solid line: no passengers, dotted line: passenger distribution "Ends" and dashed line: passenger distribution "Middle".*

The interaction between passengers and carbody can be measured by a "passenger load parameter" *P.* For each mode, this number can be calculated using the passengers' mass and the vertical mode-shape-values at the location of the passengers. For a more detailed description, see the definition in Section 5.1.2 and Appendix B.1. Here the 14 points on the inner floor shown in Figure 3-3 are used together with the passenger distributions in Figure 3-6. The mode-shapes are shown to depend on the excitation amplitude somewhat, and therefore the calculated values of *P* in Table 3-6 are given for two different excitation amplitudes.

Table 3-6 ***Values of P [kgm^2].*** *Based on measured mode shapes without passengers. Amplitude, "50%" and "25%", respectively.*

Amplitude	Passenger distribution	G1	G2	G3	G4	G5
50%	Middle	0.044	0.092	0.038	0.118	0.135
	Ends	0.022	0.024	0.075	0.076	0.052
25%	Middle	0.043	0.080	0.030	0.106	0.219
	Ends	0.021	0.016	0.088	0.066	0.054

The parameter *P* is motivated from a modelling standpoint, since it turns up as a parameter in simple interaction models. Unfortunately, the value of *P* can be hard to obtain with accuracy. *P* is proportional to the passengers' mass but proportional to the square of the deformation shapes values, and these depend, to some extent, on the interpretation and use of the frequency response functions. The difference in values of *P* obtained for the two excitation amplitudes is, to some extent, due to such difficulties. The *P*-values obtained in Table 3-6 for the torsion modes, G3 and G4, for the passenger distribution "Middle" are surprisingly high. This is partly due to the fact that the inner floor does not deform purely. Perhaps fourteen points are not enough to describe the deformation of the inner floor. Nonetheless, the values obtained here for *P* correspond agreeably with the values of *MCF* calculated in [13] with some exceptions. The relation between *P* and *MCF* will be discussed in Chapter 5.

In Figure 3-13, the measured eigenfrequency and relative damping of modes G1 to G5 are plotted as a function of the passenger load parameter *P* in the "50%" case. The values are estimated from the point accelerance curve shown in Figure 3-9.

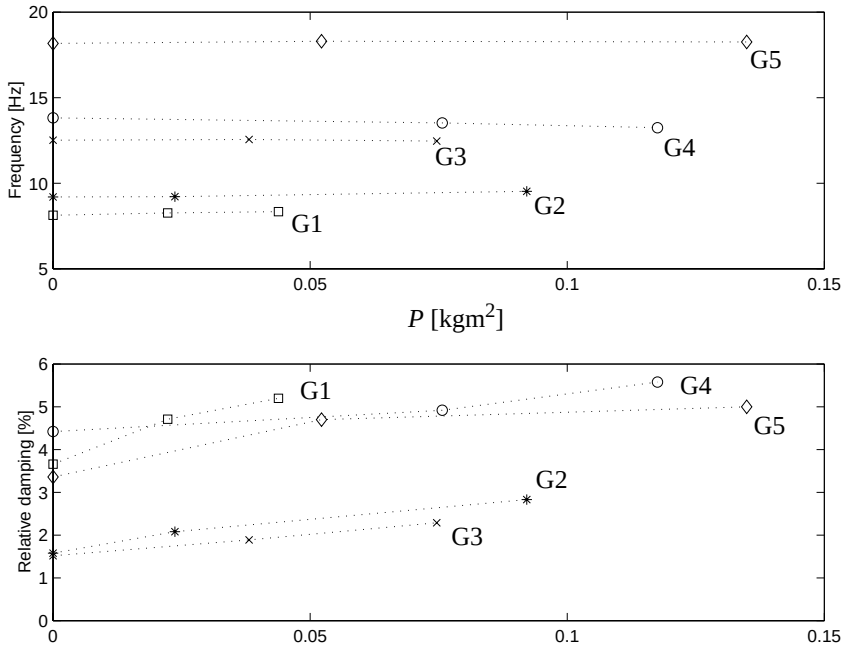

Figure 3-13 Measured undamped eigenfrequency and relative damping as a function of the passenger load parameter P for the modes G1 to G5. *Based on measured point accelerance, cf. Figure 3-9. Amplitude, "50%".*

One of the main trends found in the figure is an almost linear increase in relative damping as *P* increases. The relative damping increases significantly owing to passenger loading for most modes. For example, the relative damping of the first vertical bending mode G2 increases from 1.6% to 2.8% when the carbody is loaded half full with passengers, passenger distribution "Middle". It is likely to increase even more for a full vehicle. One may note that the two modes with the lowest eigenfrequencies, G1 and G2, interact the most with the passengers.

The eigenfrequency of the modes increases (G1, G2 and G5) or decreases (G3, G4) almost linearly with passenger load. The change in eigenfrequency is easier to evaluate from the frequency response functions than the relative damping is, but the changes are smaller.

For the amplitude of “25%”, similar results are obtained, although the trends are less clear.

An alternative view is given in Section 6.1, in connection with the comparison with model results, where root loci are shown.

3.2.3 Seat transmissibility

The vertical accelerances of the positions *S* and *F*, see Figure 3-5, can be used to calculate the seat transmissibility, i.e. the frequency response function between the acceleration on top of the seat pan (*S*) and the floor (*F*), where the acceleration at the floor is considered as input. A more detailed definition is given in Section 4.2.1 and Appendix B.1.

In Figure 3-14, the accelerance for points *S* and *F* are shown as well as seat transmissibility. A passenger weighing 80 kg was sitting on the seat. The excitation amplitude is “100%”. This high amplitude gave the best coherence.

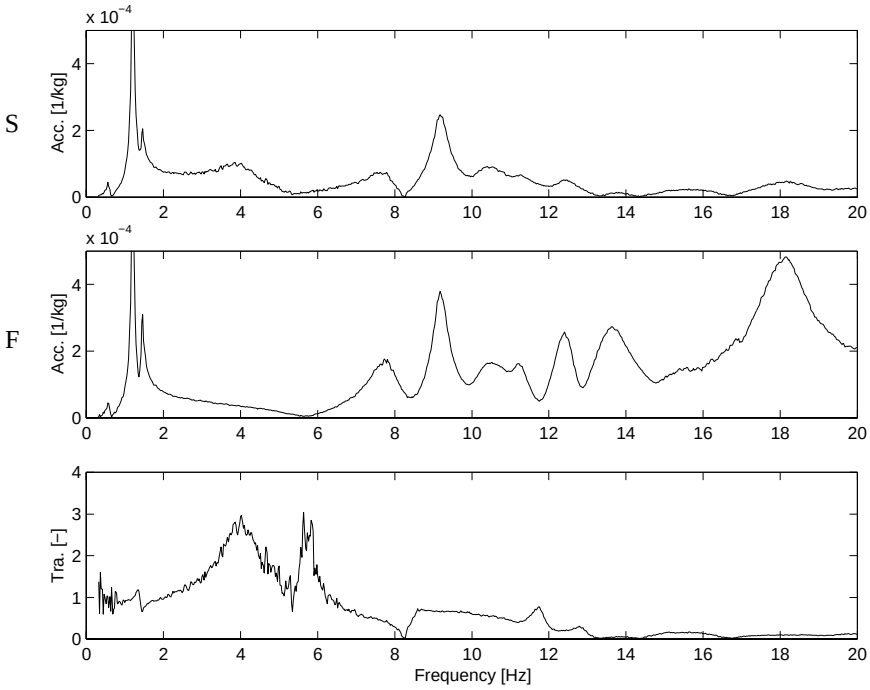

Figure 3-14 Accelerance at seat pan (S) and floor (F) as well as seat transmissibility (Tra.) (magnitude). *With a passenger seated. Excitation amplitude, “100%”. Points S and F are defined in Figure 3-5.*

Very few measurements of seat transmissibility were taken, only including two persons and one seat. This must kept in mind when interpreting the results and drawing conclusions.

However, studying Figure 3-14, one may note that the acceleration at the seat pan differs from the acceleration at the floor. Mainly, the accelerance is lower at the seat, corresponding to a seat transmissibility less than one. However, in the interval of 2 Hz to 6 Hz transmissibility is greater than one. This is what is usually obtained in seat transmissibility measurements, cf. Figure 4-4. The first peak at 4 Hz is due to a combined effect of human body dynamics and seating dynamics. The narrow peak at 6 Hz is unexpected, but might be explained by an anti-resonance; the accelerance is low around 6 Hz.

In order to investigate how much the mode shapes deform owing to one passenger, the curves in Figure 3-15 have been produced. Measurements with the empty seat have been compared to measurements with a passenger sitting in the seat, by calculating the ratio between an accelerance of the occupied seat and the same accelerance of the empty seat. A ratio of one thus means that the corresponding part of the seat is not influenced by the seated passenger. No other passengers are present.

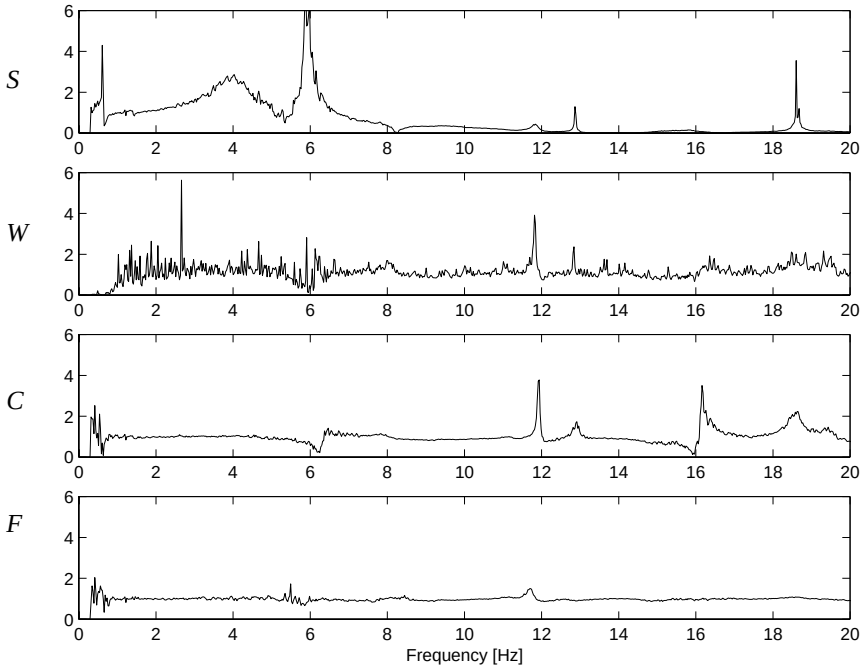

Figure 3-15 The ratio accelerance with passenger to accelerance without passenger (magnitude). *Amplitude, "100%". Points S, W, C and F are defined in Figure 3-5.*

From Figure 3-15 it is clear that the mode shape of the inner floor is hardly influenced by a single passenger. No corresponding measurements showing the influence of several passengers were carried out.

3.3 Conclusions

In conclusion, the two main trends found in the measurements are that passenger-load increases the relative damping of many carbody modes, and that the modal parameters of the carbody depend on the excitation-amplitude. The role played by relative damping is very important in resonant systems, as it determines the system's behaviour at resonance; both passenger-load and excitation-amplitude influence the carbody relative-damping.

The excitation-amplitude is here varied by a factor of 8, which is quite much. In normal running conditions, the excitation-amplitude is likely to vary much less. This makes it possible to adopt a linear carbody model, using a relative damping that is representative of normal running conditions, i.e. corresponding to an excitation-amplitude somewhere between "25%" and "50%".

The influence of passenger-load on relative damping is significant. Moreover, the measurements with and without passengers show that it is possible to establish a (linear) dependence of the relative damping on a "passenger-load parameter". This parameter will be properly introduced in Chapter 5.

The passenger-load and the excitation-amplitude also have an influence on the carbody eigenfrequencies, although this influence is less pronounced. The changes are probably too small to change the system's behaviour significantly, at least from a ride comfort point of view.

However, the observed amplitude-dependency of the eigenfrequency indicates that the damping of the carbody is partly explained by Coulomb friction.

The modal parameters obtained in this experimental modal analysis agree well with previous finite-element calculations and operating-deflection-shape measurements.

The few measurements taken of seat transmissibility agree with the results of other investigators.

Finally, note that the influence of passenger-load and excitation-amplitude on the rigid-body movement of the carbody has not been studied.

With these conclusions in mind, the models proposed in Chapter 5 concentrate on basic interaction mechanisms and thus on rather simple models.

4 Models of passengers, seats and carbody

4.1 Human body

4.1.1 Modelling

For the purposes of the present study, models that provide a simple mathematical summary of human-body dynamics are needed. The present study is restricted to vertical vibration, since, on the one hand, vertical structural vibrations proved to be the most important in the case study [13], see Figure 2-10, and on the other hand, most of the studies on human whole-body dynamics found in literature treat vertical vibrations. Few-degree-of-freedom models of this type are proposed in references [44], [47] and [51] among others.

It must be stressed that these models do not explain the motion of different human-body parts, but merely describe the seated human body exposed to vertical vibration by mathematical models. The models are based on impedance measurements: The subject sits on a stiff support that is excited, the exciting force and the resulting support acceleration are measured and the impedance, i.e. the frequency-response function between the force and the support velocity (force/velocity), is calculated. Here, the "*normalized apparent mass*", used by [51], will be used to characterize the human-body dynamics. Detailed definitions of the notions used in the present work are found in Appendix B.

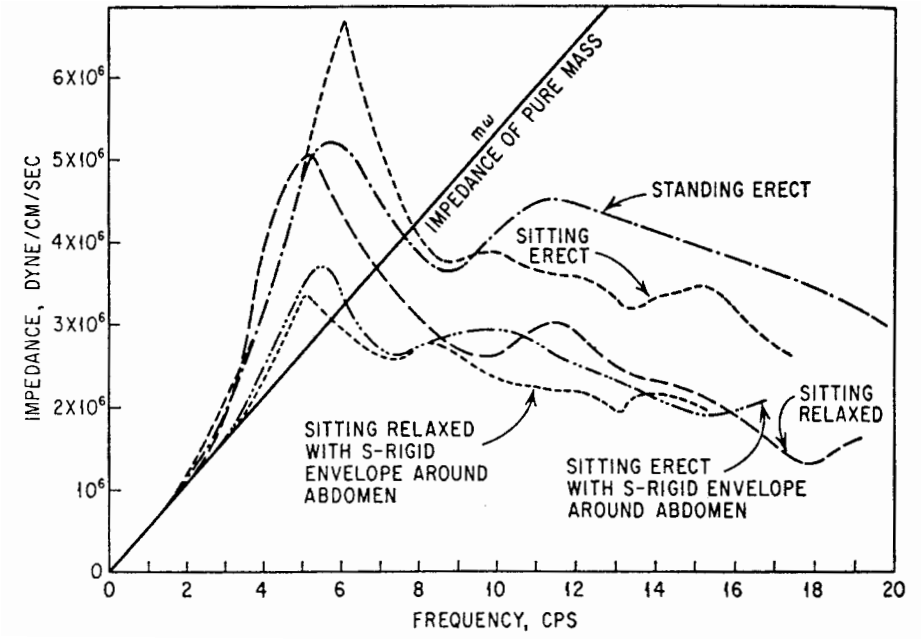

***Figure 4-1 Example of measured vertical point impedance (magnitude)**. One subject at various postures. From [40].*

Up to now, about 100 people have been measured by this method, and the investigations show similar results [51]. The most important effect is a peak in the impedance function between 4 and 6 Hz, see Figure 4-1.

The impedance depends to a large extent on the posture; sitting erect or relaxed makes a difference. Also, the excitation amplitude seems to be less important than the posture. Statistically, fitted model parameters for a group of men and a group of women differ only marginally [51].

4.1.2 Chosen models

Figure 4-2 shows two possible single-degree-of-freedom vertical models of the human body in sitting position. The model shown to the left in the figure was first proposed by Coermann in [40]. Wei and Griffin [51] propose the model shown to the right in Figure 4-2. “Model B” to the right will be used in the present study. The impedance measurements show a second peak at 10 to 14 Hz, cf. Figure 4-1, which can be taken into account by adding another sprung mass in parallel to the first mass. But single-degree-of-freedom models are used here in order to obtain small-sized models.

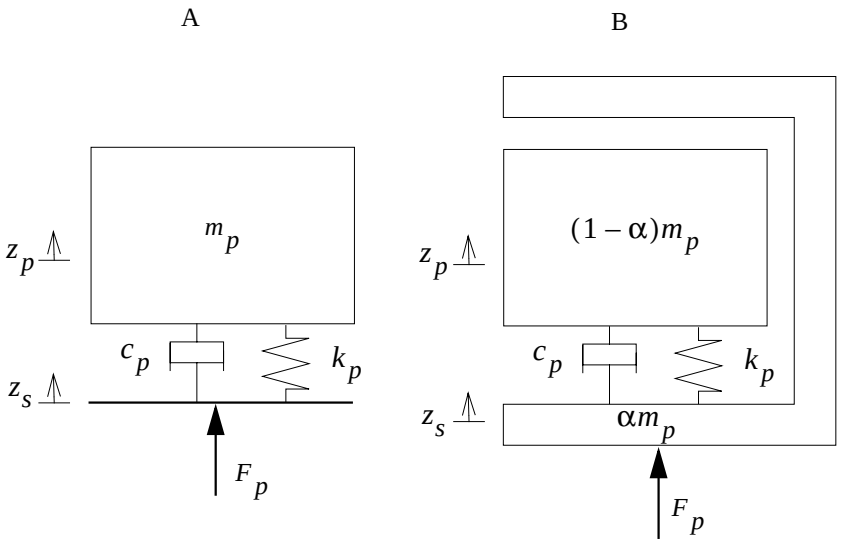

Figure 4-2 Single-degree-of freedom human-body models [40][51].

Model A to the left represents the passenger by a simple spring-damper-mass system. The human-body mass m_p is suspended on a linear spring and a linear viscous damper. The values of the spring constant k_p and the damper constant c_p can be obtained by curve-fitting to impedance measurements, cf. Figure 4-1. Published measurements [51] indicate that k_p and c_p are proportional to m_p. Here, this is assumed to be the case, writing

$$_p = \omega_p^2 m_p \tag{4-1}$$

$$c_p = 2\zeta_p \omega_p m_p \tag{4-2}$$

thereby introducing the undamped circular eigenfrequency ω_p and the relative damping ζ_p of the human-body model. Most of the values of the relative damping found in the literature are close to 50% and the undamped eigenfrequency varies between 4 and 6 Hz, cf. the peak in Figure 4-1.

After attributing a vertical degree-of-freedom z_p to the sprung mass (p as in passenger) and denoting the vertical displacement of the foundation by z_s (s as in seat), the equations of motion for the human-body model can be written as

$$\begin{aligned} m_p\ddot{z}_p + c_p(\dot{z}_p - \dot{z}_s) + k_p(z_p - z_s) &= 0 \\ c_p(\dot{z}_s - \dot{z}_p) + k_p(z_s - z_p) &= F_p \end{aligned} \tag{4-3}$$

where F_p represents the dynamic force from the carbody. The frequency response function between z_p and z_s (z_p/z_s), that is the transmissibility, is found from (4-3). With the assumptions (4-1) and (4-2), the transmissibility for Model A is

$$T_{pA}(\omega) = \frac{\omega_p^2 + 2i\zeta_p\omega_p\omega}{\omega_p^2 + 2i\zeta_p\omega_p\omega - \omega^2} \tag{4-4}$$

The vertical point impedance of Model A, $Z_{pA}(\omega) = \frac{F_p}{z_s i\omega}$ is found to be proportional to the body mass and to the transmissibility:

$$Z_{pA}(\omega) = m_p T_{pA}(\omega) i\omega \tag{4-5}$$

Model B represents the passenger by two masses. The total body mass m_p is partitioned into a sprung and an unsprung mass. The carbody force acts on the unsprung part αm_p. The fraction of unsprung mass α is typically between 0.05 and 0.2, estimated from the measurements in [51].

In this case, the equations of motion are

$$\begin{aligned} (1-\alpha)m_p\ddot{z}_p + c_p(\dot{z}_p - \dot{z}_s) + k_p(z_p - z_s) &= 0 \\ \alpha m_p\ddot{z}_s + c_p(\dot{z}_s - \dot{z}_p) + k_p(z_s - z_p) &= F_p \end{aligned} \tag{4-6}$$

showing that $\alpha = 0$ in Model B yields Model A.

The transmissibility and impedance of model B equal, respectively

$$T_{pB}(\omega) = \frac{\omega_p^2 + 2i\zeta_p\omega_p\omega}{\omega_p^2 + 2i\zeta_p\omega_p\omega - (1-\alpha)\omega^2} \tag{4-7}$$

and

$$Z_{pB}(\omega) = (1-\alpha)m_p i\omega T_{pB}(\omega) + \alpha m_p i\omega \tag{4-8}$$

The vertical human-body impedance of Model B thus consists of two terms, one term from each of the two masses.

Definition of normalized apparent mass

The human-body impedance is proportional to the body mass m_p and, therefore, the "normalized apparent mass" of a passenger is introduced:

$$T_p(\omega) = \frac{Z_p(\omega)}{m_p i\omega} \tag{4-9}$$

"Apparent mass" is defined as the frequency-response function between the force and the support acceleration (force/acceleration), and thus has the dimension [kg]. The notion "*normalized* apparent mass" of the seated human body exposed to vertical vibration is defined and used by [51]. Here it is denoted by $T_p(\omega)$ since it, in Model A, is identical to the transmissibility (z_p/z_s). For Model B, the normalized apparent mass is $T_p = (1-\alpha)T_{pB} + \alpha$. Note that the normalized apparent mass has both magnitude and phase.

The normalized apparent mass for Model B is shown in Figure 4-3, where mean human-body parameters are used: $\alpha = 0.1$, $\omega_p = 2\pi \cdot 5$ rad/s and $\zeta_p = 0.5$, based on a fit mean of 60 people given in [51].

The mean normalized apparent mass in Figure 4-3 is clearly related to the measured vertical point impedance in Figure 4-1. Most obvious is the peak between 4 and 6 Hz. The concept of mean normalized apparent mass will be utilized in Chapter 5 when modelling several passengers.

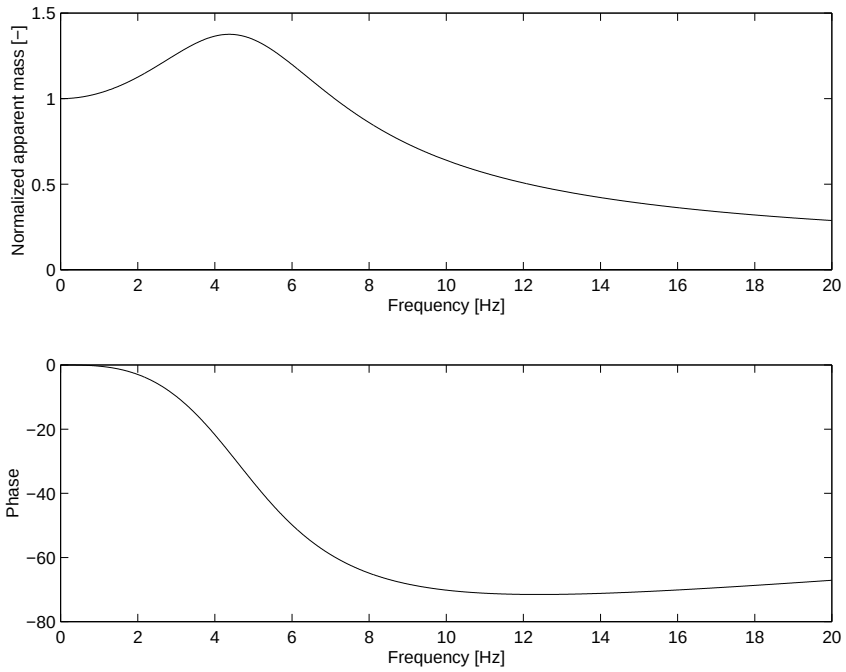

Figure 4-3 Mean normalized apparent mass of human body. *Model B with mean human-body parameters* $\alpha = 0.1$, $\omega_p = 2\pi \cdot 5$ *rad/s and* $\zeta_p = 0.5$.

4.2 Seats

4.2.1 Modelling

There are various types of rail-vehicle seats. Three main types of seat cushions and back-rests can be identified [45]. One type has a core of springs covered by foam rubber and cloth. Another type has a core of firm foam rubber covered by softer foam rubber and cloth. A third type has a core of foam rubber covered with foamed plastic and felted cloth. The seat cushion and back-rest are generally mounted on a steel construction, which is attached to the wall and/or standing on the inner floor.

Several methods of quantifying dynamic seat comfort have been proposed for different types of vehicles. There are no specific standards for evaluating rail-vehicle seats, but a general method for evaluating seat dynamics is proposed in [44], the “seat effective amplitude transmissibility”, the so-called SEAT-value. The SEAT-value compares the vibration comfort in the seat with that at the floor. More specifically, it is defined as the square root of the ratio between the comfort-weighted r.m.s. acceleration at the seat pan and at the floor, i.e.

$$SEAT\ in\ per\ cent = \sqrt{\frac{\int G_S(\omega)W^2(\omega)\mathrm{d}\omega}{\int G_F(\omega)W^2(\omega)\mathrm{d}\omega}} \times 100 \qquad (4\text{-}10)$$

where $G_S(\omega)$ is the autospectrum of the acceleration at the seat interface, $G_F(\omega)$ is the autospectrum of the acceleration at the floor and $W(\omega)$ is a comfort-weighting filter, e.g. the vertical ISO-2631 filter in Figure 2-12. A SEAT value of 100% means that sitting on the floor produces the same vibration discomfort as that experienced sitting in the seat.

From a modelling point of view, the seat is a complex dynamical system and transmits vibrations to the seated passenger via seat pan, arm-, back- and foot-rest. The vibrations are multiaxial and amplitude-dependent. In [41] an example of typical magnitude of r.m.s. acceleration for a person seated over a bogie is given. The dominant group of perceived vibration inputs consists of lateral and vertical inputs at the seat pan and the fore-and-aft motion at the back-rest. But, if unweighted r.m.s.-values are considered then vertical and lateral inputs at foot and back-rest are as important as the input at the seat pan. Available measurements and theory mainly treat the vertical direction.

Definition of seat transmissibility

Seat transmissibility is often used to characterize the vertical dynamics of a seat. The term is used here as defined in [52] with the generalization that phase information is included as well. It is defined as the frequency-response function z_s to z_f, where z_s is the vertical *displacement* of the seat pan and z_f is the vertical *displacement* of the floor at the interface between seat and floor. A person is supposed to be sitting in the seat. Note that the seat transmissibility is *not* a force-to-force frequency-response function.

The seat transmissibility can be estimated from measurements by

$$T_s(\omega) = \frac{G_{SI}(\omega)}{G_{FI}(\omega)} \qquad (4\text{-}11)$$

where $G_{SI}(\omega)$ is the cross-spectrum of the acceleration at the seat pan (S) and the exciting input force (I) and $G_{FI}(\omega)$ is the cross-spectrum of the acceleration at the floor (F) and the exciting input force. See also Appendix B.1.

Seat models may be validated against seat-transmissibility measurements, which are the most common measurements of seat dynamic properties.

Seat transmissibility is a suitable characteristics, since it is relatively easy to measure. It indicates the motion of the seat pan/passenger relative to the steady-state of the motion at the floor.

Figure 4-4 shows measured vertical transmissibilities of 10 alternative cushions fitted in a rail-vehicle seat and exposed to random-motion input with a magnitude of 0.6 m/s^2 r.m.s. [41]. The spring cushion, which is normally used as standard, has the highest transmissibility at resonance, but the choice of the most suitable cushion also depends on the vibration input at the foot of the seat as well as the sensitivity of the passenger to vibration.

The vertical stiffness of a seat is often preload dependent, and depends also on the shape and posture of the seat occupant. This means that the seat transmissibility depends on the seat occupant. Often, static comfort design criteria result in a vertical resonance frequency close to 4 Hz [44], as in the case of Figure 4-4.

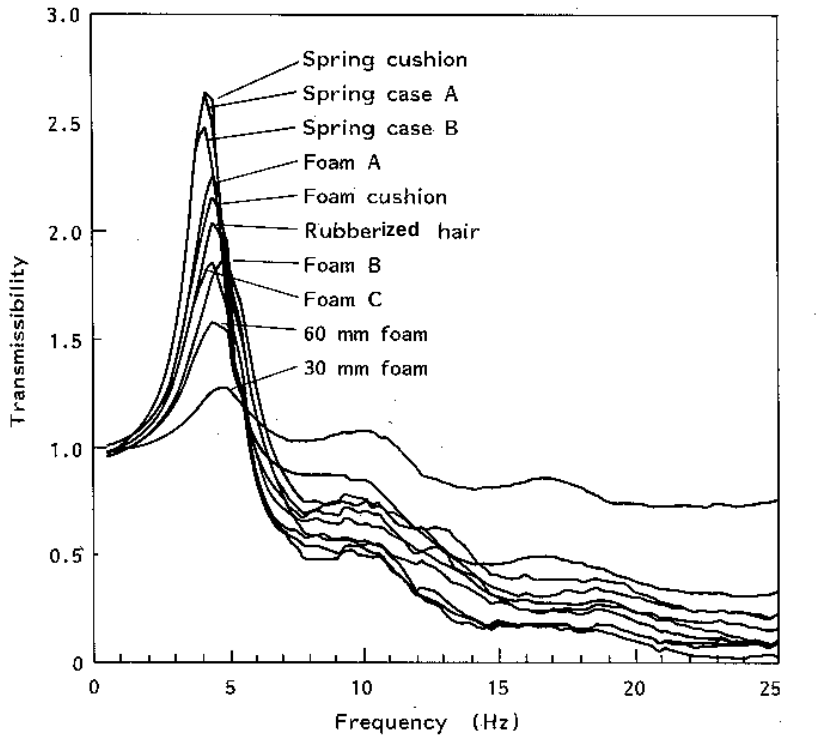

Figure 4-4 Measured seat transmissibility of rail-vehicle seats (magnitude). *From [41][44].*

4.2.2 Chosen models

Since the present study focuses on vertical dynamics, only vertical seat models are considered here. Figure 4-5 shows four possible models.

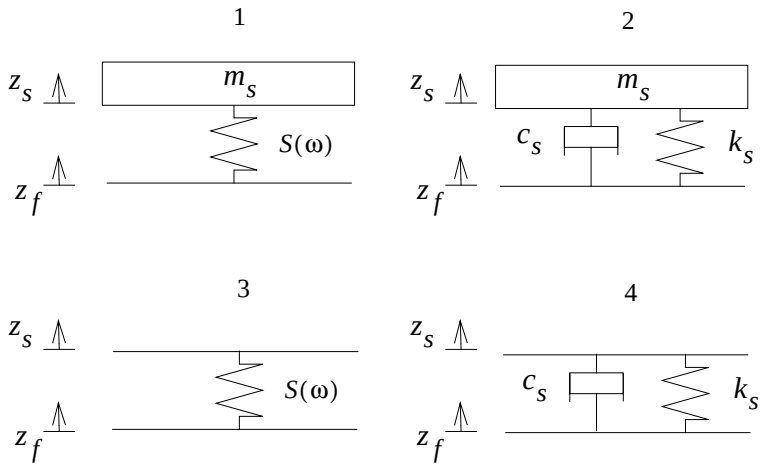

Figure 4-5 Seat models. *After [44].*

Seat model 1 is similar to a model given in [44]. The other three seat models are special cases of this model. The seat models are to be inserted between the carbody model and the human-body model. Here, z_s denotes the motion of the seat pan, see also Figure 4-2, and z_f denotes the motion of the inner floor. In seat models 1 and 2, there is a part of the seat with mass m_s that moves with the seat pan. This mass is assumed to be small in comparison with the unsprung mass of the passenger and is often negligible. The seat stiffness $S(\omega)$, i.e. the frequency-response function between force and relative displacement (force/displacement), may be general or, for instance, as assumed in models 2 and 4

$$S(\omega) = k_s + \mathrm{i}\omega c_s \tag{4-12}$$

The seat stiffness may not be well defined, since the interface between passenger and seat is rather complex. The stiffness depends on the weight of the seat occupant and the posture, etc.

The seat transmissibility, defined in Section 4.2.1, $T_s(\omega)$, is *not* solely a function of the seat parameters, but depends also on the dynamical properties of the seat occupant. In Section 5.4.1, where the combination of passenger and seat is examined in detail, it is shown that

$$T_s(\omega) = \frac{S(\omega)}{S(\omega) + Z_p(\omega)\mathrm{i}\omega - m_s\omega^2} \tag{4-13}$$

where $Z_p(\omega)$ is the impedance of the seated passenger.

4.3 Carbody model

The measurements presented in Chapter 3 show that the dynamic properties of the carbody are amplitude dependent. Here, however, a linear carbody model is assumed. The general linearized equations of motion of the carbody may be written

$$\boldsymbol{M}_c\ddot{\boldsymbol{q}} + \boldsymbol{C}_c\dot{\boldsymbol{q}} + \boldsymbol{K}_c\boldsymbol{q} = \boldsymbol{F} \tag{4-14}$$

where the subscript c refers to the carbody. The forces $\boldsymbol{F}$ are exerted by the bogies and the passengers, but here only the passengers are considered. The system is generally diagonalized so that the mass matrix $\boldsymbol{M}_c$ and the stiffness matrix $\boldsymbol{K}_c$ become diagonal. The damping matrix $\boldsymbol{C}_c$ is not automatically diagonal, but it is often assumed to be, since it permits decoupling the modal equations for the eigenmodes of the carbody

$$m_{cj}\ddot{q}_{cj} + 2m_{cj}\zeta_{cj}\omega_{cj}\dot{q}_{cj} + m_{cj}\omega_{cj}^2 q_{cj} = F_{cj} \tag{4-15}$$

where index j runs from 1 to L, the number of carbody modes included in the model. The modal mass of the carbody is denoted by m_{cj}, the relative damping by ζ_{cj} and the undamped circular eigenfrequency by ω_{cj}. The generalized degree-of-freedom of the carbody mode is q_{cj}. The mode shape of the carbody, $\boldsymbol{n}_{cj}$, may be scaled so that its modal mass equals 1 kgm^2, simplifying the expressions. This is done here. F_{cj} denotes the modal forces that are due to passengers.

A modal carbody model can be obtained by experimental modal analysis (EMA), cf. Figure 3-7 or from a finite-element model (FEM), cf. Figure 2-9. In the latter case, relative damping is normally not included, since detailed information on the damping mechanisms in the structure is normally not available. The mode-shapes obtained by experimental modal analysis may be complex-valued allowing a phase other than zero and 180 degrees between different parts of the carbody. Such modes appear when damping is non-proportional [2]. The eigenmodes should be measured/calculated for a free carbody, since the carbody is mounted via soft springs on the bogies.

The rigid-body motion of the carbody is best taken into account by a (flexible) multibody model, see, for instance, [14][35]. The interface between a multibody model and the model of a flexible body is discussed in [36].

In the following, the modal models obtained from the experimental modal analysis of the SJ-B7M will be used.

Models of passengers, seats and carbody

5 Proposed interaction models

In this chapter, models are proposed that describe the dynamical interaction between the passengers and the carbody, answering the question of how the passengers influence carbody structural dynamics and the ride comfort. To the author's knowledge, no such studies have been published before. There are, however, studies carried out where a single rail-vehicle passenger is modelled in order to investigate the dynamics of the passenger, e.g. [49].

The models proposed here are intentionally simple, leading to equations of motion of a quite general character. Owing to the generality of the equations of motion, it is worthwhile to investigate their properties. In particular, the "passenger load parameter" can be identified as a key parameter of the passenger-carbody interaction. The role played by similar parameters are discussed by other authors, e.g. [1].

The "passenger load parameter" is a central notion in the present work. It is motivated and defined in Section 5.1. In Section 5.2, basic interaction models are discussed, including possible reductions in model size. Ideas on approximate models are presented in Section 5.3. In Section 5.4, vertical seating dynamics is included in the models. A summary and conclusions of the contents of the chapter are given in Section 5.5. Important definitions are collected in Appendix B.1, and the notations are explained in Appendix B.2.

5.1 Passenger load parameter

5.1.1 Background

Consider the case in which the carbody motion is represented by a single mode shape, i.e. L=1. The mode has undamped eigenfrequency ω_c, relative damping ζ_c, modal mass m_c=1 kgm^2 and modal degree-of-freedom q_c. Suppose there are N passengers, each acting on the carbody by a vertical force F_{pi}, where i runs from 1 to N. The only forces considered are vertical. The modal force F_c acting on the carbody mode is then the sum of the force from each passenger F_{pi} times the mode's vertical displacement at the location of each passenger, here denoted d_i. That is

$$F_c(\omega) = \sum_{i=1}^{N} d_i F_{pi}(\omega) \tag{5-1}$$

The principle is illustrated in Figure 5-1.

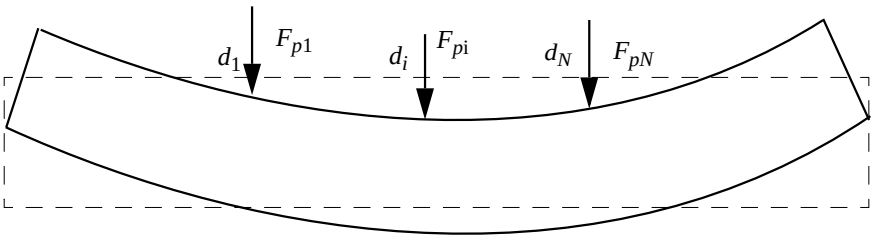

Figure 5-1 Forces from the passengers 1 to N on the carbody.

The impedance formulation permits writing each passenger force as a product of the impedance and the velocity of the carbody at the location of each passenger $d_i \mathrm{i}\omega q_c(\omega)$:

$$F_{pi}(\omega) = Z_{pi}(\omega) d_i \mathrm{i}\omega q_c(\omega) \tag{5-2}$$

where $Z_{pi}(\omega)$ is the impedance of passenger *i*.

Assumption of a mean normalized apparent mass of the human body

The models proposed in this chapter all rely on the assumption that there exists a mean normalized apparent mass $T_p(\omega)$ of the human body, cf. equation (4-9) and Figure 4-3. The impedance of passenger number *i* is then given by

$$Z_{pi}(\omega) = m_{pi} T_p(\omega) \mathrm{i}\omega \tag{5-3}$$

where m_{pi} is the mass of passenger *i*. Thus, $T_p(\omega)$ is assumed to be the same for all passengers. This approximation does not seem to be inadequate, in view of the discussion held in [51].

Inserting (5-2) and (5-3) in (5-1) results in the following expression for the modal force

$$F_c(\omega) = -\sum_{i=1}^{N} m_{pi} d_i^2 T_p(\omega) \omega^2 q_c(\omega) \tag{5-4}$$

from which one sees that it consists of a frequency-dependent part $-T_p(\omega)\omega^2 q_c(\omega)$ and a spatial part $\sum_{i=1}^{N} m_{pi} d_i^2$.

The system with "*N* passengers in a carbody" shows resemblances with other general systems, for instance the "rod with attached damped spring-mass systems" discussed in

[4]. (The rod corresponds to the carbody and the passengers to the attached spring-damper systems.) The combination of two systems and the impedance coupling method are discussed in textbooks, for instance [2].

5.1.2 Definition of passenger load parameter

In equation (5-4) one identifies a “passenger load parameter”

$$P = \sum_{i=1}^{N} m_{pi} d_i^2 \tag{5-5}$$

This parameter is frequency independent but depends on the passenger mass distribution as well as the vertical mode-shape values at the location of the passengers. A passenger sitting in a node of a mode shape does not interact with the mode, since then $d_i = 0$. It is worth noting that the apparition of this parameter relies on two assumptions, namely that
- the normalized apparent mass is assumed to be the same for all passengers, and that
- the system is not excited via the passengers.

For the general case of several carbody mode-shapes, there is one passenger load parameter per carbody mode-shape

$$P_j = \sum_{i=1}^{N} m_{pi} d_{ij}^2 \tag{5-6}$$

where j runs from 1 to L. The passenger load parameter has the dimension kgm^2.

The passenger distribution may be known for a particular case, for instance as in the measurement in Chapter 3. In general, however, all passenger distributions are equally probable, and, consequently, the best estimate is

$$m_{p1} = \ldots = m_{pi} = \ldots = m_{pN} = m_p \tag{5-7}$$

where m_p is the mass of a typical average passenger, cf. Section 4.1.2. Then one obtains a relationship between the passenger load parameter P_j and the “Modal Contribution Factor” (*MCF*) proposed in [15], see also Section 2.2.3, namely

$$P_j = m_p \sum_{i=1}^{N} d_{ij}^2 = N m_p (MCF_j)^2 \tag{5-8}$$

The value of *MCF* depends on the mode shape, and where passengers are to sit. A mode shape that mainly involves deformations of the roof has a low *MCF*-value, for instance.

Typical values of *MCF* are given in Table 2-2. From (5-8), it is clear that P_j is proportional to the total passenger mass $M_p = Nm_p$.

In summary, the passenger load parameter P_j is a measure of how much carbody mode *j* interacts with the passengers, although it does not consider frequency dependency.

5.2 Basic interaction models

5.2.1 One passenger and one carbody mode

Let the *passenger* (*N*=1) be represented by Model B, that is equation (4-6), and let the *carbody* be represented by a single mode, i.e. by equation (4-15) with *L*=1, see Figure 5-2.

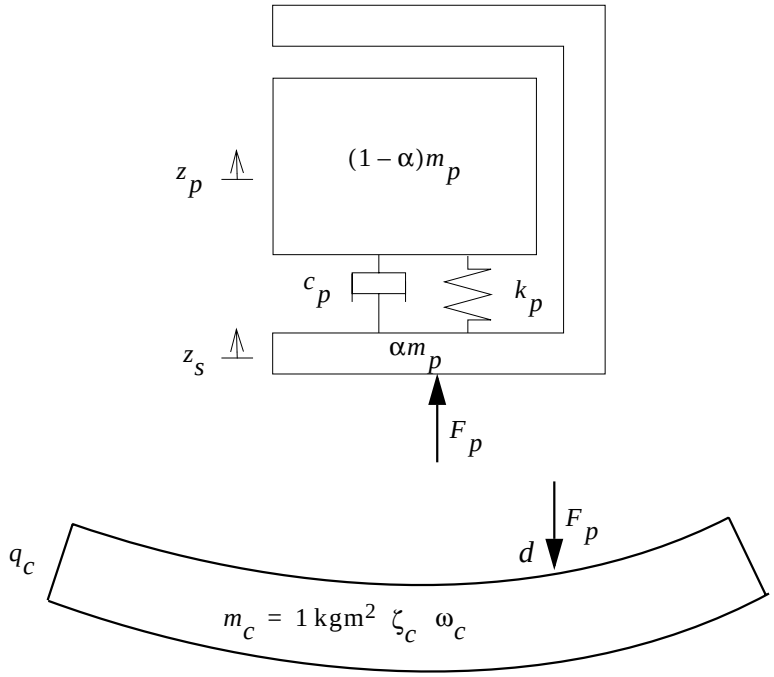

Figure 5-2 Model of one human-body and one carbody mode.

The result of a vertical point-force acting on the mode shape depends on the vertical deformation shape value *d* of the mode at this particular point. If the undamped circular eigenfrequency is denoted ω_c and the relative damping as ζ_c, then the equation of motion of the carbody mode is

$$\ddot{q}_c + 2\zeta_c\omega_c\dot{q}_c + \omega_c^2 q_c = F_p d \tag{5-9}$$

where q_c is the generalized degree-of-freedom of the carbody mode, and where it is assumed that $m_c = 1$ kgm^2.

Assume that the unsprung mass in the human-body model stays in permanent contact with the motion of the carbody at the point where the passenger sits, giving a direct relation between the carbody generalized degree-of-freedom q_c and the vertical degree-of-freedom of the unsprung mass z_s, namely

$$z_s = dq_c \tag{5-10}$$

The resulting mechanical system then has two degrees-of-freedom. If these are chosen as the carbody generalized degree-of-freedom q_c and the vertical degree-of-freedom of the sprung mass z_p then, using equations (4-6), (5-9) and (5-10), the equations of motion of the two-degree-of-freedom system can be written as

$$\boldsymbol{M}\ddot{\boldsymbol{q}} + \boldsymbol{C}\dot{\boldsymbol{q}} + \boldsymbol{K}\boldsymbol{q} = \boldsymbol{0} \tag{5-11}$$

with

$$\begin{aligned} \boldsymbol{q} &= \begin{bmatrix} z_p \\ q_c \end{bmatrix} & \boldsymbol{M} &= \begin{bmatrix} (1-\alpha)m_p & 0 \\ sym & 1+\alpha m_p d^2 \end{bmatrix} \\ \boldsymbol{C} &= 2\begin{bmatrix} \zeta_p\omega_p m_p & -\zeta_p\omega_p m_p d \\ sym & \zeta_c\omega_c + \zeta_p\omega_p m_p d^2 \end{bmatrix} & \boldsymbol{K} &= \begin{bmatrix} \omega_p^2 m_p & -\omega_p^2 m_p d \\ sym & \omega_c^2 + \omega_p^2 m_p d^2 \end{bmatrix} \end{aligned} \tag{5-12}$$

The roots λ of the coupled system are found by solving the characteristic equation

$$\begin{aligned} &(\omega_p^2 + 2\zeta_p\omega_p\lambda + (1-\alpha)\lambda^2)(\omega_c^2 + 2\zeta_c\omega_c\lambda + \lambda^2) \\ &+ P\lambda^2(\omega_p^2 + 2\zeta_p\omega_p\lambda + \alpha(1-\alpha)\lambda^2) = 0 \end{aligned} \tag{5-13}$$

where the passenger load parameter

$$P = m_p d^2 \tag{5-14}$$

is identified as a key parameter, cf. (5-5).

The coefficients in the polynomial in (5-13) are real, and, therefore, any complex roots are complex-conjugated pairs. The four roots of the coupled system are all functions of P, as expressed by equation (5-13). In this sense, the parameter P measures the interaction between the carbody mode and the passenger. As P approaches zero, two of the roots, i.e. the “carbody-mode roots”, approach the roots of the empty carbody

$-\omega_c(\zeta_c \pm i\sqrt{1-\zeta_c^2})$. The other two roots approach the roots of the isolated human-body model.

Numerical example

In Figure 5-3, root loci for one of the carbody roots and one of the human-body roots are plotted as a function of the passenger load parameter *P*, for three sets of human-body parameters, see Table 5-1. Only roots with positive imaginary parts are shown in the figure. The passenger load parameter *P*, cf. (5-14), varies from 0 to 1 kgm^2 in steps of 0.05 kgm^2.

Table 5-1 Three sets of human-body parameters.

	$f_p = \omega_p/2\pi$	ζ_p	α
1	5 Hz	50%	0.1
2	5 Hz	25%	0.1
3	Unsprung mass		1.0

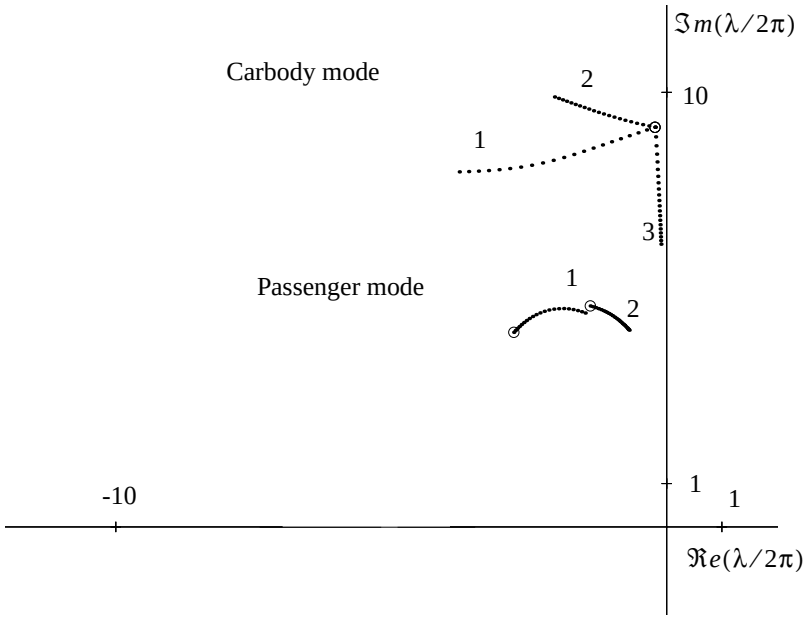

Figure 5-3 Root loci of carbody mode and human-body mode for different sets of human-body parameters. *$0 \le P \le 1$ kgm^2 by steps of 0.05 kgm^2, circle corresponds to P=0. Carbody mode G2, cf. Table 3-4. Human-body parameter sets 1, 2 and 3 from Table 5-1.*

Parameter set 1 corresponds to typical values from [51]. In parameter set 2, passenger relative-damping has been halved. The third parameter set corresponds to the limiting case with all passenger mass lumped to the carbody, i.e. $\alpha = 1$.

This example shows that if the passenger is modelled as a single unsprung mass (set 3), then the carbody-mode eigenfrequency decreases and the relative damping does not change significantly when *P* increases. If the passenger is modelled by Model B (set 1 and 2), then carbody-mode relative-damping always increases as *P* increases as shown by the figure. Carbody-mode eigenfrequency decreases (set 1), or increases (set 2), depending on the values taken by the human-body parameters.

The relative damping of the passenger mode decreases with increasing *P*.

The comparison to measurement results made in Chapter 6 shows that modelling the human body as an unsprung mass only (set 3) is inappropriate.

The special case of a vertical rigid carbody-model ($\zeta_c = \omega_c = 0$ and m_c being the carbody mass) merits consideration. In this case (5-13) changes to

$$((m_c + m_p)(\omega_p^2 + 2\zeta_p\omega_p\lambda) + (m_c + \alpha m_p)(1-\alpha)\lambda^2)\lambda^2 = 0 \qquad (5\text{-}15)$$

showing that the rigid-body motion of the carbody is not affected by the passengers for an isolated passenger-carbody system ($\lambda = 0$ is still a solution). This is only true for the ideal case of an isolated passenger-carbody system, however. With the carbody mounted on the bogies, the system has an eigenfrequency and a relative damping that are determined by the carbody mass-properties and the characteristics of the suspension. This eigenfrequency and this relative damping are affected by the passenger load.

5.2.2 Inclusion of several passengers

The model in Section 5.2.1 is now generalized to the case with several passengers ($N > 1$), cf. Section 5.1.1 and Figure 5-1. The passengers are assumed to be alike from a mechanical modelling point of view, i.e. the "human-body parameters" α, ω_p and ζ_p are the same for all passengers, corresponding to the assumption of equation (5-3).

Suppose there are *N* passengers sitting at different locations and having different masses m_{pi}. The assumption of equation (5-7) is thus not made. The index *i* refers to the passengers and runs from 1 to *N*. Denote the vertical displacement value of the mode where each passenger sits by d_i. Attribute two degrees-of-freedom z_{pi} and z_{si} to each passenger. Each passenger is then described by a system corresponding to equation (4-6).

The force on the carbody from passenger *i* is now to be multiplied with d_i, and the total force is obtained by summing over all passengers, so that (5-9) turns into

$$\ddot{q}_c + 2\zeta_c\omega_c\dot{q}_c + \omega_c^2 q_c = \sum_{i=1}^{N} F_{pi} d_i \tag{5-16}$$

In this case (5-10) is replaced by

$$z_{si} = d_i q_c \tag{5-17}$$

with i running from 1 to N.

The equations of motion for this case may then be written as $\boldsymbol{M}\ddot{\boldsymbol{q}} + \boldsymbol{C}\dot{\boldsymbol{q}} + \boldsymbol{K}\boldsymbol{q} = \boldsymbol{0}$ with

$$\boldsymbol{q} = \begin{bmatrix} z_{p1} \\ \cdots \\ z_{pN} \\ q_c \end{bmatrix} \quad \boldsymbol{M} = \begin{bmatrix} (1-\alpha)m_{p1} & & 0 & 0 \\ & \cdots & & \\ & & (1-\alpha)m_{pN} & 0 \\ sym & & & 1+\alpha P \end{bmatrix}$$

$$\boldsymbol{C} = 2\begin{bmatrix} \zeta_p\omega_p m_{p1} & & 0 & -\zeta_p\omega_p m_{p1} d_1 \\ & \cdots & & \\ & & \zeta_p\omega_p m_{pN} & -\zeta_p\omega_p m_{pN} d_N \\ sym & & & \zeta_c\omega_c + \zeta_p\omega_p P \end{bmatrix} \tag{5-18}$$

$$\boldsymbol{K} = \begin{bmatrix} \omega_p^2 m_{p1} & & 0 & -\omega_p^2 m_{p1} d_1 \\ & \cdots & & \\ & & \omega_p^2 m_{pN} & -\omega_p^2 m_{pN} d_N \\ sym & & & \omega_c^2 + \omega_p^2 P \end{bmatrix}$$

The characteristic equation of this system has $2N+2$ roots. As in the previous case, the "carbody-mode roots" approach $-\omega_c(\zeta_c \pm i\sqrt{1-\zeta_c^2})$ as P approaches zero, where now

$$P = \sum_{i=1}^{N} m_{pi} d_i^2 \tag{5-19}$$

Also as above, two of the roots approach the roots of the isolated human-body mode. The remaining $2N$-2 roots correspond to modes that do not involve any motion of the carbody, they are redundant.

The redundancy can be used to reduce the system. In fact, by multiplying (5-17) by the Model B transmissibility T_{pB} and introducing a generalized passenger degree-of-freedom $q_p = T_{pB} q_c$, the following is achieved

$$z_{pi} = T_{pB} z_{si} = d_i T_{pB} q_c = d_i q_p \tag{5-20}$$

with i running from 1 to N.

The redundancy and the possibility of reducing the number of degrees-of-freedom rely on two assumptions, namely that
- the normalized apparent mass T_p is assumed to be the same for all passengers, and that
- the system is not excited via the passengers.

(For Model B, the normalized apparent mass is $T_p = (1-\alpha)T_{pB} + \alpha$.)

The equations of motion of the resulting two-degree-of-freedom system can be written as $\boldsymbol{M}\ddot{\boldsymbol{q}} + \boldsymbol{C}\dot{\boldsymbol{q}} + \boldsymbol{K}\boldsymbol{q} = \boldsymbol{0}$ with

$$\boldsymbol{q} = \begin{bmatrix} q_p \\ q_c \end{bmatrix} \qquad \boldsymbol{M} = \begin{bmatrix} (1-\alpha)P & 0 \\ 0 & 1+\alpha P \end{bmatrix}$$
$$\boldsymbol{C} = 2\begin{bmatrix} \zeta_p \omega_p P & -\zeta_p \omega_p P \\ sym & \zeta_c \omega_c + \zeta_p \omega_p P \end{bmatrix} \quad \boldsymbol{K} = \begin{bmatrix} \omega_p^2 P & -\omega_p^2 P \\ sym & \omega_c^2 + \omega_p^2 P \end{bmatrix} \tag{5-21}$$

clearly showing the important role played by P.

The displacement z_{pi} of each passenger may be retrieved from (5-20).

5.2.3 Several passengers and carbody modes

The model in Section 5.2.2 is now further generalized to also include several carbody modes.

Assume there are N passengers, each described by “Model B”, and L carbody modes described by equation (4-15). This system will be referred to as the (N,L)-system and is shown in Figure 5-4.

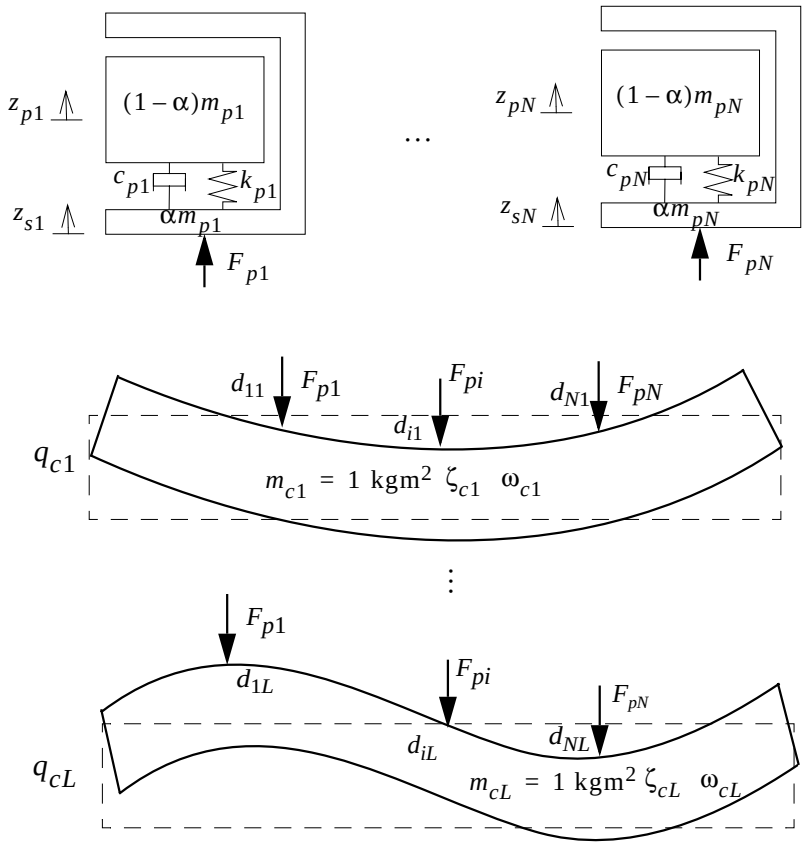

Figure 5-4 N passengers and L carbody modes, referred to as the (N,L)-system.

The system has N passenger degrees-of-freedom and L carbody degrees-of-freedom, namely the vertical displacement of each passenger, and the modal carbody-degrees-of-freedom:

$$\boldsymbol{z}_p = \begin{bmatrix} z_{p1} \\ \dots \\ z_{pN} \end{bmatrix} \quad \boldsymbol{q}_c = \begin{bmatrix} q_{c1} \\ \dots \\ q_{cL} \end{bmatrix} \tag{5-22}$$

Let the carbody modes be indexed by j running from 1 to L, and denote the vertical displacement value of the carbody mode j where passenger i sits by d_{ij}. These displacements are collected in the $N \times L$ matrix

$$\boldsymbol{D} = \begin{bmatrix} d_{11} & & d_{1L} \\ & \cdots & \\ d_{N1} & & d_{NL} \end{bmatrix} \tag{5-23}$$

which describes the "geometry" of the interaction. Each column of $\boldsymbol{D}$ may be regarded as a carbody mode shape restricted to the locations of the passengers. Each row of $\boldsymbol{D}$ contains the vertical displacements of the carbody mode-shapes at one of the passenger locations.

The carbody eigenmodes for an empty carbody are by definition uncoupled. The passengers introduce a coupling between the modes, which is a consequence of the fact that (5-17) must be replaced by

$$z_{si} = \sum_{j=1}^{L} d_{ij} q_{cj} \tag{5-24}$$

which also may be written as $\boldsymbol{z}_s = \boldsymbol{D}\boldsymbol{q}_c$ with $\boldsymbol{z}_s = \begin{bmatrix} z_{s1} & \cdots & z_{sN} \end{bmatrix}^T$.

The following $L \times L$ "passenger load matrix" can be identified in the equations of motion of the mechanical system of several passengers and carbody mode-shapes:

$$\boldsymbol{P} = \sum_{i=1}^{N} \begin{bmatrix} m_{pi} d_{i1}^2 & & m_{pi} d_{i1} d_{iL} \\ & \cdots & \\ sym & & m_{pi} d_{iL}^2 \end{bmatrix} \tag{5-25}$$

which also may be written $\boldsymbol{P} = \boldsymbol{D}^T \boldsymbol{M}_p \boldsymbol{D}$ with

$$\boldsymbol{M}_p = \begin{bmatrix} m_{p1} & & 0 \\ & \cdots & \\ sym & & m_{pN} \end{bmatrix} \tag{5-26}$$

The matrix $\boldsymbol{P}$ is a slight generalization of the passenger load parameter. In fact, the diagonal terms can be easily recognized as the passenger load parameters defined in equation (5-6). The off-diagonal terms quantify the coupling that the passengers introduce between the carbody mode-shapes. If these are zero, then the passengers do not introduce such a coupling. A numerical example based on the case study is given in Section 5.3.

The equations of motion are now $\boldsymbol{M}\ddot{\boldsymbol{q}} + \boldsymbol{C}\dot{\boldsymbol{q}} + \boldsymbol{K}\boldsymbol{q} = \boldsymbol{0}$ where

$$\boldsymbol{q} = \begin{bmatrix} \boldsymbol{z}_p \\ \boldsymbol{q}_c \end{bmatrix} \qquad \boldsymbol{M} = \begin{bmatrix} (1-\alpha)\boldsymbol{M}_p & \boldsymbol{0} \\ \boldsymbol{0} & \boldsymbol{I} + \alpha\boldsymbol{P} \end{bmatrix}$$
$$\boldsymbol{C} = \begin{bmatrix} 2\zeta_p\omega_p\boldsymbol{M}_p & -2\zeta_p\omega_p\boldsymbol{M}_p\boldsymbol{D} \\ -2\zeta_p\omega_p\boldsymbol{D}^T\boldsymbol{M}_p & \boldsymbol{C}_c + 2\zeta_p\omega_p\boldsymbol{P} \end{bmatrix} \quad \boldsymbol{K} = \begin{bmatrix} \omega_p^2\boldsymbol{M}_p & -\omega_p^2\boldsymbol{M}_p\boldsymbol{D} \\ -\omega_p^2\boldsymbol{D}^T\boldsymbol{M}_p & \boldsymbol{K}_c + \omega_p^2\boldsymbol{P} \end{bmatrix} \tag{5-27}$$

with diagonal matrices

$$\boldsymbol{C}_c = 2\begin{bmatrix} \zeta_{c1}\omega_{c1} & & 0 \\ & \cdots & \\ sym & & \zeta_{cL}\omega_{cL} \end{bmatrix} \quad \boldsymbol{K}_c = \begin{bmatrix} \omega_{c1}^2 & & 0 \\ & \cdots & \\ sym & & \omega_{cL}^2 \end{bmatrix} \tag{5-28}$$

and $\boldsymbol{I}$ being the $L \times L$ identity matrix representing the orthonormalized masses of the carbody modes.

The “carbody roots” are now a function of the matrix $\boldsymbol{P}$. The characteristic equation of system (5-27) depends only on the human-body parameters, the modal parameters of the carbody and the passenger load matrix $\boldsymbol{P}$.

Provided $N > L$, which is likely in most applications, the (N,L)-system of (5-27) can be reduced without approximation to a system with 2L degrees-of-freedom, cf. the case for $L = 1$ in Section 5.2.2. The reduction is accomplished by introducing L generalized passenger degrees-of-freedom q_{pj} instead of the N physical degrees-of-freedom z_{pi}. The reduced system will be referred to as the (L,L)-system.

The relation between the generalized and the physical passenger-degrees-of-freedom is analogous to (5-20), namely

$$\boldsymbol{z}_p = T_{pB}\boldsymbol{z}_s = \boldsymbol{D}T_{pB}\boldsymbol{q}_c = \boldsymbol{D}\boldsymbol{q}_p \tag{5-29}$$

with $\boldsymbol{q}_p = \begin{bmatrix} q_{p1} & \cdots & q_{pL} \end{bmatrix}^T$ defined by $\boldsymbol{q}_p = T_{pB}\boldsymbol{q}_c$

The equations of motion for the reduced system are obtained by inserting (5-29) into (5-27). It reads $\boldsymbol{M}\ddot{\boldsymbol{q}} + \boldsymbol{C}\dot{\boldsymbol{q}} + \boldsymbol{K}\boldsymbol{q} = \boldsymbol{0}$ with

$$\boldsymbol{q} = \begin{bmatrix} \boldsymbol{q}_p \\ \boldsymbol{q}_c \end{bmatrix} \qquad \boldsymbol{M} = \begin{bmatrix} (1-\alpha)\boldsymbol{P} & \boldsymbol{0} \\ \boldsymbol{0} & \boldsymbol{I} + \alpha\boldsymbol{P} \end{bmatrix}$$
$$\boldsymbol{C} = \begin{bmatrix} 2\zeta_p\omega_p\boldsymbol{P} & -2\zeta_p\omega_p\boldsymbol{P} \\ sym & \boldsymbol{C}_c + 2\zeta_p\omega_p\boldsymbol{P} \end{bmatrix} \quad \boldsymbol{K} = \begin{bmatrix} \omega_p^2\boldsymbol{P} & -\omega_p^2\boldsymbol{P} \\ sym & \boldsymbol{K}_c + \omega_p^2\boldsymbol{P} \end{bmatrix} \tag{5-30}$$

This system is analogous to (5-21). From (5-30), it is seen how the carbody mode degrees-of-freedom are coupled to each other by the off-diagonal terms of the passenger matrix $\boldsymbol{P}$, and also how the passenger degrees-of-freedom are coupled to each other. This means, for instance, that the vertical bending mode and a torsion mode may be coupled by the passengers yielding mixed torsion-vertical bending modes. Note that $\boldsymbol{I} + \alpha\boldsymbol{P}$, $\boldsymbol{C}_c + 2\zeta_p\omega_p\boldsymbol{P}$ and $\boldsymbol{K}_c + \omega_p^2\boldsymbol{P}$ are not necessarily simultaneously diagonalizable. The reduced system contains less degrees-of-freedom at the price of a loss of diagonality.

The possibility to reduce the system from $N + L$ to $2L$, i.e. by N-L degrees-of-freedom, may also be shown by studying then eigenvalue problem of the (N,L)-system. As stated in Section 5.2.2, the possibility relies on two assumptions, namely that
- the normalized apparent mass is assumed to be the same for all passengers, and that
- the system is not excited via the passengers.

In short, the first fact yields N-L eigenvectors of the system whose motion is restricted to the passengers, they do not involve any motion of the carbody. Therefore, by the second fact, these N-L eigenmodes are not excited and can be removed, thereby reducing the total number degrees-of-freedom to $2L$. The principle is illustrated for N=2 and L=1 in Figure 5-5.

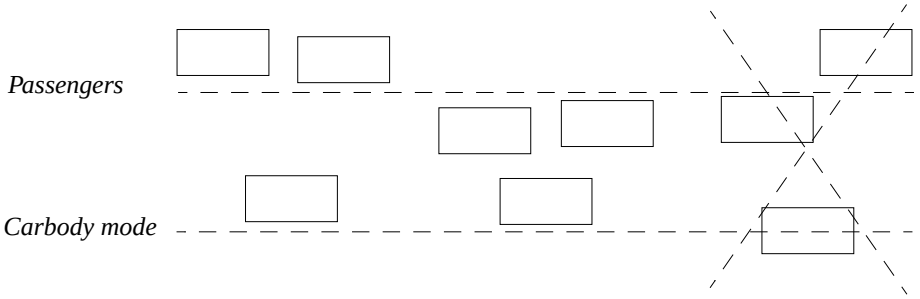

Figure 5-5 ***The three eigenmodes of the (N=2,L=1)-system.*** *The one at right can be removed, since it cannot be excited by any force acting on the carbody.*

To end this Section, a somewhat more formal proof this claim.

Proof: Let $\boldsymbol{C}_p = 2\zeta_p\omega_p\boldsymbol{M}_p$ and $\boldsymbol{K}_p = \omega_p^2\boldsymbol{M}_p$. Denote the solutions of the eigenvalue-problem $((1-\alpha)\boldsymbol{M}_p\lambda^2 + \boldsymbol{C}_p\lambda + \boldsymbol{K}_p)\boldsymbol{n} = \boldsymbol{0}$ by $(\lambda_p,\boldsymbol{n}_p)$ There are N such solutions, since the matrices have dimension N. The eigenvectors $\boldsymbol{n}_p$ are arbitrary, owing to the proportionality of the matrices. We want to show, for $N > L$, that there are exactly $N - L$

linearly independent solutions (eigenvectors) of the form $\boldsymbol{n}_{p+c} = \begin{bmatrix} \boldsymbol{n}_p \\ \boldsymbol{0} \end{bmatrix}$ to the eigenvalue-problem $(\boldsymbol{M}\lambda^2 + \boldsymbol{C}\lambda + \boldsymbol{K})\boldsymbol{n} = \boldsymbol{0}$ with $\boldsymbol{M}$, $\boldsymbol{C}$ and $\boldsymbol{K}$ defined in (5-27), since these eigenvectors are the only ones that cannot not be excited by forces on the carbody. We calculate

$$(\boldsymbol{M}\lambda_p^2 + \boldsymbol{C}\lambda_p + \boldsymbol{K})\begin{bmatrix} \boldsymbol{n}_p \\ \boldsymbol{0} \end{bmatrix} = \begin{bmatrix} ((1-\alpha)\boldsymbol{M}_p\lambda_p^2 + \boldsymbol{C}_p\lambda_p + \boldsymbol{K}_p)\boldsymbol{n}_p \\ -\boldsymbol{D}^T(\boldsymbol{C}_p\lambda_p + \boldsymbol{K}_p)\boldsymbol{n}_p \end{bmatrix} = \begin{bmatrix} \boldsymbol{0} \\ \boldsymbol{D}^T(1-\alpha)\boldsymbol{M}_p\lambda_p^2\boldsymbol{n}_p \end{bmatrix}$$

Therefore $(\lambda_p, \boldsymbol{n}_{p+c})$ is a solution to $(\boldsymbol{M}\lambda^2 + \boldsymbol{C}\lambda + \boldsymbol{K})\boldsymbol{n} = \boldsymbol{0}$ if and only if $\boldsymbol{D}^T\boldsymbol{M}_p\boldsymbol{n}_p = \boldsymbol{0}$. The matrix $\boldsymbol{D}^T\boldsymbol{M}_p$ has the same rank as $\boldsymbol{D}$, namely L. Therefore, the linear equation $\boldsymbol{D}^T\boldsymbol{M}_p\boldsymbol{n}_p = \boldsymbol{0}$ has $N-L$ indeterminates, see e.g. [5], which means that $\boldsymbol{D}^T\boldsymbol{M}_p\boldsymbol{n}_p = \boldsymbol{0}$ has $N-L$ linearly independent solutions, and, consequently, that there are $N-L$ solutions (eigenvectors) of the form $\boldsymbol{n}_{p+c} = \begin{bmatrix} \boldsymbol{n}_p \\ \boldsymbol{0} \end{bmatrix}$ to the eigenvalue-problem $(\boldsymbol{M}\lambda^2 + \boldsymbol{C}\lambda + \boldsymbol{K})\boldsymbol{n} = \boldsymbol{0}$.

5.3 Approximate models

In this Section, an idea is introduced on how to approximate models. The idea is to compare two models in terms of their characteristic equations using the passenger load parameter as a quantifier of the approximation. The idea can be described as a Taylor expansion, see [5], in the passenger load parameter, of the characteristic equation.

The use of such approximate models is clear from the previous discussion. For instance, one would like to approximate the off-diagonal terms in $\boldsymbol{P}$ by zero. A question of whether this would be an adequate approximation then arises. Another, more far-reaching approximation involves reducing the number of degrees-of-freedom further by representing the passenger load by a single degree-of-freedom.

The theory is first presented, followed by an analytical and a numerical example, with values taken from the case study.

It can be shown[1] that the characteristic equation of the “exact model” (5-27) is of the following form

1. The key to the proof is that $rank(\boldsymbol{P}) = rank(\boldsymbol{D}^T\boldsymbol{M}_p\boldsymbol{D}) = rank(\boldsymbol{D}^T\boldsymbol{D}) = rank(\boldsymbol{D}) = min(L,N)$ and that the number of non-zero roots to the characteristic equation is equal to $rank(\boldsymbol{P})$.

$$g_0(\lambda) + \sum_l P_l^{(1)} g_{1l}(\lambda) + \ldots + \sum_l P_l^{(K)} g_{Kl}(\lambda) = 0 \qquad (5\text{-}31)$$

where $K = \min(L,N)$ and the g:s are polynomials in λ of order $2N+2L$ independent of d_{ij}. $g_0(\lambda) = 0$ is the characteristic equation of the uncoupled system, i.e. $g_0(\lambda) = (\lambda - \lambda_p)^N \prod_{j=1}^{L} (\lambda - \lambda_{cj})$ with somewhat simplified notation[2].

The coefficients $P_l^{(k)}$, where k runs from 1 to K, are introduced as a generalization of the passenger load parameters. The superscript *(k)* denotes the order of generalization; $P_l^{(k)}$ is a product of k elements of $\boldsymbol{P}$. The index l counts the number of terms in the sums.

Definition of an approximate model

An approximate model of the "exact model" (5-27) is a system in which the term $g_0(\lambda) + \sum P_l^{(1)} g_{1l}(\lambda)$ *of its characteristic equation is identical to that of (5-31).*

The approximation is adequate provided that the term $\sum P_l^{(2)} g_{1l}(\lambda) + \ldots + \sum P_l^{(K)} g_{Kl}(\lambda)$ is negligible. This is the case if $P_l^{(k)} \ll P_l^{(1)}$ for $k \geq 2$.

Two different approximate models (to the exact "(N,L)-model") are considered in the following: an "$L \times (1,1)$-model", that is a system consisting of L uncoupled systems of the type in equation (5-21), and a "(1,L)-model" that is a model with only one passenger degree-of-freedom and L carbody degrees-of-freedom.

Using this latter model also means a reduction of the degrees-of-freedom to L+1. Such a reduction is plausible only if the passenger degrees-of-freedom are not to be calculated in the subsequent analysis.

Analytical example

Let $N \geq L = 2$. Then the equations of motion of the $L \times (1,1)$-model can be written as $\boldsymbol{M}\ddot{\boldsymbol{q}} + \boldsymbol{C}\dot{\boldsymbol{q}} + \boldsymbol{K}\boldsymbol{q} = \boldsymbol{0}$ with

2. The short-hand notation $(\lambda - \lambda_p)$ etc. is used in this Section for $(\lambda - \lambda_p)(\lambda - \overline{\lambda_p})$ where $\overline{\lambda_p}$ is the complex conjugate of λ_p. In analogy with the above short-hand notation, λ should be read λ^2.

$$\boldsymbol{q} = \begin{bmatrix} q_{p1} \\ q_{p2} \\ q_{c1} \\ q_{c2} \end{bmatrix} \qquad \boldsymbol{M} = \begin{bmatrix} (1-\alpha)P_1 & 0 & 0 & 0 \\ 0 & (1-\alpha)P_2 & 0 & 0 \\ & & 1+\alpha P_1 & 0 \\ sym & & & 1+\alpha P_2 \end{bmatrix}$$

$$\boldsymbol{C} = 2\begin{bmatrix} \zeta_p\omega_p P_1 & 0 & -\zeta_p\omega_p P_1 & 0 \\ & \zeta_p\omega_p P_2 & 0 & -\zeta_p\omega_p P_2 \\ & & \zeta_{c1}\omega_{c1} + \zeta_p\omega_p P_1 & 0 \\ sym & & & \zeta_{c2}\omega_{c2} + \zeta_p\omega_p P_2 \end{bmatrix} \tag{5-32}$$

$$\boldsymbol{K} = \begin{bmatrix} \omega_p^2 P_1 & 0 & -\omega_p^2 P_1 & 0 \\ & \omega_p^2 P_2 & 0 & -\omega_p^2 P_2 \\ & & \omega_{c1}^2 + \omega_p^2 P_1 & 0 \\ sym & & & \omega_{c2}^2 + \omega_p P_2 \end{bmatrix}$$

Note that this system is obtained from (5-30) by letting the off-diagonal terms in $\boldsymbol{P}$ be zero. The simplification means that the coupling between carbody modes by the passengers is neglected. The approximate system (5-32) is much more advantageous from a computational point of view, owing to the diagonality of $\boldsymbol{P}$.

The equations of motion for (1,*L*)-model are $\boldsymbol{M}\ddot{\boldsymbol{q}} + \boldsymbol{C}\dot{\boldsymbol{q}} + \boldsymbol{K}\boldsymbol{q} = \boldsymbol{0}$ with

$$\boldsymbol{q} = \begin{bmatrix} q_p \\ q_{c1} \\ q_{c2} \end{bmatrix} \qquad \boldsymbol{M} = \begin{bmatrix} (1-\alpha)Nm_p & 0 & 0 \\ & 1+\alpha P_1 & 0 \\ sym & & 1+\alpha P_2 \end{bmatrix}$$

$$\boldsymbol{C} = 2\begin{bmatrix} \zeta_p\omega_p Nm_p & -\zeta_p\omega_p Nm_p MCF_1 & -\zeta_p\omega_p Nm_p MCF_2 \\ & \zeta_{c1}\omega_{c1} + \zeta_p\omega_p P_1 & 0 \\ sym & & \zeta_{c2}\omega_{c2} + \zeta_p\omega_p P_2 \end{bmatrix} \tag{5-33}$$

$$\boldsymbol{K} = \begin{bmatrix} \omega_p^2 Nm_p & -\omega_p^2 Nm_p MCF_1 & -\omega_p^2 Nm_p MCF_2 \\ & \omega_{c1}^2 + \omega_p^2 P_1 & 0 \\ sym & & \omega_{c2}^2 + \omega_p^2 P_2 \end{bmatrix}$$

These equations are obtained by lumping the total passenger mass Nm_p to the single generalized passenger-degree-of-freedom. The modal contribution factors (MCF_1 and

MCF_2) are used as mean displacement-values for carbody modes 1 and 2, respectively. The relation between MCF_j and P_j is discussed in Section 5.1.2, where the relation $P_j = Nm_p(MCF_j)^2$ is shown to hold, if it is assumed that the passengers all have the same weight.

In the simple case of N=L=2, the polynomial g_0 is $g_0(\lambda) = (\lambda-\lambda_p)^2(\lambda-\lambda_{c1})(\lambda-\lambda_{c2})$ using the short-hand notation defined in the footnote earlier; the polynomial is thus of degree eight.

The characteristic equation of the exact *(L,L)*-model is, in this case, defined by

$$\begin{aligned} P_1^{(1)} &= P_1 = m_{p1}d_{11}^2 + m_{p2}d_{21}^2 & g_{11}(\lambda) &= \lambda(\lambda-\lambda_p)(\lambda-\lambda_{c2}) \\ P_2^{(1)} &= P_2 = m_{p1}d_{12}^2 + m_{p2}d_{22}^2 & g_{12}(\lambda) &= \lambda(\lambda-\lambda_p)(\lambda-\lambda_{c1}) \\ P_1^{(2)} &= m_{p1}m_{p2}(d_{11}d_{22}-d_{12}d_{21})^2 & g_{21}(\lambda) &= \lambda^2 \end{aligned} \qquad (5\text{-}34)$$

As for the $L\times(1,1)$-model, it turns out that the only difference is that

$$P_1^{(2)} = P_1P_2$$

The (1,*L*)-system also has a different g_{21}:

$$P_1^{(2)} = P_1P_2 \qquad g_{21}(\lambda) = \lambda^2 - 1$$

Thus, according to the definition, both the $L\times(1,1)$-model and the *(*1,*L)*-model are approximate models to the exact (*L*,*L*)-model.

Numerical example

Let *L*=5 and consider the carbody-modes G1 to G5 in Chapter 3. Consider the passenger distribution “Middle” in Figure 3-6. The number of passenger groups is *N*=8. The modal parameters, the passenger mass-distribution, the vertical mode-shape-values and the ***P***-matrix are summarized in Table 5-2, Table 5-3 and Table 5-4.

Table 5-2 Modal parameters of carbody-modes G1 to G5.

j	1	2	3	4	5
f_{cj} (Hz)	8.1	9.2	12.5	13.5	18.2
ζ_{cj} (%)	3.7	1.6	1.5	4.4	3.4

Table 5-3 ***Passenger-group masses and vertical mode-shape values.*** *Carbody-modes G1 to G5 and case "Middle".*

i	1	2	3	4	5	6	7	8
m_{pi} [kg]	209	245	398	386	262	160	259	290
d_{i1} [mm]	-5.3	-4.5	3.6	-5.8	3.7	2.4	-5.5	2.9
d_{i2} [mm]	4.5	4.9	7.6	7.8	5.2	4.0	6.9	6.8
d_{i3} [mm]	-4.2	7.9	3.7	4.6	-1.7	3.3	-2.4	2.0
d_{i4} [mm]	-6.4	-4.0	11.6	10.2	-1.7	5.2	2.3	4.1
d_{i5} [mm]	6.3	-4.9	7.8	3.9	-3.1	7.0	9.2	14.2

Table 5-4 ***The P-matrix for carbody-modes G1 to G5.*** *[kgm^2]*

	G1	G2	G3	G4	G5
G1	0.044	-0.015	0.004	0.006	-0.001
G2		0.092	0.030	0.068	0.080
G3			0.038	0.038	0.011
G4				0.118	0.007
G5	*sym*				0.135

The human-body parameters are $\alpha = 0.1$, $f_p = 6$ Hz and $\zeta_p = 0.5$.

In Figure 5-6, a comparison, in terms of root locus, between the "exact" (L,L)-model (dots), the $L \times (1,1)$-model (circles) and the (1,L)-model (crosses) is shown.

As is evident from the figure, all three models lie closely together in their prediction. Measured values for the empty carbody, cf. Table 3-4, are indicated (by stars) for the sake of comparison. Both approximate models are thus appropriate. The largest difference appears for modes G1 and G4 using the (1,L)-model. Here, also, the magnitude of the passenger load parameters P_j are well below 1. The highest value is 0.135 kgm^2, see Table 5-4. The second-order-generalized passenger-load parameters are therefore small, in the order of 0.01 kg^{2}m^4.

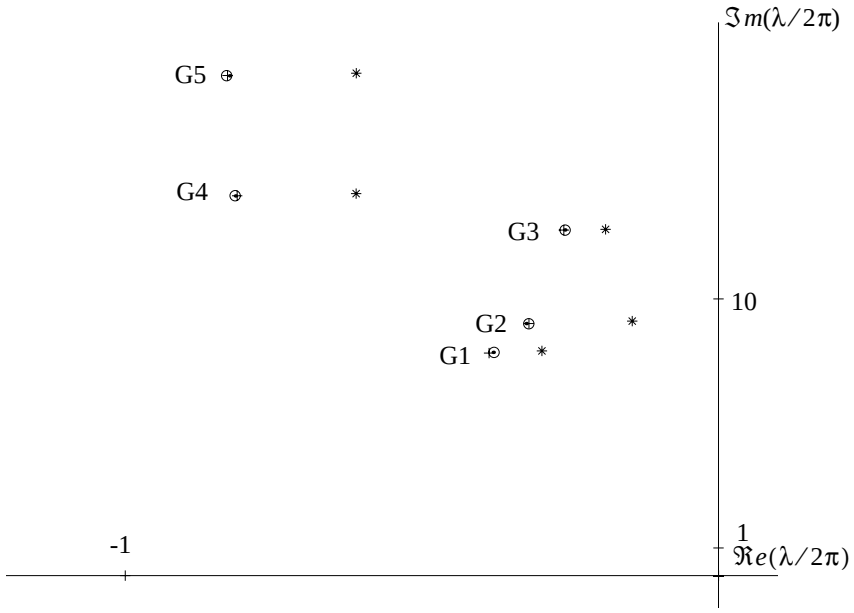

Figure 5-6 ***Root-locus comparison between the (L,L)-model (dots), the $L\times(1,1)$-model (circles) and the (1,L)-model (crosses).*** *N.B. the scale. Measured values for the empty carbody are indicated (stars) for comparison.*

5.4 Inclusion of seating dynamics

5.4.1 Passenger and seat model

The following model is adopted from [44]. Consider a passenger with impedance $Z_p(\omega)$ sitting on a seat modelled by the seat model 1 in Figure 4-5. The resulting system is illustrated in Figure 5-7.

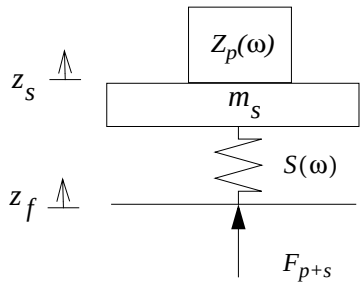

Figure 5-7 ***Passenger and seat model.***

Force equilibrium at the top of the spring yields

$$S(\omega)(z_f - z_s) = (Z_p(\omega)\mathrm{i}\omega - m_s\omega^2)z_s \tag{5-35}$$

from which the seat transmissibility, i.e. the frequency-response function between the *displacements* z_s and z_f, i.e. z_s/z_f, is

$$T_s(\omega) = \frac{S(\omega)}{S(\omega) + Z_p(\omega)\mathrm{i}\omega - m_s\omega^2} \tag{5-36}$$

From Figure 5-7, it is clear that the mass m_s follows the passenger. It represents the upper part of the seat-pan. It may be weighing some tenths of a kilogram and might therefore be neglected as compared to the weight of the seat occupant.

As the magnitude of S increases, corresponding to a stiffer seat, the seat transmissibility $T_s(\omega)$ approaches unity. In other words, sitting on an infinitely stiff seat is like sitting directly on the floor.

The force F_{p+s} is

$$F_{p+s} = S(\omega)(z_f - z_s) = (Z_p(\omega)\mathrm{i}\omega - m_s\omega^2)z_s = (Z_p(\omega)\mathrm{i}\omega - m_s\omega^2)T_s(\omega)z_f \tag{5-37}$$

From equation (5-37), one finds that this passenger-seat impedance $Z_{p+s}(\omega) = \frac{F_{p+s}}{z_s\mathrm{i}\omega}$ is

$$Z_{p+s}(\omega) = (Z_p(\omega) + m_s\mathrm{i}\omega)T_s(\omega) \tag{5-38}$$

The normalized apparent mass of the passenger-seat system is, in analogy with (4-9):

$$T_{p+s}(\omega) = (T_p(\omega) + m_s/m_p)T_s(\omega) \tag{5-39}$$

If m_s/m_p is assumed to be a constant, then the normalized apparent mass of the passenger-seat system becomes independent of the individual body mass. This simplifying assumption is made here by making the (stronger) assumption

$$m_s/m_p = 0 \tag{5-40}$$

This approximation should be adequate, since m_s is small compared to m_p. The assumption will make the passenger load parameter useful, also in this case, where seat transmissibility is taken into account.

Finally, one may note that the passenger-seat normalized apparent mass $T_{p+s}(\omega)$ is proportional to the seat transmissibility $T_s(\omega)$, and that for a totally stiff seat $T_{p+s}(\omega) = T_p(\omega)$ holds.

5.4.2 Passenger-seat-carbody model

To begin with, one passenger on a seat and one carbody mode are considered. Let the *passenger* be represented by Model B and the seat by Model 2, see Figure 5-8.

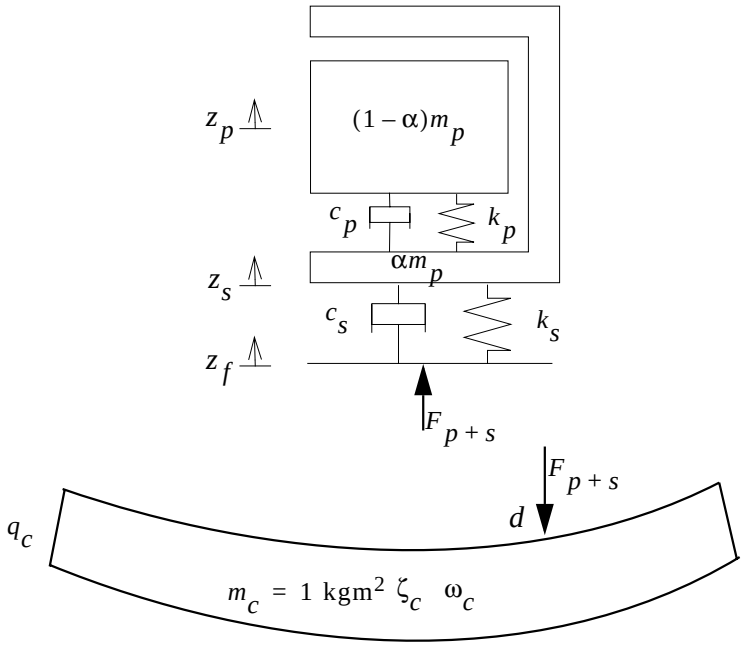

Figure 5-8 Proposed passenger-seat-carbody model.

The unsprung mass in the human-body model stays in permanent contact with the seat-pan motion, that is the z_s of the human-body model is identical to the z_s of the seat model. Moreover, z_f is directly related to q_c by

$$z_f = dq_c \tag{5-41}$$

cf. (5-10). The equations of motion of the system are then $\boldsymbol{M}\ddot{\boldsymbol{q}} + \boldsymbol{C}\dot{\boldsymbol{q}} + \boldsymbol{K}\boldsymbol{q} = \boldsymbol{0}$ with

$$\boldsymbol{q} = \begin{bmatrix} z_p \\ z_s \\ q_c \end{bmatrix} \quad \boldsymbol{M} = \begin{bmatrix} (1-\alpha)m_p & 0 & 0 \\ 0 & \alpha m_p & 0 \\ 0 & 0 & 1 \end{bmatrix}$$

$$\boldsymbol{C} = \begin{bmatrix} 2\zeta_p\omega_p m_p & -2\zeta_p\omega_p m_p & 0 \\ -2\zeta_p\omega_p m_p & 2\zeta_p\omega_p m_p + c_s & -c_s d \\ 0 & -c_s d & 2\zeta_c\omega_c + c_s d^2 \end{bmatrix} \tag{5-42}$$

$$\boldsymbol{K} = \begin{bmatrix} \omega_p^2 m_p & -\omega_p^2 m_p & 0 \\ -\omega_p^2 m_p & \omega_p^2 m_p + k_s & -k_s d \\ 0 & -k_s d & \omega_c^2 + k_s d^2 \end{bmatrix}$$

The characteristic equation for the passenger-seat-carbody model is

$$\begin{aligned} &(\omega_p^2 + 2\zeta_p\omega_p\lambda + (1-\alpha)\lambda^2)(\omega_c^2 + 2\zeta_c\omega_c\lambda + \lambda^2) + \\ &\left(P + \frac{m_p}{k_s + \lambda c_s}(\lambda^2 + 2\zeta_c\omega_c\lambda + \omega_c^2)\right)\lambda^2(\omega_p^2 + 2\zeta_p\omega_p\lambda + \alpha(1-\alpha)\lambda^2) = 0 \end{aligned} \tag{5-43}$$

Note that this equation is identical to (5-13) for $\frac{m_p}{k_s + \lambda c_s}(\lambda^2 + 2\zeta_c\omega_c\lambda + \omega_c^2) = 0$. Hence, in a sense the quotient $\frac{m_p}{(k_s + \lambda c_s)P}$ quantifies the relative importance of the seat dynamics. It would be convenient if the seat parameters c_s and k_s were proportional to m_p, since this would simplify the equations of motion and the characteristic equation. In fact, since many current conventional seats tend to have a vertical resonance frequency close to 4 Hz [44], k_s is, in a sense, proportional to m_p. The proportionality does not necessarily hold for c_s, however. But, if (5-7) is assumed, then the quotient c_s/m_p is the same for all passengers.

Numerical example

In the following example k_s is varied in the interval of $64 \text{ kN/m} < k_s < 96 \text{ kN/m}$ for a person weighing 80 kg. The choice of seat parameters is based on fitted parameter values, see Figure 3-14 and Figure 6-6. In Figure 5-9 the sensitivity of the relative damping towards seat stiffness is illustrated.

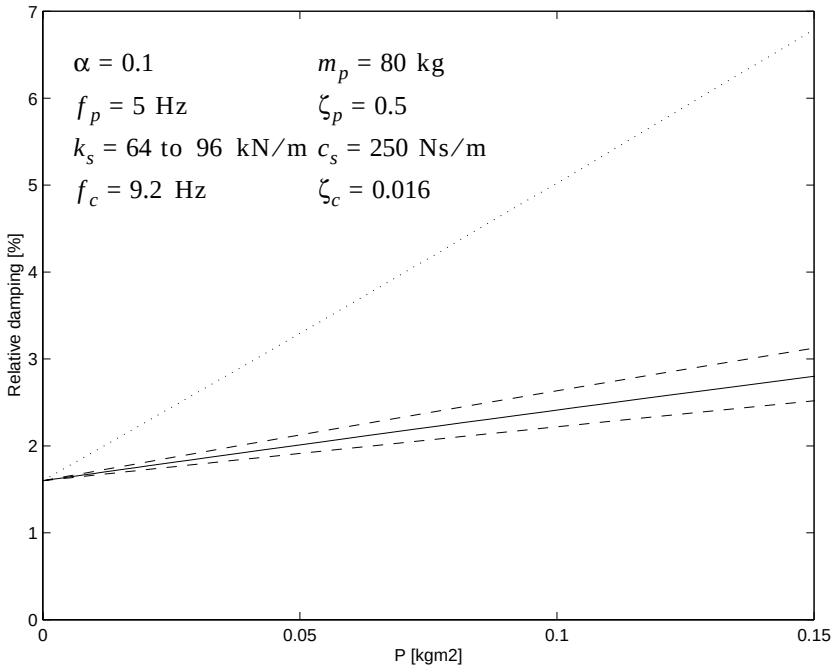

Figure 5-9 ***Relative damping of the carbody mode G2 as a function of the passenger load parameter P. Illustration of the sensitivity towards seat stiffness.*** *The dotted line corresponds to very high seat stiffness. The solid line corresponds to a typical value of k_s (80 kN/m for a person weighing 80 kg). The dashed lines show the result of a 20% variation in seat stiffness.*

From Figure 5-9, it is obvious that the introduction of the seat in the model has a significant influence on the interaction between carbody and passengers. For a seat with a very high stiffness, the curve, i.e. the dotted curve, approaches that of the passenger-carbody model. For a softer seat, the predicted interaction between passenger and carbody becomes less important owing to the fact that the passengers are then more loosely coupled to the carbody.

5.4.3 Several passengers, seats and carbody modes

The passenger-seat-carbody model can be generalized to include *N* passengers, *N* seats and *L* carbody modes, referred to as the (*N*+*N*,*L*)-model. In this case (5-41) changes to

$$\boldsymbol{z}_f = \boldsymbol{D}\boldsymbol{q}_c \tag{5-44}$$

The equations of motion are analogous to (5-42) and read $\boldsymbol{M}\ddot{\boldsymbol{q}} + \boldsymbol{C}\dot{\boldsymbol{q}} + \boldsymbol{K}\boldsymbol{q} = \boldsymbol{0}$ with

$$\boldsymbol{q} = \begin{bmatrix} \boldsymbol{z}_p \\ \boldsymbol{z}_s \\ \boldsymbol{q}_c \end{bmatrix} \quad \boldsymbol{M} = \begin{bmatrix} (1-\alpha)\boldsymbol{M}_p & 0 & 0 \\ & \alpha\boldsymbol{M}_p & 0 \\ sym & & \boldsymbol{I} \end{bmatrix}$$

$$\boldsymbol{C} = \begin{bmatrix} 2\zeta_p\omega_p\boldsymbol{M}_p & -2\zeta_p\omega_p\boldsymbol{M}_p & 0 \\ & 2\zeta_p\omega_p\boldsymbol{M}_p + \boldsymbol{C}_s & -\boldsymbol{C}_s\boldsymbol{D} \\ sym & & \boldsymbol{C}_c + \boldsymbol{D}^T\boldsymbol{C}_s\boldsymbol{D} \end{bmatrix} \tag{5-45}$$

$$\boldsymbol{K} = \begin{bmatrix} \omega_p^2\boldsymbol{M}_p & -\omega_p^2\boldsymbol{M}_p & 0 \\ & \omega_p^2\boldsymbol{M}_p + \boldsymbol{K}_s & -\boldsymbol{K}_s\boldsymbol{D} \\ sym & & \boldsymbol{K}_c + \boldsymbol{D}^T\boldsymbol{K}_s\boldsymbol{D} \end{bmatrix}$$

where

$$\boldsymbol{K}_s = \begin{bmatrix} k_{s1} & & 0 \\ & \cdots & \\ 0 & & k_{sN} \end{bmatrix} \quad \boldsymbol{C}_s = \begin{bmatrix} c_{s1} & & 0 \\ & \cdots & \\ 0 & & c_{sN} \end{bmatrix}$$

with $k_{s1} \ldots k_{sN}$ and $c_{s1} \ldots c_{sN}$ being, respectively, the stiffness and damping constants of the seats. It is clear from (5-45) that if it is assumed that $\boldsymbol{K}_s$ and $\boldsymbol{C}_s$ are proportional to $\boldsymbol{M}_p$, then the $\boldsymbol{P}$-matrix will again appear in the equations of motion. As in the simpler case of Section 5.4.2, the assumption that $\boldsymbol{K}_s$ is proportional to $\boldsymbol{M}_p$ seems reasonable, in view of the measurements presented in [52]. The assumption on $\boldsymbol{C}_s$ might be less adequate, although it would simplify the equations. It would, for instance, be then possible to reduce the system to an exact (L+L,L) system, in analogy with the reduction made in Section 5.2.3. Here also, quotients of the type $\dfrac{m_p}{(k_s + \lambda c_s)P}$ may be studied in order to quantify the relative importance of the seat properties.

5.4.4 Seat transmissibility

The parameters c_s and k_s in Figure 5-8 may be estimated from measured seat transmissibility using equation (5-36) with $m_s = 0$. However, this expression also contains the human-body impedance of the seat occupant, which in modelling depends on the undamped circular eigenfrequency ω_p, the relative damping ζ_p, the fraction of unsprung mass α and the mass m_p. Therefore, assuming the mass m_p is known, the remaining five parameters must be obtained simultaneously by curve-fitting. This is

possible because a variation of the different parameters yields different changes in the shape of the transmissibility curves. Moreover, the human-body parameters should differ only little from standard values. The influence of the variation of k_s and c_s is illustrated in Figure 5-10, cf. Figure 4-4. See also Section 6.2.

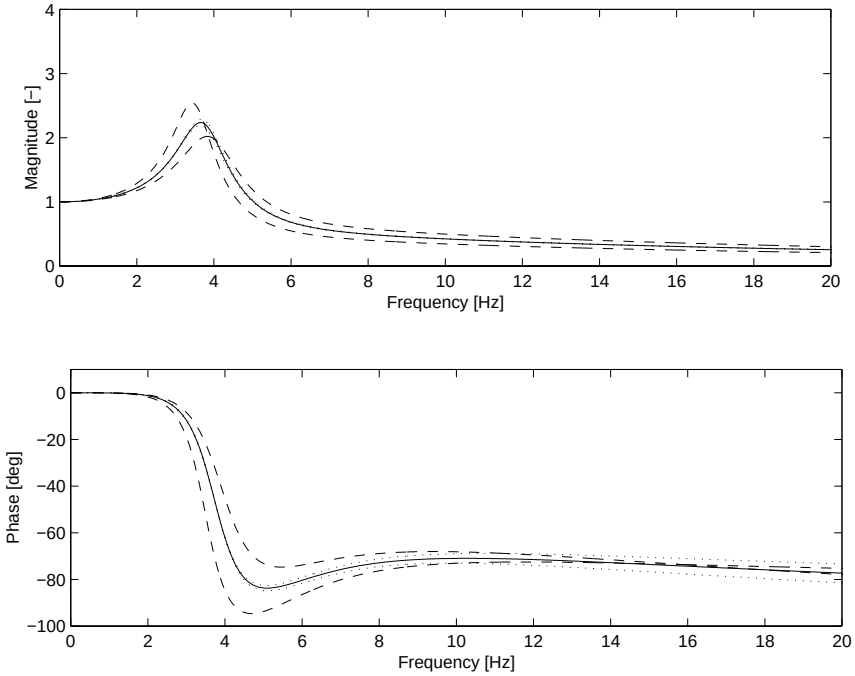

Figure 5-10 Seat transmissibility. *Dashed lines: ±20 % variation of the parameter k_s. Dotted lines: ±20 % variation of the parameter c_s. Nominal passenger and seat parameters as in Figure 5-9.*

5.5 Summary and conclusions

In summary, the proposed models of the passenger-carbody interaction that are derived in this chapter are simple and general. They are intended to explain and estimate the main influence of the passengers on the carbody dynamics and to predict vibration levels for ride-comfort evaluation. The passengers are modelled by human-body models found in literature. A modal model of the carbody is used.

The main assumption on which these simple models are based is that the passengers are supposed to be alike, viewed as mechanical systems. Their normalized apparent mass, a term used by [51], is assumed to be the same for each passenger. Important key parameter are the passenger load parameters, or in a more generalized form, the “passenger load matrix”. It describes how the passengers affect each individual carbody mode, and also how they couple the carbody modes to each other.

The passenger-carbody model is equivalent to the case with infinitely stiff seats.

Simple seat models are difficult to achieve, owing to the complexity and diversity in design. Here, a simple vertical seat model is proposed, but it is based on quite far-reaching assumptions. Firstly, it is a priori only applicable to seats of the same type as in the case study. Secondly, it is assumed that the only interaction that takes place between seat and passenger is a vertical force at the seat pan. However, the model allows one to describe how seat stiffness and damping affects the passenger-carbody interaction, at least in principle.

A contribution is made to the field of what might be called reduction and approximation theory. It is shown that the dynamics of L carbody modes and $N>L$ passengers can be reduced without approximation to a system with $2L$ degrees-of-freedom, provided that each passenger is modelled by a single degree-of-freedom. The idea of approximate models is introduced, meaning that dynamical systems are compared in terms of their characteristic equation and the passenger load parameter. The same principles can be used when seating dynamics is considered.

The proposed interaction models are validated against measurements in Chapter 6, and they are implemented and utilized in time-domain simulations in Chapter 7.

6 Comparison of model and measurement results

The predictions of the proposed models of Chapter 5 are compared here with results of the measurements in Chapter 3. Essentially two types of measurements have been made: passenger-load measurements, see Section 6.1, and seat-transmissibility measurements, see Section 6.2

6.1 Passenger load

Measurements and model predictions are compared here in terms of root loci of the carbody modes and in terms of frequency-response curves. The two passenger distributions “Middle” and “Ends” are considered, with *N*=8 and 10, respectively, cf. Figure 3-6. In the model predictions, the *P*-values obtained from the measurements are used, see Table 5-4. Also, the measured carbody eigenfrequencies and the relative-damping values of the empty carbody are used in the model prediction.

Figure 6-1 shows measurement results for the excitation amplitude of “50%”.

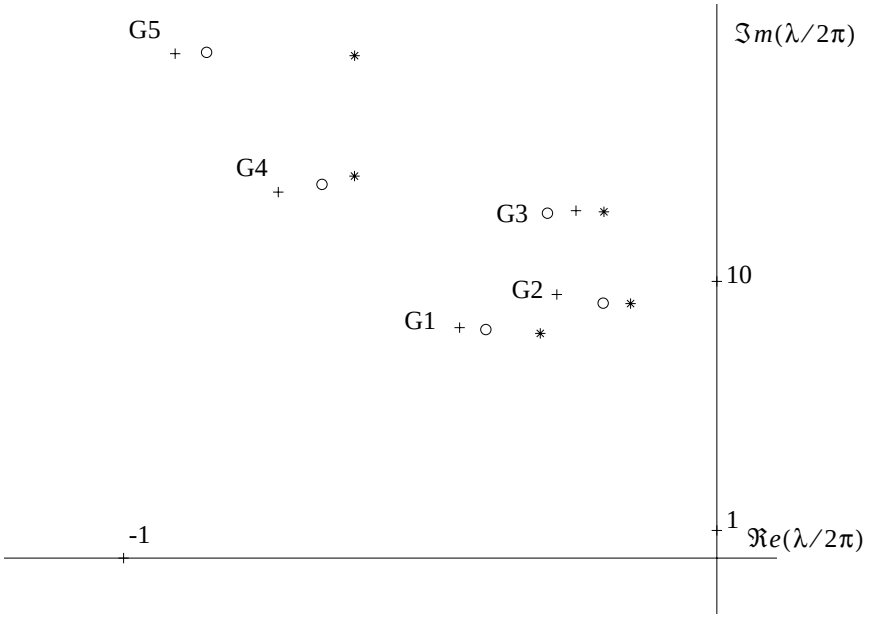

Figure 6-1 ***Measured, i.e. synthesized, root loci of five carbody modes for empty carbody and two different passenger distributions.*** *Amplitude, “50%”. N.B. the scale. Stars: empty carbody, circles: passenger distribution “Ends” and crosses: passenger distribution “Middle”.*

The figure summarizes the results of the passenger-load measurements by showing root loci for the five identified global carbody modes for the passenger distributions “Middle” and “Ends” as well as for the empty carbody. An alternative view is given in Figure 3-13, which also contains information on the *P*-values. As observed in connection to that

figure, the main trends are an almost linear increase in relative damping with *P*, and a linear change (an increase in most cases) in undamped eigenfrequency with *P*.

Two types of models are considered here, the passenger-carbody model proposed in Section 5.2.3 and the passenger-seat-carbody model proposed in Section 5.4.3. It is shown in Section 5.3 that the reduced (*L*,*L*)-model, the approximate $L \times (1,1)$-model and the approximate (1,*L*)-model give almost identical results for the SJ-B7M vehicle. Only results of the reduced (*L*,*L*)-passenger-carbody model and the (*L*+*L*,*L*) passenger-seat-carbody model are therefore shown here.

All model results are based on the "50%-amplitude" *P*-values, and can thus be compared to the root loci of Figure 6-1.

Figure 6-2 shows the root loci of the proposed (*L*,*L*)-passenger-carbody model.

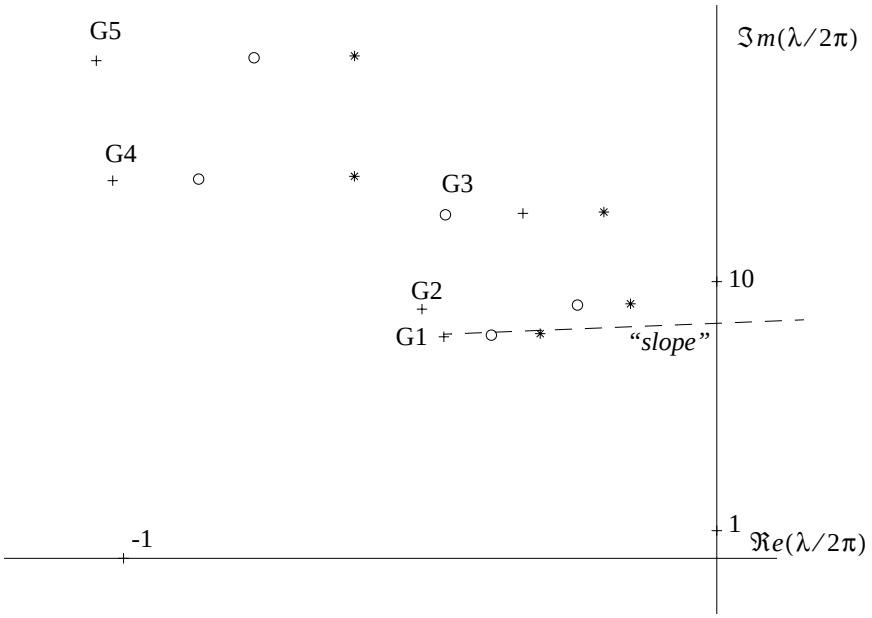

Figure 6-2 ***Predicted root loci of five carbody modes for empty carbody and two different passenger distributions.*** *Proposed (L,L)-passenger-carbody model with L=5, f_p = 6 Hz, ζ_p = 0.5 and α = 0.1. N.B. the scale. Stars: empty carbody (identical to measurements), circles: passenger distribution "Ends" and crosses: passenger distribution "Middle". To be compared with Figure 6-1.*

The trends observed in the measurement data are captured in the predictions, the order of crosses and stars are the same, and the relative spacing between the stars, crosses and circles is satisfactory. The predicted interaction is nevertheless exaggerated, i.e. the absolute spacing is too large (G1 being an exception), but this is not surprising, since an infinitely stiff seat is assumed in the prediction model. But the "slope", as defined in Figure 6-2, is, in some cases, inclined in the wrong direction.

Figure 6-3 shows the prediction of the proposed (*L*+*L*,*L*)-passenger-seat-carbody model with the seat and human-body parameters obtained from the seat-transmissibility measurements presented in Section 6.2: f_p = 6 Hz, ζ_p = 0.5, α = 0.1, c_s = 250 Ns/m and k_s = 84 kN/m for a human-body mass of m_p = 80 kg.

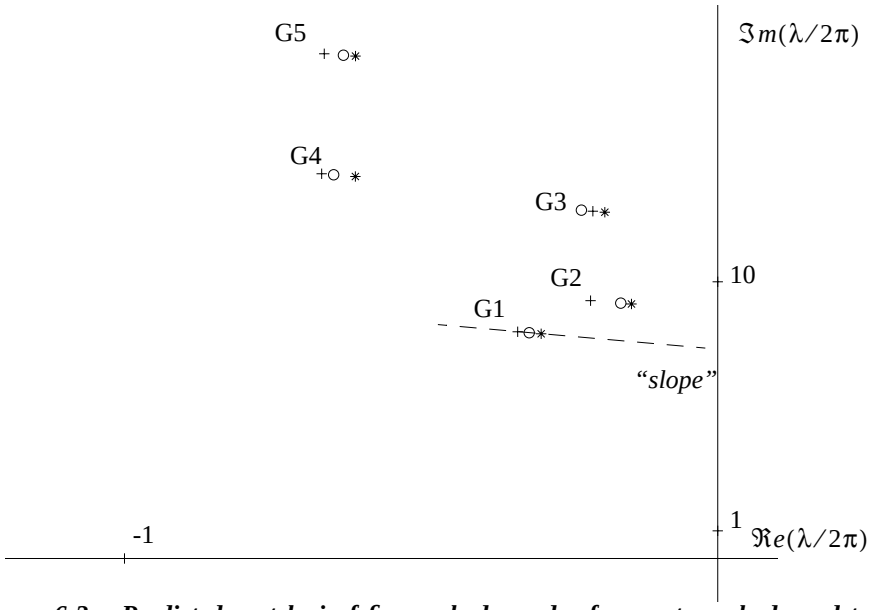

Figure 6-3 ***Predicted root loci of five carbody modes for empty carbody and two different passenger distributions.*** *Proposed (L+L,L)-passenger-seat-carbody model with L=5, f_p = 6 Hz, ζ_p = 0.5, α = 0.1, c_s = 250 Ns/m, k_s = 84 kN/m and m_s = 0 for m_p = 80 kg. N.B. the scale. Stars: empty carbody (identical to measurements), circles: passenger distribution "Ends" and crosses: passenger distribution "Middle".*

As seen from the figure, the passenger-seat-carbody model predicts significantly smaller interaction than the passenger-carbody model does. This is expected as discussed in Section 5.4; for a softer seat the predicted interaction between passenger and carbody becomes less important owing to the fact that the passenger are more loosely coupled to the carbody. The passenger-seat-carbody model also predicts a smaller interaction than what is observed in the measurements, cf. Figure 6-1. However, the predicted "slopes" generally agree better with the measurements for the passenger-seat-carbody model than for the passenger-carbody model.

Based on the measurements, one may conclude that the passenger-carbody model gives a suitable upper-boundary, while the passenger-seat-carbody model gives a lower boundary for the interaction.

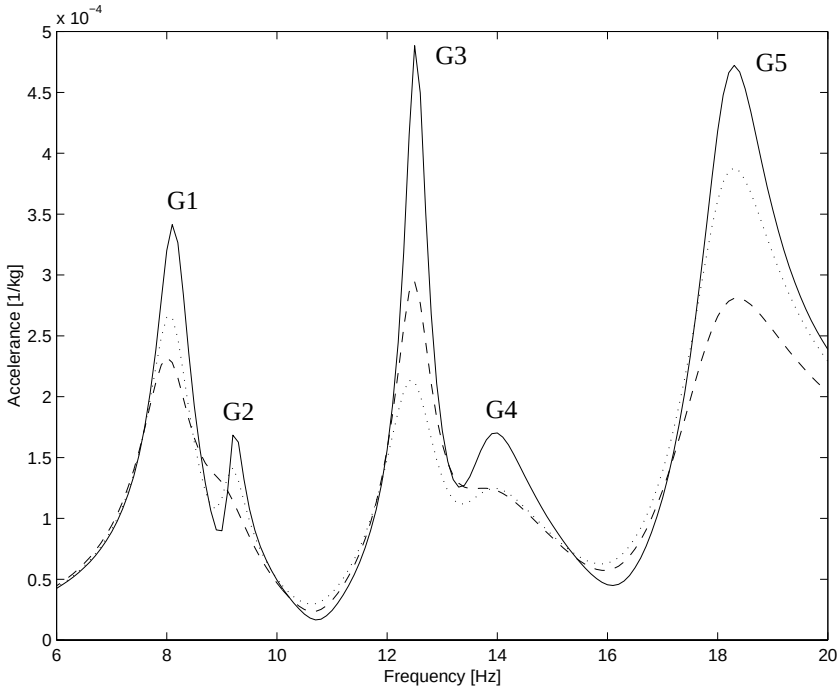

Figure 6-4 ***Predicted point accelerance (magnitude).*** *Proposed (L,L)-passenger-carbody model with L=5, f_p=6 Hz, ζ_p = 0.5 and α=0.1. Solid line: empty carbody (identical to Figure 3-10), dotted line: passenger distribution "Ends" and dashed line: passenger distribution "Middle". To be compared with Figure 3-9 and Figure 3-10.*

Figure 6-4 and Figure 6-5 show the predicted point accelerance based on the (*L*,*L*)-passenger-carbody and the (*L*+*L*,*L*)-passenger-seat-carbody model, respectively. The point accelerance is obtained by including an external force acting on the five carbody modes in the equations of motion in Chapter 5. The vertical displacement values at the excitation point are used to calculate the modal forces on the five carbody modes.

A comparison of these to the synthesized point accelerance in Figure 3-10 and the measured point accelerance in Figure 3-9 gives an idea of how faithful the models are. The passenger-carbody model shows the best agreement for modes G1 and G5, while the passenger-seat-carbody model is better for the modes G2, G3 and G4. The synthesized point accelerance lies in between the two predicted accelerance curves, which supports the statement above that the passenger-carbody model seems to give a suitable upper-boundary, while the passenger-seat-carbody model gives a lower boundary for the interaction.

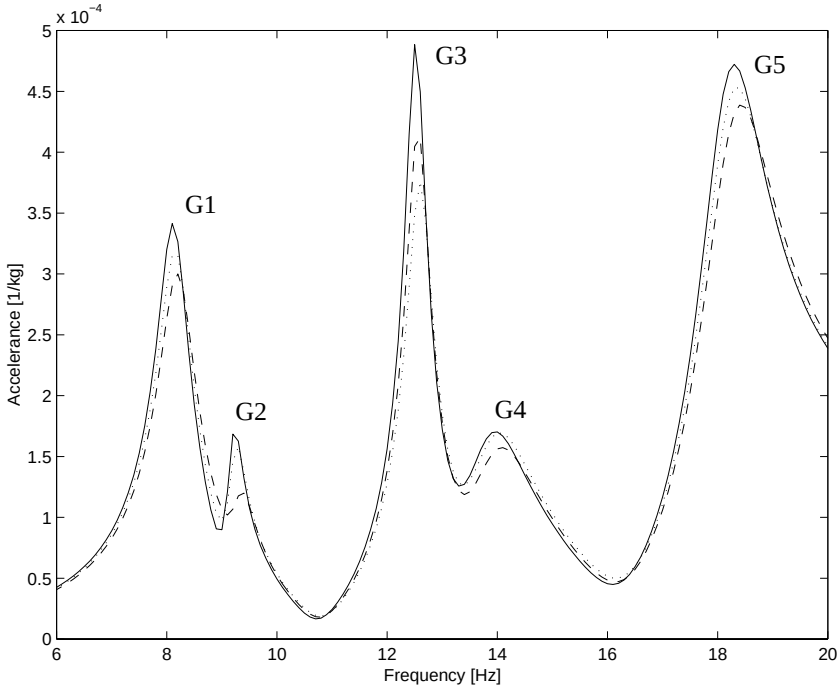

Figure 6-5 ***Predicted point accelerance (magnitude).*** *Proposed (L+L,L)-passenger-seat-carbody model with L=5, f_p=6 Hz, ζ_p = 0.5, α = 0.1, c_s = 250 Ns/m, k_s= 84 kN/m and m_s = 0 for m_p = 80 kg. Solid line: empty carbody (identical to Figure 3-10), dotted line: passenger distribution "Ends" and dashed line: passenger distribution "Middle". To be compared with Figure 3-9 and Figure 3-10.*

6.2 Seat transmissibility

The seat-transmissibility measurements make it possible to estimate the dynamical parameters of the seat, i.e. the seat stiffness and the seat damping.

Figure 6-6 shows the measured seat transmissibility of seat 24 in the SJ-B7M vehicle and a corresponding fitted-model seat transmissibility. The solid line corresponds to the seat transmissibility measured at a "100%" excitation amplitude, cf. Figure 3-14. The dashed line corresponds to the model prediction with fitted seat parameters. The fitting was made manually focusing on the measured magnitude peak at 4 Hz, and the magnitude for frequencies above 10 Hz. The passenger-seat model of Section 5.4.2 is used, that is the seat-pan mass is neglected. Nearly average human-body parameter values are obtained: f_p = 6 Hz, ζ_p = 0.5 and α = 0.1. The fitted seat parameters are c_s = 250 Ns/m and k_s = 84 kN/m. The weight of the seat occupant is m_p=80 kg.

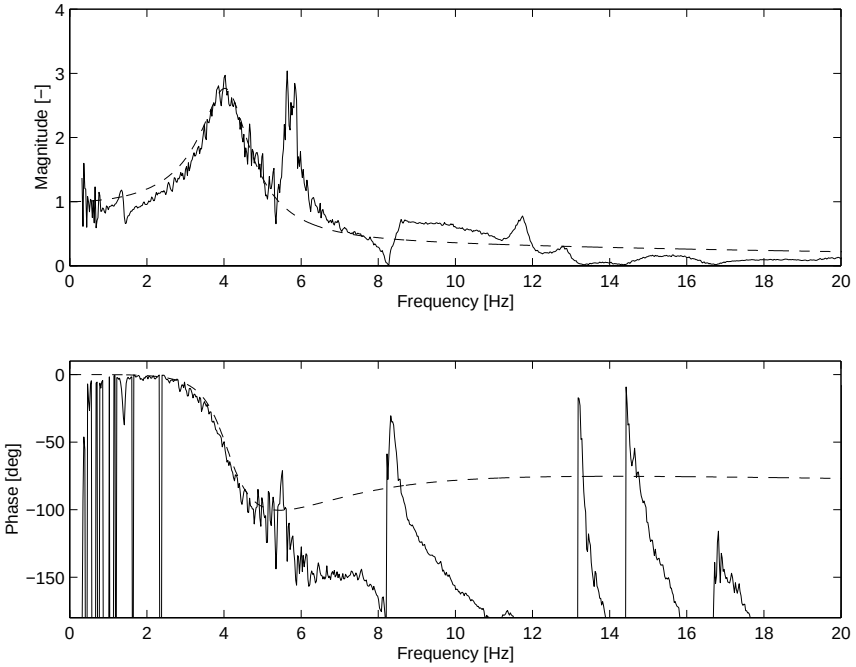

Figure 6-6 ***Measured and fitted model seat transmissibility.*** *Solid line: measured. Dashed line: fitted model.*

It is clear that the model does not reproduce all features of the measured seat transmissibility. The peak at 6 Hz is neglected, for instance. And the fit of the phase is poor above 5 Hz. However, the fit at the peak of 4 Hz is rather good, and the parameter values obtained are reasonable. It should also be kept in mind that, ideally, the model response should have been compared with seat-transmissibility measurements for all 35 passengers.

6.3 Conclusions

In conclusion, the comparison is rather favourable for the proposed models, and the passenger distribution can be taken into account using the passenger load parameter.

The passenger-carbody model overestimates the interaction, whereas the passenger-seat-carbody model gives a lower boundary for the interaction. As concluded in Section 5.5, the assumptions made for the passenger-seat models are far-reaching, and, therefore, the predictions may not be expected to be fully reliable. However, in view of the comparison presented in the present chapter, it seems as though the passenger-seat-carbody model is adequate and useful, at least to give a lower boundary for the interaction. Finally, it is worthwhile to repeat, in this context, the comment made in relation to Figure 5-3, that the alternative to model the passengers as unsprung masses is not recommended, since such a model fails to predict the increase in relative damping and it also underestimates the eigenfrequencies.

7 Track-induced passenger-carbody interaction

7.1 Implementation of passenger models for simulation

The measurements and the models presented in Chapters 3 and 5, as well as the results of Chapter 6, point to some basic mechanisms in the interaction between passengers and carbody global mode-shapes, but when it comes to implementation in a simulation software for rail-vehicle dynamics, a number of additional questions arise, such as: how accurate is available data? How accurate is the rest of the model? What should be predicted? What level of accuracy in prediction is needed? Is computational time crucial? Are model complexity and user-friendliness crucial?

The model choice stands between:
- the passenger-carbody model or the passenger-seat-carbody model
- using the original, the reduced or an approximate model.

From the validation carried out in the previous chapter it is concluded that the passenger-carbody model gives a reasonable upper boundary for the interaction. The passenger-seat-carbody model, on the other hand, gives a reasonable lower boundary. Here, both the passenger-carbody model and the passenger-seat-carbody model are therefore implemented in the GENSYS model described in Chapter 2.

It is shown in Chapter 5 that the (1,L)-model is an adequate approximation of the original (N,L)-model, at least in terms of root locus for the measured cases. Here, both a (1,L)-model and an (N,L)-model are implemented. From a computational viewpoint, the (1,L)-model is preferable, since it introduces only one extra degree-of-freedom, whereas the original model needs N extra degrees-of-freedom. 2N extra degrees-of freedom are needed for the original passenger-seat-carbody model.

In practice, the reduced models cannot be straightforwardly used without implementing the reduction process into the core of the simulation code. Note also that there must be three passenger degrees-of-freedom corresponding to carbody bounce (vertical displacement), roll (rotation about the longitudinal axis) and pitch (rotation about the lateral axis), respectively, for the reduced passenger-carbody model, giving L+3 passenger degrees-of-freedom. The kind of implementation mentioned above is not made here.

Four models are thus demonstrated in this chapter:
- the (N,L)-passenger-carbody model
- the (1,L)-passenger-carbody model
- the (N+N,L)-passenger-seat-carbody model and
- the (1+1,L)-passenger-seat-carbody model.

A short note on the actual implementation: the carbody structural modes are added to the rigid carbody modes. The unsprung mass of the passengers, αM_p, where M_p denotes the total mass of the passengers, is modelled by adding mass and the corresponding moments of inertia to the original carbody mass-properties. The coupling to the carbody

rigid-body modes is thus taken into account. However, in the longitudinal direction, in the lateral direction and in yaw (rotation about vertical axis), the total mass must be added, since only vertical forces between passengers and carbody are considered in the present models. The unsprung part of the passengers are modelled as masses with only a vertical degree-of-freedom. The masses are mounted on linear springs and linear viscous dampers attached to the carbody. For the (1,*L*)-model and the (1+1,*L*)-model, the *MCF* are used as generalized vertical displacements, cf. (5-33).

7.2 Example: Complete simulation

The present example builds on the measurements and simulations presented in Section 2.1. In Figure 2-10, results from measurement and simulation are compared in terms of comfort-weighted vertical r.m.s.-values of acceleration. Here, the same simulation model is used, modified only to include passengers and seats. The main aim of this example is to investigate the influence of passenger load on ride comfort.

The human body parameters are f_p = 6 Hz, ζ_p = 0.5 and α = 0.1. The seat parameters are m_s = 0 kg, k_s =75 kN/m and c_s = 300 Ns/m for the assumed average human-body mass of m_p = 75 kg. The carbody modal-contribution-factors (*MCF*) of the eight calculated modes, cf. Figure 2-9, are given in Table 2-2. The relation between *MCF* and *P* is discussed in Section 5.1.2. The same carbody relative damping as in [13], that is 1%, is used for the sake of comparison. Here *N*=10, corresponding to the 10 acceleration positions in the side-sills used during the on-track measurements, cf. Figure 2-1. The mass of several passengers is thus lumped to each one of the accelerometer positions.

Two parameter studies are carried out. In Section 7.2.1, the total passenger mass M_p is varied between 0 and 6,000 kg, corresponding to a full vehicle with 80 passengers. In Section 7.2.2, the passengers are not included, but the carbody relative damping is varied. The aim of the latter sensitivity study is twofold. Firstly, to show how the influence of the passenger load on the carbody mode-shape can be approximately modelled by increasing the relative damping of the carbody mode-shapes. In this case, however, it is difficult to decide how much relative damping should be increased, but once again, the passenger-load parameters can be used, cf. Figure 5-9. The second aim is to investigate how sensitive ride comfort is to carbody relative damping. It is worthwhile to repeat in this context that the carbody relative damping is seldom known exactly in practice.

7.2.1 Parameter study: Passenger mass

Figure 7-1 shows the prediction made by an (*N*,*L*)-model with *N*=10 passenger groups and *L*=8 carbody mode shapes. The simulation results can thus be compared with those of Figure 2-10.

In this case, the total number of carbody modes that interact with the passengers is 8+3=11, including the three carbody rigid-body modes bounce, roll and pitch. Since, in this case *L*=8, only the (1,*L*) and (1+1,*L*) models imply a reduction.

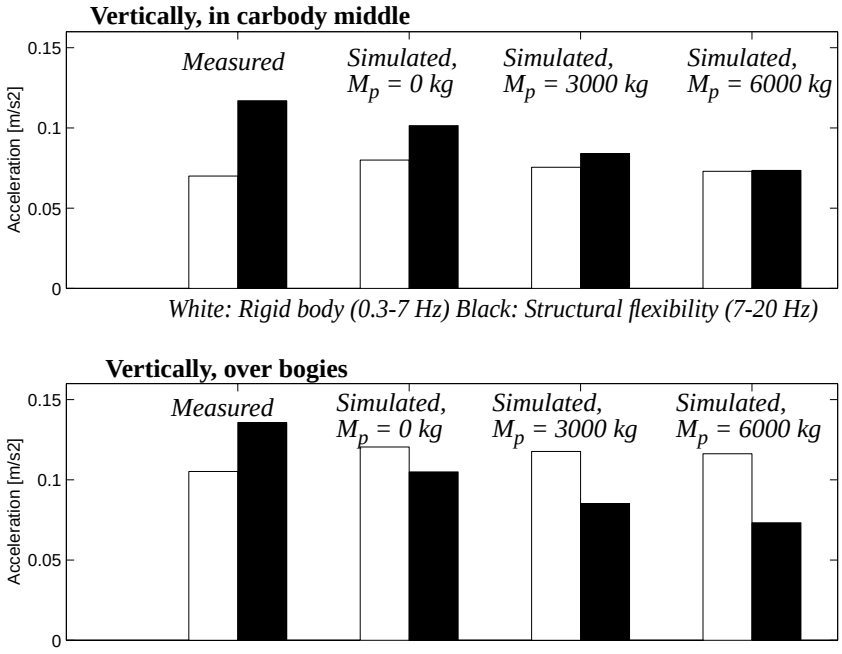

Figure 7-1 ***Comfort-weighted vertical acceleration (r.m.s.) in side-sills in carbody middle and over bogies as a function of total passenger mass predicted by the (N,L)-passenger-carbody model.*** *White corresponds to rigid-body motion and black corresponds to structural-flexibility vibration.*

Comfort-weighted r.m.s.-values of vertical acceleration in the side-sills of the carbody middle and over the bogies are shown. Average values of two and four points, respectively, are used. White corresponds to the frequency interval of 0.3 to 7 Hz (essentially rigid-body motion) and black corresponds to the frequency interval of 7 to 20 Hz (essentially structural-flexibility vibration). Note that these cannot be added directly to obtain the total r.m.s.-value. See also Figure 2-10. As observed in Section 2.1, the agreement between simulated and measured rigid-body motion (0.3 to 7 Hz) is good, while structural-flexibility vibration (7 to 20 Hz) is not fully excited in the simulation as compared to the measurements.

The passengers influence both rigid-body vibration and structural flexibility vibration according to the simulations. The structural flexibility comfort-weighted vibration (r.m.s) decreases by some 30% for a fully loaded vehicle. The change in rigid-body vibration is smaller.

Figure 7-2 shows the simulation results obtained with the (1,*L*)-passenger-carbody model. The values in the carbody middle differ little from those of the (N,*L*)-model, but the decrease in acceleration over the bogies is smaller using this (1,*L*)-model.

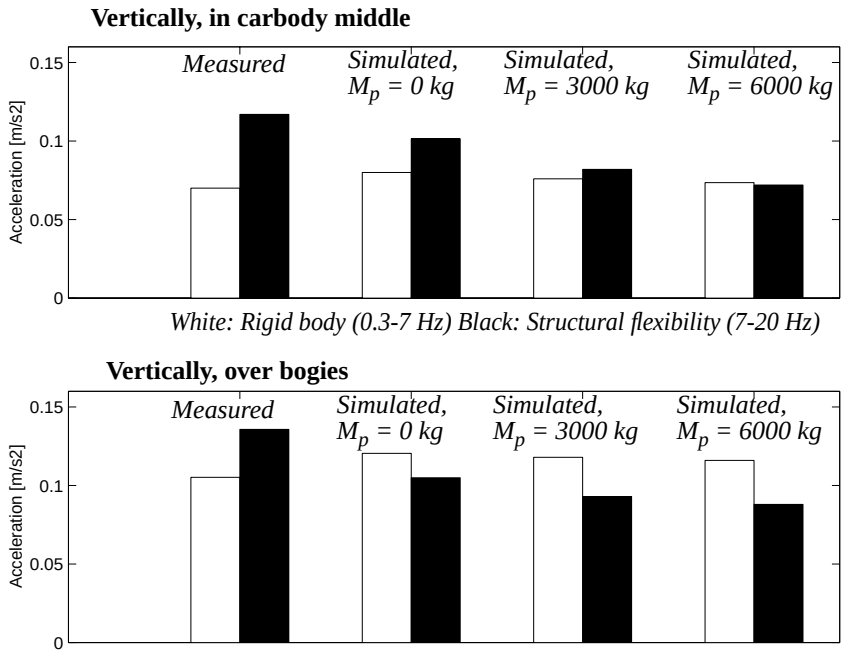

Figure 7-2 Comfort-weighted vertical acceleration (r.m.s.) in side-sills in carbody middle and over bogies as a function of total passenger mass predicted by the (1,L)-passenger-carbody model.

In top of Figure 7-3, the prediction made by the (*N*+*N*,*L*)-passenger-seat-model is shown. It is to be compared with the predictions of the (*N*,*L*)-passenger-carbody model in Figure 7-1. The (*N*+*N*,*L*)-model also predicts a decrease in structural vibration level when passengers are introduced, although the decrease is less than for the corresponding passenger-carbody model in Figure 7-1. Structural vibration in the middle of the carbody is predicted to decrease by some 15%, while the corresponding value over the bogies is some 3% for a fully loaded vehicle.

Note that the predictions in Figure 7-3 concern the vibration level at the floor, or here rather in the side-sills. In order to obtain the corresponding vibration levels at the seat-pan, measured, or modelled, seat-transmissibility curves, cf. Figure 6-6, can be utilized.

The prediction made by (1+1,*L*)-passenger-seat-carbody model, cf. bottom of Figure 7-3, is quite similar to that of the exact (*N*+*N*,*L*)-passenger-seat-carbody-model. This supports the conclusions made in Section 5.3, namely that the approximate models should give fairly accurate results, cf. Figure 5-6.

From the model validation in Chapter 6 one would judge that the “true” values lie somewhere in between the predictions made by the passenger-carbody models and the passenger-seat-carbody models, somewhat closer to the prediction by the passenger-seat-carbody model.

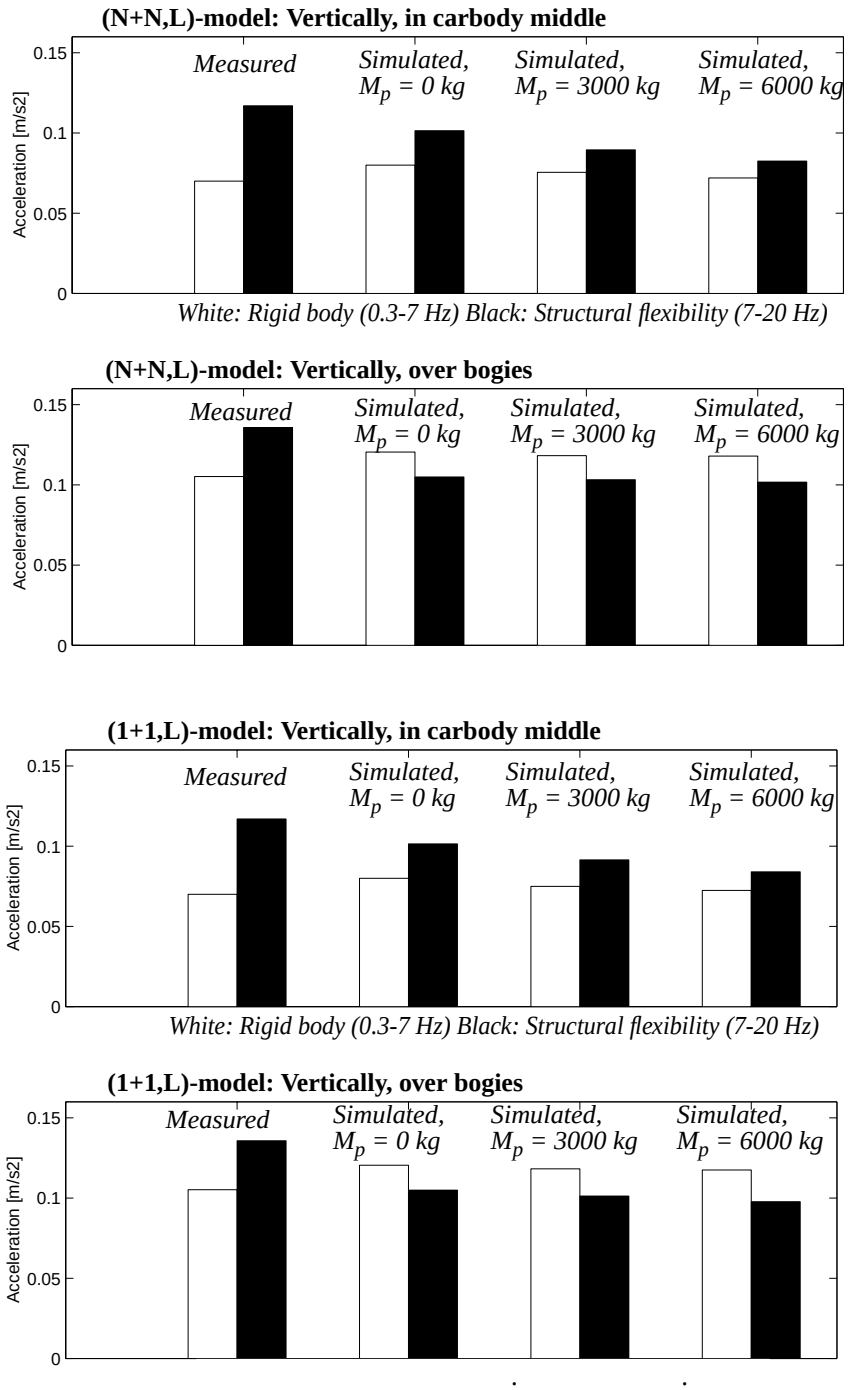

Figure 7-3 Comfort-weighted vertical acceleration (r.m.s.) in side-sills in carbody middle and over bogies as a function of total passenger mass predicted by the (N+N,L)- and (1+1,L)-passenger-seat-carbody models.

7.2.2 Parameter study: Carbody relative damping

The measurements presented in Chapter 3 showed that the main influence of passenger loading is an increase of relative damping of the carbody structural modes. Therefore, a brief parameter study of the carbody relative damping is conducted. The passenger models are not used here.

Figure 7-4 shows comfort-weighted vertical acceleration (r.m.s.) in the side-sills in carbody middle and over bogies as a function of carbody relative damping. The same relative damping is given to all modes.

As can be seen, an increase of carbody relative damping from 1% to 4% gives results similar to an increase in passenger mass from 0 to 6,000 kg. This agrees with previous prediction on how much the relative damping of the carbody-dominated modes increases as a function of the passenger load, cf. Figure 7-1 and Figure 3-13.

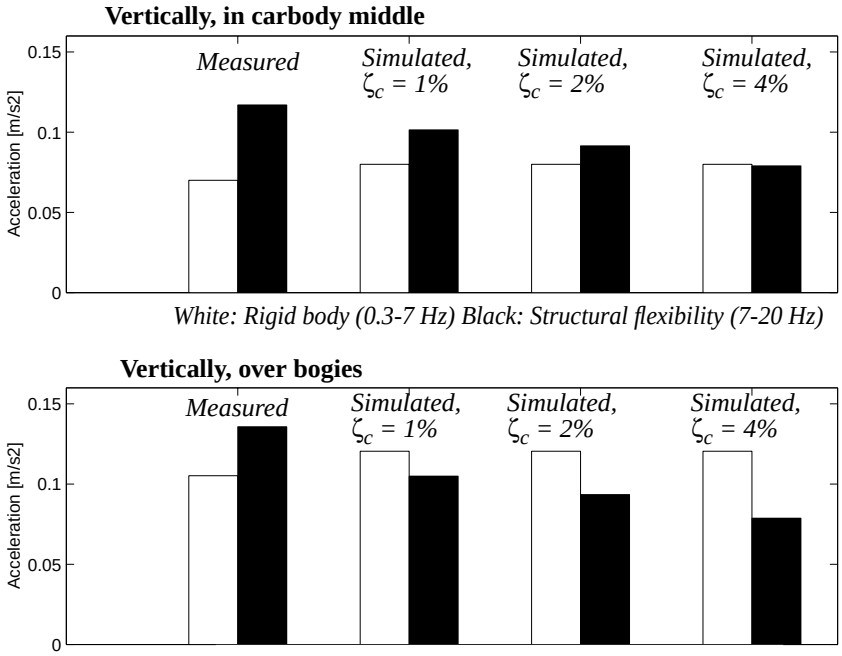

Figure 7-4 ***Comfort weighted vertical acceleration (r.m.s.) in side-sills in carbody middle and over bogies as a function of carbody relative damping.*** *A relative damping of 1% is also used in Section 7.2.1 and in the case study in Chapter 2. The passenger models are not used.*

7.3 Conclusions

The parameter studies that are conducted in this chapter show that passengers would have an appreciable influence on the dynamics of the carbody and on ride comfort. The main influence can be seen as an increased damping of the carbody structural modes.

However, for a more complete picture of the dynamics involved, the passenger(-seat)-carbody models are recommended. They are easy to implement and the increase in computational cost is minimal. Primarily, the passenger-carbody model is recommended, since it gives an upper boundary on the interaction, although it probably underestimates the vibration levels, cf. Section 6.3. Also, it relies on easily accessible data. If seat parameters are available, however, then the model can easily be extended to include the seats.

Note that, in order to predict acceleration levels and ride comfort at the seat-pan, a model of the seat is needed. Seat-transmissibility curves contain valuable information to this end.

There is another important aspect, namely the reliability of the rail-vehicle model as such. If the predictions made by the rail-vehicle model are not reliable, then it is not worthwhile to include the passengers. Previous work [13] showed that the excitation of the carbody modes in the simulation is quite sensitive to a number of factors, in particular the modelling of the carbody-bogie interface.

Also, the relative-damping values of the empty carbody are an important aspect. Often these values are not known reliably. They cannot be calculated from finite-element models, since it would require a detailed knowledge of the damping mechanisms of the entire structure. The values may be obtained by experimental modal analysis, but this supposes that the vehicle in question exists. Often rules-of-thumb are used, with values ranging from 2% to 5% [6], which is in the same range as the possible additional damping due to passengers. There is also, as observed earlier, a dependence on excitation amplitude.

In conclusion, the simple and easy-to-use models presented here are recommended to be used to model the passengers whenever the rest of the vehicle model is fully reliable. One must be aware of the simplifications, in particular that only vertical forces are taken into account between passengers, seats and carbody.

Finally, to conclude this chapter, some recommendations are given.

Practical recommendations on how to model passengers in rail vehicle dynamics

Based on the present case study, the following recommendations are given on how to model and estimate the influence of passenger load on ride comfort.

The best alternative is to implement the reduced models into the simulation software. The number of degrees-of-freedom would then be kept to a minimum, and a high level of user-friendliness could be achieved. The only required input data would be the total passenger mass M_p and a specification of the area in which passengers are to sit. Seat stiffness and damping constants could also be input. The software would then calculate (and output) the informative $\boldsymbol{P}$-matrix, and perform the necessary reduction before starting the simulation.

But, in case the reduced models are *not* implemented, the following is recommended:

No carbody relative damping data is available

Set carbody relative damping to 2% for the empty vehicle.
Set carbody relative damping to 4% for the fully loaded vehicle.
Add passenger mass and resulting moments of inertia to rigid carbody modes.

Carbody relative damping data available, but the modelling of the inner floor is poor.

Use available carbody relative damping for empty vehicle.
Increase carbody relative damping by 2% for fully loaded vehicle.
Add passenger mass and resulting moments of inertia to rigid carbody modes.

Carbody relative damping is data available and the modelling of the inner floor is good.

It is highly recommended that the ***P***-matrix be calculated, since it gives information on which carbody modes are important, and also what modes that risk being coupled by the passengers.
Let L be the number of carbody modes (typically 10), and M_p (typically 6,000 kg) be the total passenger mass. Choose N representative locations where passengers are seated. N should be equal to $L+3$ or slightly superior. Attach a point mass with a vertical degree-of-freedom (only) to each one of the N chosen points. The mass should be mounted on a linear spring and a linear viscous damper in parallel, with the following data:

Mass: $0.9 \cdot M_p / N$ kg

Spring: $M_p / N \cdot 4 \cdot \pi^2 \cdot 25$ N/m

Damper: $M_p / N \cdot 4 \cdot \pi \cdot 0.5 \cdot 5$ Ns/m

Add mass and moments of inertia to the rigid carbody corresponding to $0.1 \cdot M_p$ in vertical, roll and pitch directions, and corresponding to M_p in longitudinal, lateral and yaw directions.

As in the previous case, but seat data is also available.

As above, it is highly recommended that the ***P***-matrix be calculated.
The seat is modelled by a linear spring and a linear viscous damper. (Typically, for a person weighing 75 kg: k_s=75 kN/m and c_s=250 Ns/m.)
A mass with a vertical degree-of-freedom should be mounted at each one of the N chosen locations. Data:

Mass: $0.1 \cdot M_p / N$ kg

Spring: $M_p / N / 75 \cdot k_s$ N/m

Damper: $M_p / N / 75 \cdot c_s$ Ns/m

Mount another mass on the top of each mass, with

Mass: $0.9 \cdot M_p / N$ kg

Spring: $M_p / N \cdot 4 \cdot \pi^2 \cdot 25$ N/m

Damper: $M_p / N \cdot 4 \cdot \pi \cdot 0.5 \cdot 5$ Ns/m

Add mass and moments of inertia corresponding to M_p to the rigid carbody in longitudinal, lateral and yaw directions.

8 Concluding remarks

8.1 Conclusions

On the one hand, a set of on-track measurements of carbody operating-deflection shapes and spectral analysis of acceleration in the carbody show that the structural flexibility of the carbody accounts for a substantial part of the vertical vibration level. On the other hand, previous simulation with a flexible multibody model of the corresponding rail vehicle shows that there are several factors to which simulation results are sensitive. These two facts, the importance and the sensitivity, emphasize the need for validated models of the carbody in rail-vehicle dynamics. Also, customer demand on good ride comfort and present standards put the passengers in focus, calling for validated models of the passenger-vehicle interaction.

From the present work, which investigates these matters, several types of conclusions may be drawn, e.g. regarding the studied vehicle, on the use of various measurement techniques and the reliability of various models and simulation results.

To begin with, the study of carbody, passenger and ride comfort in rail-vehicle dynamics has many aspects and involves a number of disciplines from physiology, via mathematics and mechanics, to vibration measurements. Some kind of limitation is necessary, and the present study concentrates on the system dynamics aspects; how do the mechanical systems interact?

It must be concluded that available software for modelling and performing simulation of a flexible carbody in rail-vehicle dynamics meets simulation needs well. There is, however, a need of guidelines for how to model carbody structural flexibility. Correct model data is essential, although not sufficient. Equally important is an awareness of the sensitivity of the vehicle model.

One conclusion drawn from the on-track measurements is that operating-deflection-shape analysis together with power-spectral analysis constitutes a powerful tool investigating vibrations, and, in particular, vibrations that are due to structural flexibility, in the carbody.

The proposed four criteria for selecting important carbody mode shapes should be seen as guidelines in finding the essentials of the carbody dynamics from a ride comfort point of view. One of the criteria, i.e. the modal-contribution-factor criterion, is shown to play an important role as a key parameter in the dynamical system consisting of passengers and carbody. As a generalization a “passenger load parameter”, also taking into account the mass distribution of the passengers, is proposed.

The experimental-modal-analysis measurements of the passenger-carbody system show that the interaction between passengers and carbody is significant. The measurements also show that the excitation amplitude has a significant influence on the modal parameters of the carbody eigenmodes. A trend can be established that relative damping

of the carbody-dominated eigenmodes increases with passenger load. The eigenfrequency increases with passenger load in most cases.

The increase in damping is predicted by a rather simple model, namely the combination of the modal carbody model and vertical human-body models from literature. The passenger-carbody model slightly overestimates the interaction, however, but this is expected, since the flexibility of the seat is not taken into account.

The main assumption on which the proposed models are based is that the passengers are supposed to be alike, viewed as mechanical systems. The “normalized apparent mass” is assumed to be the same for each passenger. Due to the generality of the problem, i.e. the common modal model and the validated human-body model, the proposed passenger-carbody model should work for other rail vehicles as well.

Simple seat models are difficult to achieve, due to the complexity and diversity in design. Here, a simple vertical seat model is proposed, but it is based on quite bold assumptions. Firstly, it is a priori only applicable to seats of the same type as in the case study. Secondly, it is assumed that the only interaction that takes place between seat and passenger is a vertical force at the seat pan. However, the model allows describing how seat stiffness and damping affects the passenger-carbody interaction, at least in principle.

The passenger-carbody model and the passenger-seat-carbody can be used to estimate an upper and a lower boundary for the interaction. From the present study, it is clear that the passengers cannot be modelled by merely adding mass to the carbody structure, since this would not introduce any damping. Such a simplification would also lower the carbody eigenfrequencies, whereas a slight increase is observed in the measurements.

The “passenger-load parameters”, which are easily calculated provided that carbody-mode-shape data are available, are shown to be suitable parameters to quantify the passenger-carbody interaction. As a generalization, the “passenger-load matrix” may be utilized. It describes how the passengers affect each individual mode, and also how they couple the carbody modes to each other.

A method to obtain reduced models of the passenger(-seat)-carbody system is proposed. Also, an idea is presented as to how to define and use approximate models of the passenger(-seat)-carbody system. It is shown that a simpler model, e.g. a model neglecting the cross-coupling between carbody modes that are due to passenger load, can be used if the passenger load is low.

Based on the present case study, recommendations can be given as to how to model passengers in rail-vehicle dynamics. Depending on available vehicle data, models of various complexity are recommended, ranging from simple rules-of-thumb to models including seat dynamics.

8.2 Further development

Further development can be outlined in different directions.

The role played by the seat needs to be investigated further, including measurements as well as modelling. One possibility is to create a more detailed model of the present vehicle, in particular a more detailed description of the seats. The result risks becoming specific and not applicable to vehicles and other seats than those in the case study. It would, therefore, be of interest to identify mechanisms in a wide range of seats, to see if there are some mechanisms that are common and worthwhile to model.

It is highly recommended that the “reduced models” presented here be implemented in simulation software for rail-vehicle dynamics, since this would improve user-friendliness and reduce computational costs.

Modelling and understanding of carbody interior dynamics, e.g. of inner floor and walls, are important to improve the modelling of passenger-carbody interaction. Such models are necessary whenever measurements are not possible.

The proposed models should be used to evaluate different design solutions. For instance, what kind of dynamics characteristics should a rail-vehicle seat have?

The ideas on model reduction and approximate systems could be investigated further. For instance, there should be an interesting mathematical framework of “approximation theory in dynamical systems”.

Concluding remarks

A References

A.1 General and structural dynamics

[1] Bamberger, Y.: *Notes pour la majeure "Vibrations"*, Ecole Polytechnique, Paris (1990)

[2] Ewins, D. J.: *Modal Testing: Theory and Practice*, Research Studies Press (1991)

[3] Clough, R. W. and Penzien, J.: *Dynamics of structures*, Sec. Ed., McGraw-Hill (1993)

[4] Cremer, L., Heckl, M. and Ungar, E. E.: *Structure-Borne Sound*, Sec. Ed., Springer Verlag (1988)

[5] Råde, L. and Westergren, B.: *Beta Mathematics Handbook*, Sec. Ed., Studentlitteratur (1990)

A.2 Rail vehicle dynamics

[6] Adtranz: *Vehicle model data*. Not public.

[7] Andereg, K. and Weichelt, P.: *Der Einfluß von Ausrüstung und Zuladung auf die vertikale Biegeschwingung eines Eisenbahn-Personenwagens*, ZEV-Glas. Ann., Vol. 114, pp. 39-41 (1990)

[8] Andersson, E., Berg, M. and Stichel, S.: *Rail vehicle dynamics - Fundamentals and Guidelines*, Division of Railway Technology, Department of Vehicle Engineering, KTH (1999)

[9] ASEA:, *Bogies for railway vehicles*, ASEA Pamphlet A 12-0006 E Reg. 6111 (1986)

[10] Berg, M.: *A model for rubber springs in the dynamic analysis of rail vehicles*, IMechE Journal of Rail and Rapid Transit, Proceedings Part F, Vol. 211, pp. 95-108 (1997)

[11] Brüel & Kjaer: *Dynamic Design Verification of a Prototype Rapid Transit Train using Modal Analysis*, Application Notes (1982)

[12] Carlbom, P.: *Structural flexibility models for rail vehicle dynamics analysis - a pilot study*, KTH/FKT/FR 96/18, Division of Railway Technology, Department of Vehicle Engineering, KTH (1996)

[13] Carlbom, P.: *Structural flexibility in a rail vehicle car body*, KTH/FKT/FR 98/37, Division of Railway Technology, Department of Vehicle Engineering, KTH (1998)

[14] Carlbom, P.: *Structural flexibility in rail vehicles - Equations of motion and model reduction*, KTH/FKT/FR 98/38, Division of Railway Technology, Department of Vehicle Engineering, KTH (1998)

[15] Carlbom, P.: *Track-induced structural vibrations in rail vehicle car bodies*, Licentiate thesis, KTH/FKT/LA-98/36, Division of Railway Technology, Department of Vehicle Engineering, KTH (1998)

[16] Carlbom, P.: *Structural flexibility: Simulation and on-track measurements of rail vehicle carbody dynamics*, Proceedings of VSDIA 1998 (editor: Zobory, I.), pp. 95-104, TU Budapest (in print)

[17] Carlbom, P.: *Combining MBS with FEM for rail vehicle dynamics analysis*, accepted for publication in Journal of Multibody System Dynamics (2000)

[18] Carlbom, P.: *Passenger and carbody interaction in rail vehicle dynamic*s, Proceedings of MBD-MST 2000, pp. 115-126, University of Bradford (2000)

[19] Cléon, L. M. and Sauvage, G.: *Rail Vehicles' Riding Quality and Comfort Related to Theoretical and Experimental Optimization, Application to High Speed Trains*, IAVSD Extensive Summaries: 9th symposium, pp. 107-114, Linköping (1985)

[20] Coutellier, D., Ravalard, Y. and Oudin, J.: *Reanalysis by modal synthesis of railway vehicle structures*, IMechE Journal of Rail and Rapid Transit, Proceedings Part F, Vol. 205, pp. 101-107 (1991)

[21] von Dellmann, T.: *Drehgestellanlenkungen und deren Auswirkungen auf die Strukturschwingungen von Reisezugwagenkästen*, ZEV-Glas. Ann., Vol. 122, pp. 400-407 (1988)

[22] Diepen, P.: *Horizontaldynamik von Drehgestellfahrzeugen*, Doctoral thesis, TU Braunschweig (1991)

[23] Dietz, S.: *Vibration and Fatigue Analysis of Vehicle Systems Using Component Modes*, Doctoral thesis, VDI Verlag GmbH, Düsseldorf (1999)

[24] Eriksson, P.: *A Study of Ride Comfort Optimization of Buses*, Licentiate thesis, Publication 00:1, Department of Structural Mechanics, Chalmers University of Technology, Göteborg (2000)

[25] Fanti, G., Berti, G. and Vianello, A.: *Dynamic analysis of rail vehicles by means of models of equivalent finite elements* (In Italian), Ingegneria Ferroviara, Vol. 43(5), pp. 257-263 (1988)

[26] Garg, V. K. and Dukkipati, R. V.: *Dynamics of Railway Vehicle Dynamics*, Academic Press (1984)

[27] Iwnicki, S. (editor): *The Manchester Benchmarks for Rail Vehicle Simulation*, Supplement to Vehicle System Dynamics, Vol. 31 (1999)

[28] Jonson, L.: *Experimental modal analysis of an X10 carbody* (In Swedish: Experimentell modalanalys av X10 motorvagnskorg), M.Sc. thesis, KTH (1984)

[29] Kalker, J. J.: *Three dimensional elastic bodies in rolling contact*, Kluwer Academic Publishers, Dordrecht, The Netherlands (1990)

[30] Knothe, K. and Böhm, F.: *History of Stability of Railway and Road Vehicles*, Vehicle System Dynamics, Vol. 31, pp. 283-323 (1999)

[31] Ofierzynsky, M. and Brundish, V.: *Fahrkomfort von Schienenfahrzeugen - Die Zuverlässigkeit moderner Simulationstechnik*, ZEV-Glas. Ann., Vol. 124, pp. 109-119 (2000)

[32] von Reiß, G. and Schraut, R.: *Zur Berechnung und Messung des Schwingungsverhaltens und des Fahrkomforts von Schienenfahrzeugen*, ZEV-Glas. Ann., Vol. 113(3), pp. 66-75 (1989)

[33] Richard, J.: *Natural Frequencies of Bernoulli-Euler Beams Resting on Two Elastic Supports: Application to Railway Vehicles*, Vehicle System Dynamics, Vol. 9, pp. 309-326 (1980)

[34] Suzuki, Y. and Akutsu, K.: *Theoretical Analysis of Flexural Vibration of Car Body*, Quarterly Report of RTRI, Vol. 31(1), pp. 42-48 (1990)

[35] Wallrapp, O.: *Entwicklung rechnergestützter Methoden der Mehrkörperdynamik in der Fahrzeugtechnik*, DFVLR-FB 89-17 (1989)

[36] Wallrapp, O.: *Standard Input Data of Flexible Members in Multibody Systems* (In: Advanced Multibody System Dynamics - Simulation and Software Tools), Kluwer Academic Publishers (1993)

[37] Wollström, M.: *On vibration characteristics of floating floors*, Licentiate thesis, KTH/FKT/L-00/31, Division of Railway Technology, Department of Vehicle Engineering, KTH (2000)

A.3 Human body and seating dynamics

[38] von Bekesy, G.: *Über die Empfindlichkeit des Stehenden und Sitzenden Menschen gegen sinusförmige Erschütterungen*, Akustische Zeitschrift, Vol. 4, pp. 360-369 (1939)

[39] Berger, E. J. and Gilmore, B. J.: *Seat Dynamics Parameters for Ride Quality*, SAE Transaction, Journal of Passenger Cars, Vol. 112(6), pp. 283-290 (1994)

[40] Coermann, R. R.: *The Mechanical Impedance of the Human Body in Sitting and Standing Position at Low Frequencies*, Human Factors, Vol. 4, pp. 227-253 (1962)

[41] Corbridge, C., Griffin, M. J. and Harborough, P. R.: *Seat Dynamics and Passenger Comfort*, IMechE Journal of Rail and Rapid Transit, Proceedings Part F, Vol. 203, pp. 57-64 (1999)

[42] Dieckmann, D.: *Einfluß vertikaler mechanisher Schwingungen auf den Menschen* Int. Zeitung angewendte Physiologie einschliesslich Arbeitsphysiologie, Vol. 16, pp. 519-564 (1957)

[43] Fairley, T.E. and Griffin, M.J.: *The apparent mass of the seated human body: vertical vibration*, Journal of Biomechanics, Vol. 22, pp. 81-94 (1989)

[44] Griffin, M. J.: *Handbook of Human Vibration*, Academic Press Limited (1990)

[45] Hansson, L.: *Seat environment design - A maximum of comfort in a minimum of space* (In Swedish: Utformning av sittplatser. Maximal komfort på minimalt utrymme*)*, M. Sc. thesis, KTH/FKT/EX-96/26-SE, Division of Railway Technology, Department of Vehicle Engineering, KTH (1996)

[46] Harris, C. M.: *Shock and Vibration Handbook*, Third Ed., McGraw-Hill (1988)

[47] ISO: *Vibration and shock - mechanical driving point impedance of the human body*, ISO 5982 (1981)

[48] Miwa, T.: *Mechanical Impedance of the Human Body in Various Postures*, Industrial Health, Vol. 13, pp. 1-22 (1975)

[49] Olsson, K.: *Dynamic seat models of today within Adtranz*, Adtranz (1998). Not public.

[50] Wasserman, R. R.: *Human Aspects of Occupational Vibration*, Elsevier (1987)

[51] Wei, L. and Griffin, M. J.: *Mathematical models for the apparent mass of the seated human body exposed to vertical vibration*, Journal of Sound and Vibration, Vol. 212(5), pp. 855-874 (1998)

[52] Wei, L. and Griffin, M. J.: *The prediction of seat transmissibility from measures of seat impedance*, Journal of Sound and Vibration, Vol. 214(1), pp. 121-137 (1998)

A.4 Ride comfort

[53] CEN: *Railway applications - Ride comfort for passengers - Measurements and evaluation*, ENV 12299, Brussels (1999)

[54] Förstberg, J.: *Ride comfort and motion sickness in tilting trains - Human responses to motion environments in train and simulator experiments*, Doctoral thesis, KTH/ FKT/D-00/28-SE, Division of Railway Technology, Department of Vehicle Engineering, KTH (2000)

[55] Helberg, W. and Sperling, E.: *Verfaren zur Beurteilung der Laufeigenschaften von Fahrzeugen*, Organ für die Fortschritte des Eisenbahnwesens, Vol. 12, pp. 176-187 (1941)

[56] ISO: *Guide to the evaluation of human exposure to whole-body mechanical vibration and shock*, ISO 1631, Geneva: ISO (1975)

[57] ISO: *Mechanical vibration and shock - Evaluation of human exposure to whole-body vibration - Part 1: General requirements*, ISO 2631-1.2:1997 (E), Geneva: ISO 2631 (1997)

[58] Kottenhoff, K.: *Future passenger trains - Vehicle concepts for increased attractiveness and effectiveness*, Licentiate thesis, KTH/IP/FR-94/3-SE, Division of Traffic and Transport Planning, Department of Infrastructure and Planning, KTH (1994)

A.5 User's guides etc.

[59] DEsolver AB: *GENSYS User's guide, revision 0003*, Östersund, Sweden (2000)

[60] LMS International: *LMS CADA-X Running Mode Analysis Manual, Revision 3.2*, Leuven, Belgium (1992)

[61] MathWorks, Inc.: *MATLAB, User's Guide* (1998)

[62] Swanson Analysis System, Inc.: *ANSYS User's Manual Revision* 5.1 (1994)

References

B Definitions and notations

B.1 Definitions

B.1.1 General

Some general definitions are collected and explained here. A good textbook is [2].

Accelerance

Accelerance is the frequency-response-function “acceleration to force”. The dimension is [1/kg].

Apparent mass

Apparent mass is the frequency-response-function “force to acceleration”. The dimension is [kg].

Autospectrum

The autospectrum gives information on the frequency content of a signal. It may be defined as the Fourier transform of the correlation function.

Correlation function

See cross-correlation function.

Cross-correlation function

The cross-correlation function between two signals x and y is defined by

$$r_{xy}(\tau) = \lim_{t \to \infty} \frac{1}{2T} \int_{-T}^{T} x(t) y(t+\tau) dt \tag{B-1}$$

The correlation-function for the signal x is obtained by replacing y by x in (B-1).

Cross-spectrum

The cross-spectrum may be defined as the Fourier transform of the cross-correlation function.

Frequency-response-function

Frequency response functions can be used to describe the dynamics of a system. Suppose that a system is excited by a harmonic input (force or motion), $I(\omega)$, where ω is the circular frequency of the input. The system gives an output $O(\omega)$ (force or motion). The frequency-response-function is then defined as $O(\omega)/I(\omega)$ and is complex-valued. Accelerance, apparent mass, impedance, dynamics stiffness and transmissibility are all frequency-response-functions.

Frequency-response-function estimate

A frequency-response-function can be estimated from two measured signals, where one is considered as input and the other as output. A number of estimates are possible. *For instance*, the "source correlation technique" is used here to estimate seat transmissibility

$$T_s(\omega) = \frac{G_{SI}(\omega)}{G_{FI}(\omega)} \tag{B-2}$$

where $G_{SI}(\omega)$ is the cross-spectrum of the acceleration at the seat pan (S) (considered as output) and the exciting input force (I) (a correlated source) and $G_{FI}(\omega)$ is the cross-spectrum of the acceleration at the floor (F) (considered as input) and (I) (the correlated source).

Impedance

Impedance is the frequency-response-function "force to velocity". The dimension is [Ns/m].

Operating Deflection Shape (ODS)

An operating deflection shape of a rail-vehicle carbody describes how the carbody vibrates at a particular frequency when the rail-vehicle is running on the track. Compared to eigenmodes of a carbody, which are determined by the dynamical properties alone, an ODS also depends on the magnitude and frequency content of the excitation forces.

Point accelerance, point impedance

"Point" means that both signals are measured at the same point and in the same direction.

Power Spectral Density (PSD)

See Autospectrum.

Relative damping

In this work relative damping is used to quantify damping. It is defined by

$$\zeta = \frac{c}{2\sqrt{mk}} \tag{B-3}$$

Root mean square value

Two types of root mean square (r.m.s.) values are used in this work, a temporal r.m.s.-value and a spatial r.m.s.-value. The *temporal* r.m.s-value of a signal *a* for a time period *T* is defined by

$$a_{rms} = \sqrt{\frac{1}{T}\int_0^T |a(t)|^2 dt} \tag{B-4}$$

A *spatial* average of an entity *a* is taken over a number *N* of points in space

$$a_{rms} = \sqrt{\frac{1}{N}\sum_{i=1}^{N} |a_i|^2} \tag{B-5}$$

Stiffness

Stiffness (dynamic stiffness) is the frequency-response-function “force to displacement”. The dimension is [N/m].

Transmissibility

In this work the term “transmissibility” is used for acceleration transmissibility, and *not* for force transmissibility. Acceleration transmissibility is defined as a frequency-response function between two acceleration signals, or equivalently, between two velocity signals, or two displacement signals. Force transmissibility, on the other hand, is defined as a frequency-response function between two force signals. It has the dimension [-].

B.1.2 More specific

Central definitions of the present work are collected and explained here.

Human-body impedance

Human-body impedance refers to the frequency-response-function “force to velocity”, where the force is the vertical force that the human body exerts on the seat pan and the velocity is the exciting vertical velocity of the seat pan. It is assumed that there are no other excitation sources than the motion of the seat. Other motions and forces than vertical are not taken into account. The human-body impedance of an average passenger is denoted by $Z_p(\omega)$ and has the dimension [Ns/m].

Modal contribution factor

The modal contribution factor (*MCF*) is proposed in [15] as a value to rank carbody mode shapes with respect to their contribution to ride discomfort in general. A high *MCF* indicates that the mode contributes much to ride discomfort. It is defined as the spatial root mean square of the vertical (or lateral) carbody mode-shape-values at a number *N* of points where passengers are seated:

$$MCF_j = \sqrt{\sum_{i=1}^{N} d_{ij}^2 / N} \tag{B-6}$$

where MCF_j is the Modal Contribution Factor of carbody-mode number *j*. The vertical displacement of mode number *j* at a point numbered *i* is denoted

by d_{ij}. *MCF* for lateral and longitudinal directions can also be defined. The modes are supposed to be scaled to have a modal mass of 1 kgm^2. *MCF* has the dimension [m].

Normalized apparent mass

Normalized apparent mass is a suitable characteristics of the human-body vertical dynamics. The term normalized apparent mass is used here as defined in [51], with the generalization that also phase information is included, i.e. it is a complex-valued quantity. The apparent mass is normalized with respect to the body mass of the subject, yielding a static value ($\omega = 0$) of 1, see Figure 4-3. Normalized apparent mass has the same dimension as transmissibility, namely [-]. In Model A, see Figure 4-2, it is identical to the transmissibility, cf. (4-4). Therefore, the normalized apparent mass of a passenger is denoted by $T_p(\omega)$ and defined by

$$T_p(\omega) = \frac{Z_p(\omega)}{m_p \mathrm{i}\omega} \tag{B-7}$$

where $Z_p(\omega)$ is the vertical point impedance of the human body and m_p is the human-body mass. The normalized apparent mass is a key entity in the present work. It expresses the frequency dependency of the human-body dynamics, and this frequency dependency is *assumed to be the same for all passengers*.

Passenger load parameter

The passenger load parameter is introduced in this work to quantify the interaction between a carbody mode shape and the passengers. It is defined as

$$P_j = \sum_{i=1}^{N} m_{pi} d_{ij}^2 \tag{B-8}$$

where N is the number of passengers, m_{pi} is the mass of passenger number i, d_{ij} is the vertical displacement of carbody-mode number j at the location of passenger number i and P_j is the passenger load parameter of carbody-mode number j. The passenger load parameter is thus a mass-weighted sum of squares of carbody vertical displacement-values, and, thereby, closely related to a spatial r.m.s.-value. It has dimension [kgm^2].

Passenger load matrix

The passenger load matrix $\boldsymbol{P}$ consists of the elements

$$P_{jk} = \sum_{i=1}^{N} m_{pi} d_{ij} d_{ik} \tag{B-9}$$

where N is the number of passengers, m_{pi} is the mass of passenger number i and, finally, d_{ij} and d_{ik} are the vertical displacement of carbody-mode number j and k, respectively, at the location of passenger number i. Note that the elements on the matrix-diagonal are identical to the passenger load parameters. The off-diagonal terms quantify the coupling introduced between the carbody modes by the action of the passenger load. The dimension is [kgm^2].

Seat stiffness

Only vertical forces and motions are considered in the passenger-carbody interface. The (dynamic) seat stiffness is consequently defined as the frequency response function "force to displacement", where the force is the vertical force transmitted through the seat and the displacement is the relative vertical displacement between the seat pan and the floor. Seat stiffness has the dimension [N/m].

Seat transmissibility

The term seat transmissibility is used as defined in [52], with the generalization that also phase information is included. It is here defined as the frequency response function between z_s and z_f, where z_s is the *vertical displacement* of the seat pan and z_f is the *vertical displacement* of the floor at the interface between seat and floor. It may be estimated by

$$T_s(\omega) = \frac{G_{SI}(\omega)}{G_{FI}(\omega)} \tag{B-10}$$

where $G_{SI}(\omega)$ is the cross-spectrum of the vertical acceleration at the seat pan (S) and an exciting input force (I) and $G_{FI}(\omega)$ is the cross-spectrum of the vertical acceleration at the floor (F) and the exciting input force. It has the dimension [-].

Vertical mode-shape value, vertical displacement of carbody mode etc.

The deformation (displacement) of a carbody mode-shape in the vertical direction at a particular point in the carbody. Denoted by d. The dimension is [m].

B.2 Notations

B.2.1 Latin

$\boldsymbol{C}$	Damping matrix [Ns/m]
$\boldsymbol{C}_c$	Carbody damping matrix [Ns/m]
$\boldsymbol{C}_s$	Diagonal matrix containing c_{si} [Ns/m]
c_p	Damper constant in human-body model [Ns/m]

c_{pi}	Damper constant in human-body model, passenger *i* [Ns/m]
c_s	Damper constant in seat model [Ns/m]
c_{si}	Damper constant of seat *i* [Ns/m]
$\boldsymbol{D}$	Matrix consisting of all d_{ij} [m]
d	Vertical displacement of carbody mode at location of passenger [m]
d_i	Vertical displacement of carbody mode at the location of passenger *i* [m]
d_{ij}	Vertical displacement of carbody mode *j* at the location of passenger *i* [m]
$\boldsymbol{F}$, $\boldsymbol{F}(t)$	Force column matrix [N]
F	Force [N]
F_{cj}	Modal force on carbody mode *j* owing to passengers [Nm]
F_p	Interaction force between passenger and carbody [N]
F_{pi}	Interaction force between passenger *i* and carbody [N]
F_{p+s}	Interaction force between passenger-seat system and carbody [N]
f_p	Eigenfrequency in human body model
$G_S(\omega)$	Autospectrum of a signal measured at the point S
$G_{SI}(\omega)$	Cross-spectrum of a signal measured at the point S and input signal I
g	Polynomial in λ
$\boldsymbol{I}$	Identity matrix
i	$\sqrt{-1}$
$\boldsymbol{K}$	Stiffness matrix [N/m]
$\boldsymbol{K}_c$	Carbody stiffness matrix [N/m]
$\boldsymbol{K}_s$	Diagonal matrix containing k_{si} [N/m]
K	Min (L,N)
k_p	Spring constant in human-body model [N/m]
k_{pi}	Spring constant in human-body model, passenger *i* [N/m]
k_s	Spring constant in seat model [N/m]
k_{si}	Spring constant of seat *i* [N/m]
L	Number of carbody modes
$\boldsymbol{M}$	Mass matrix [kg]
$\boldsymbol{M}_c$	Carbody mass matrix [kg]
$\boldsymbol{M}_p$	Diagonal matrix containing m_{pi} [kgm^2]
M_p	Total mass of all passengers [kg]
m_{cj}	Modal mass of carbody-mode number *j*. Assumed to be equal to 1 kgm^2.
m_p	Mass of a typical passenger [kg]
m_{pi}	Mass of passenger number *i*
m_s	Mass of seat-pan moving with the passenger [kg]
MCF_j	Modal Contribution Factor of carbody-mode number *j* [m]
MPF_{ij}	Modal Participation Factor of mode *j* with respect to force distribution *i* [-]
N	Number of passengers, passenger groups, “important locations”

$\boldsymbol{n}_{cj}$	Mode-shape column-matrix of carbody eigenmode number j
$\boldsymbol{n}_p$	Generalized mode-shape column-matrix of passengers
$\boldsymbol{n}_{p+c}$	Mode-shape column-matrix of the passenger-carbody system
$\boldsymbol{P}$	Passenger load matrix containing the P_{ij} [kgm^2]
P_j	Passenger load parameter of carbody-mode number j [kgm^2]
P_{ij}	Coupling between carbody mode i and carbody mode j owing to passenger load [kgm^2]
$P_l^{(k)}$	Generalized passenger load parameter [kg^{k}m^{2k}]
$\boldsymbol{q}$	Degrees-of-freedom column matrix [may be mixed]
$\boldsymbol{q}_c$	Column matrix containing q_{cj} [-]
q_{cj}	Carbody modal-degree-of-freedom number j [-]
q_{pj}	Generalized passenger degree-of-freedom number j [-]
$\boldsymbol{R}$	Force distribution column matrix [Ns^2]
$S(\omega)$	Seat stiffness [N/m]
$T_p(\omega)$	Normalized apparent mass of a typical passenger [-]
$T_{pA}(\omega)$	Transmissibility z_p/z_s in passenger Model A [-]
$T_{pB}(\omega)$	Transmissibility z_p/z_s in passenger Model B [-]
$T_{p+s}(\omega)$	Normalized apparent mass of passenger-seat system [-]
$T_s(\omega)$	Vertical seat transmissibility [-]
$W(\omega)$	Comfort-weighting filter [-]
$Z_p(\omega)$	Impedance of passenger [Ns/m]
$Z_{pA}(\omega)$	Impedance of passenger in Model A [Ns/m]
$Z_{pB}(\omega)$	Impedance of passenger in Model B [Ns/m]
$Z_{pi}(\omega)$	Impedance of passenger number i [Ns/m]
$Z_{p+s}(\omega)$	Impedance of passenger-seat system [Ns/m]
$\boldsymbol{z}_f$	Column matrix containing z_{fi} [m]
z_f	Vertical motion of floor at the foot of the seat [m]
z_{fi}	Vertical motion of floor at the foot of seat number i [m]
$\boldsymbol{z}_p$	Column matrix containing z_{pi} [m]
z_p	Vertical displacement of passenger [m]
z_{pi}	Vertical displacement of passenger number i [m]
$\boldsymbol{z}_s$	Column matrix containing z_{si} [m]
z_s	Vertical displacement of seat [m]
z_{si}	Vertical displacement of seat number i [m]

B.2.2 Greek

α	Fraction of unsprung human-body mass in human-body models [-]
$\alpha(t)$	Time-varying coefficient [s^{-2}]
ζ_{cj}	Relative damping of carbody-mode number j [-]
ζ_p	Relative damping in human-body models [-]

λ	Root of characteristic equation
λ_c	Carbody mode root of characteristic equation
ω	Circular frequency [rad/s]
ω_{cj}	Circular eigenfrequency of carbody-mode number *j* [rad/s]
ω_p	Circular eigenfrequency in human-body model [rad/s]

B.2.3 Indexes

c	Carbody
cj	Carbody eigenmode number *j*
f	Foot of seat, floor
i	Counts passengers, runs from 1 to *N*
j	Counts mode shapes, runs from 1 to *L*
l	Counts generalized passenger load parameters
p	Passenger
pi	Passenger number *i*
p+s	Passenger and seat combined
s	Seat

B.2.4 Locations in carbody

A	In side-sill, over bogie
B	In side-sill, between A and C
C	In side-sill, in the middle of the carbody Also: on the console of seat 24
F	At the floor, at the foot of seat 24
S	On the top of the seat-pan of seat 24
W	Under the wooden plate of seat 24

B.2.5 Abbreviations

CEN	Comité Européen de Normalisation
EMA	Experimental Modal Analysis
FEM	Finite Element Method
ISO	International Standard Organization
ODS	Operation Deflection Shape
PSD	Power Spectral Density

B.3 Railway glossary

Adtranz
: A supplier of railway equipment

B7M
: A Swedish passenger rail vehicle

Banverket
: The Swedish National Rail Administration

Bogie
: A running gear that can move relative to the carbody and in which the wheelsets are mounted

Bolster beam
: Part of some bogies

Cant
: The difference in height between left and right rails

Carbody
: Part of the vehicle that carries load. The carbody rests on the bogies

Gauge
: The nominal lateral distance between the inner edges of the two rails. Standard gauge is 1.435 m.

GENSYS
: A simulation software for rail-vehicle dynamics

ISO-2631
: A standard for evaluation of vibration-related comfort

Lateral
: Direction in the plane of the floor and perpendicular to the direction of travel

Longitudinal
: Direction of travel

Ride comfort
: “Comfort” is “a state of being relaxed and feeling no pain” and “ride comfort” is the state of being relaxed and feeling no pain when riding a vehicle. There are standard procedures for how to evaluate ride comfort. See also [54].

Side-sill
: A longitudinal beam at the junction of carbody floor and side-wall

SJ
: Swedish State Railways

S4M
: A variant of the Swedish passenger rail-vehicle B7M furnished for office working

Track irregularities
: Irregularities of the track that give rise to vibrations

Vertical
: Direction perpendicular to the carbody floor.

Wheelset
: A set of two wheels on an axle. The wheels cannot move relatively to each other, and this fact makes it possible to keep the rail vehicle on track.

Wz
: A ride-comfort index